Electronic Supplementary Material (ESI) for Chemical Science.

Shape-selective crystallisation of fluxional carbon cages

Aisha N. Bismillah, Jiri Sturala, Brette M. Chapin, Dimitry S. Yufit, Paul Hodgkinson and Paul R. McGonigal*

Department of Chemistry, Durham University, Lower Mountjoy, Stockton Road, Durham, DH1 3LE, UK.

Table of Contents

Supporting Information

1. General Methods

Materials: All reagents were purchased from commercial suppliers (Sigma-Aldrich, Acros Organics, or Alfa Aesar) and used without further purification.

Instrumentation and Analytical Techniques: Analytical thin-layer chromatography (TLC) was performed on neutral aluminium sheet silica gel plates and visualised under UV irradiation (254 nm). Nuclear magnetic resonance (NMR) spectra were recorded using a Bruker Advance (III)-400 (^{1}H 400.130 MHz and ^{13}C 100.613 MHz), Varian Inova-500 (^{1}H 500.130 MHz and ^{13}C 125.758 MHz), Varian VNMRS-600 (^{1}H 600.130 MHz and ^{13}C 150.903 MHz) or a Varian VNMRS-700 (^{1}H 700.130 MHz and ^{13}C 176.048 MHz) spectrometer, at a constant temperature of 298 K unless otherwise stated. For variable-temperature measurements, operating temperatures were calibrated using an internal calibration solution of MeOH and glycerol. Chemical shifts (δ) are reported in parts per million (ppm) relative to the signals corresponding to residual non-deuterated solvents [$CDCl_3$: δ = 7.26 or 77.16. CD_2Cl_2: δ = 5.32 or 54.00]. Coupling constants (J) are reported in Hertz (Hz). ^{13}C NMR Experiments were proton-decoupled, whereas ^{19}F NMR experiments are coupled and referenced to an internal standard, hexafluorobenzene (HFB, δ = 164.99 ppm), unless otherwise stated. Assignments of ^{1}H and ^{13}C NMR signals were accomplished by two-dimensional NMR spectroscopy (COSY, NOESY, HSQC, HMBC). NMR spectra were processed using MestReNova version 11. Data are reported as follows: chemical shift; multiplicity; coupling constants; integral and assignment. Solid-State NMR spectra were recorded on a V-NMRS-400 (^{1}H 399.88 MHz and ^{13}C 105.56 MHz). The spectra were acquired using cross-polarisation with a 90-s recycle delay and 5-ms contact time for **1b′** ms and 30-s recycle delay and a 7-ms contact time for **1a**. All spectra were recorded at ambient probe temperature (approximately 25 °C) and at a spin rate of 10 kHz. Spectra are reported relative to an external sample of neat tetramethylsilane (referencing was carried out by setting the high-

frequency signal from adamantane to 38.5 ppm). Low-resolution ASAP-MS were performed using a Waters Xevo QTOF equipped with an Atmospheric Solids Analysis Probe (ASAP). High-resolution electrospray (HR-ESI) and ASAP (HR-ASAP) mass spectra were measured using a Waters LCT Premier XE high resolution, accurate mass UPLC ES MS (also with ASAP ion source). Melting points were recorded using a Gallenkamp (Sanyo) apparatus and are uncorrected. The X-ray single-crystal diffraction data for 1-(4-fluorophenyl)tricyclo[3.3.1.$0^{2,8}$]nona-3,6-dien-9-one, **1a**, **1c**, **1d**, and **1e′** were collected at 120.0(2) K using λMoKα radiation (λ = 0.71073 Å) on a Bruker D8Venture (Photon100 CMOS detector, IμS-microsource, focusing mirrors) diffractometer and for compound **1b′** on an Agilent XCalibur (Sapphire-3 CCD detector, fine-focus sealed tube, graphite monochromator) diffractometer, both equipped with a Cryostream (Oxford Cryosystems) open-flow nitrogen cryostats. Multi-temperature measurements for compounds **1a** and **1b′** were performed on the latter instrument. The heating rate was 120°/h in both cases. All structures were solved by direct method and refined by full-matrix least squares on F^2 for all data using Olex2[1] and SHELXT[2] software. All non-disordered non-hydrogen atoms were refined anisotropically, hydrogen atoms were located in the difference Fourier maps and refined isotropically. The hydrogen atoms in high-temperature structures **1a** and **1b′** were placed into calculated positions and refined in riding mode. Crystallographic data for the structure have been deposited with the Cambridge Crystallographic Data Centre as supplementary publication CCDC-1857573–1857583, 1857874.

2. Synthetic Procedures

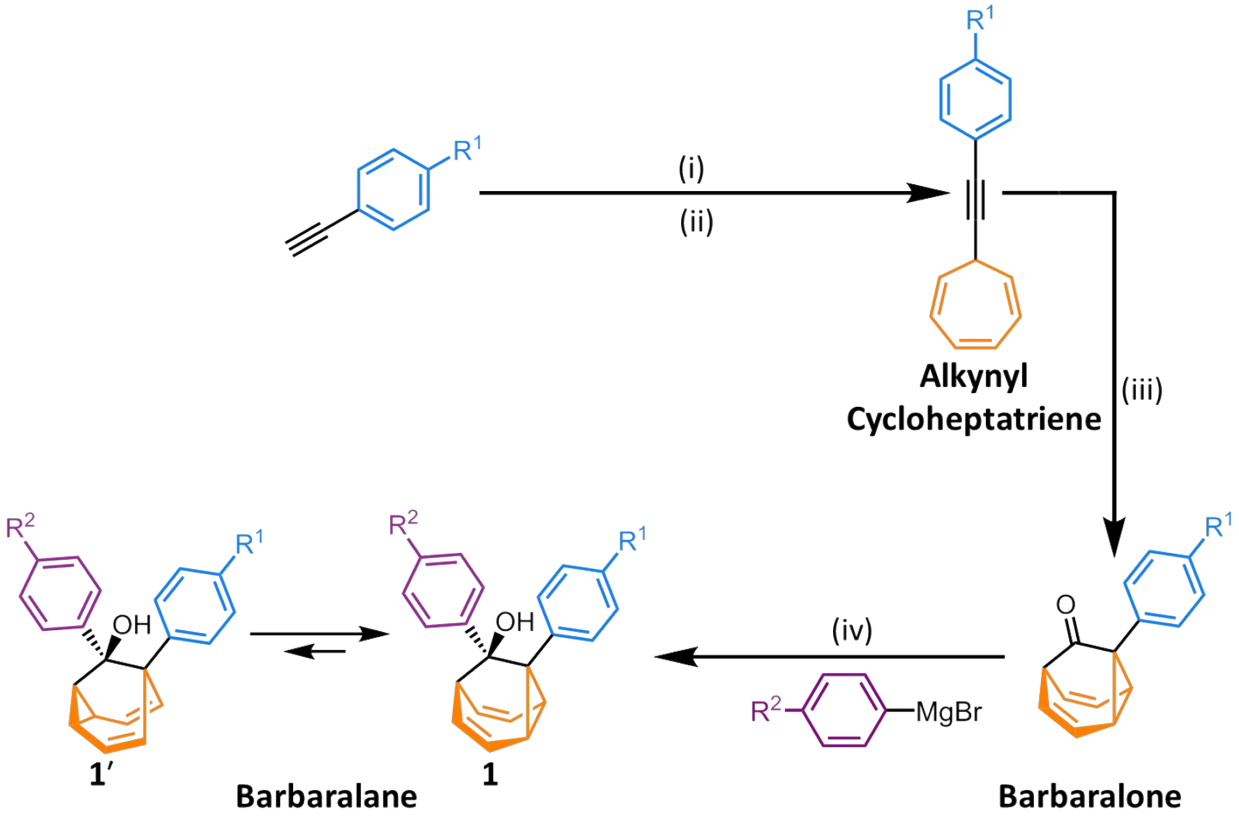

Scheme S1. General synthesis of substituted **Alkynyl Cycloheptatrienes**, **Barbaralones** and **Barbaralanes** according to modified literature[3,4] procedures. Reagents and Conditions: (i) *n*-BuLi / THF / -78 °C / 40 min, (ii) Tropylium Tetrafluoroborate / rt / 16 h, (iii) IPr Au(MeCN)BF_4 (5 mol%) / Ph_2SO / CH_2Cl_2 / rt / 16 h, (iv) either (a) THF / 0 °C to rt / 16 h or (b) Diglyme / Bu_4NI / THF / 0 °C to rt / 16 h.

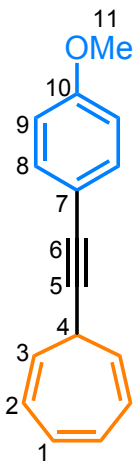

7-[2-(4-Anisyl)ethynyl]cyclohepta-1,3,5-triene: 4-Ethynylanisole (330 mg, 2.5 mmol) was placed into an oven-dried round-bottomed flask fitted with a septum under a N_2 atmosphere. Anhydrous THF (15 mL) was added and the resulting solution was cooled to –78 °C before adding *n*-BuLi (1.0 mL, 2.56 mmol, 2.5 M in hexanes) and stirring for 40 min at this temperature. Tropylium tetrafluoroborate (455 mg, 2.5 mmol) was added, and the mixture was allowed to reach rt and stirred for 16 h. The reaction was quenched with a saturated aqueous solution of NH_4Cl (30 mL), then extracted with EtOAc (3 × 20 mL). The combined organic extracts were dried over $MgSO_4$,

filtered and the solvent removed under reduced pressure. The crude residue was purified by column chromatography (Teledyne Isco CombiFlash Rf+ system, 24 g SiO_2, hexanes−EtOAc, gradient elution) to yield the title compound as a pale yellow solid (470 mg, 2.11 mmol, 85%). **M.P.** 70 – 72 °C (lit.[3] 69 – 71 °C). **^{1}H NMR** (400 MHz, $CDCl_3$) δ 7.40 (d, *J* = 8.7 Hz, 2H, H_8), 6.84 (d, *J* = 8.7 Hz, 2H, H_9), 6.78 – 6.53 (m, 2H, H_1), 6.28 – 6.09 (m, 2H, H_2), 5.51 – 5.31 (m, 2H, H_3), 3.81 (s, 3H, H_{11}), 2.69 (tt, *J* = 5.6, 1.5 Hz, 1H, H_4). **^{13}C NMR** (151 MHz, $CDCl_3$) δ 159.5 (C_{10}), 133.2 (C_8), 131.2 (C_1), 124.8 (C_2), 123.6 (C_3), 115.7 (C_7), 114.0 (C_9), 89.7 (C_5), 80.5 (C_6), 55.4 (C_{11}), 32.4 (C_4). **HR-ASAP-MS** *m/z* = 223.1123 $[M+H]^+$ (calculated for $C_{16}H_{15}O^+$ = 223.1117).

Spectroscopic data were consistent with those published previously.[3,4]

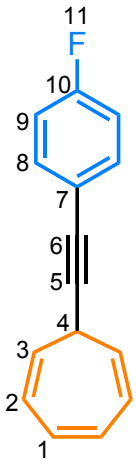

7-[2-(4-Fluorophenyl)ethynyl]cyclohepta-1,3,5-triene: 1-Ethynyl-4-fluorobenzene (600 mg, 5.0 mmol) was placed into an oven-dried round-bottomed flask fitted with a septum under a N_2 atmosphere. Anhydrous THF (15 mL) was added and the resulting solution was cooled to –78 °C before adding *n*-BuLi (1.0 mL, 2.56 mmol, 2.5 M in hexanes) and stirring for 40 min at this temperature. Tropylium tetrafluoroborate (910 mg, 5.0 mmol) was added, and the mixture was allowed to reach rt and stirred for 16 h. The reaction was quenched with a saturated aqueous solution of NH_4Cl (30 mL), then extracted with EtOAc (3 × 20 mL). The combined organic extracts were dried over $MgSO_4$, filtered and the solvent removed under reduced pressure. The crude residue was purified by column chromatography (Teledyne Isco CombiFlash Rf+ system, 24 g SiO_2, hexanes−EtOAc, gradient elution) to yield the title compound as a yellow oil (852 mg, 3.88 mmol, 81%). **^{1}H NMR**

(400 MHz, $CDCl_3$) δ 7.53 – 7.34 (m, 2H, H_8), 7.08 – 6.93 (m, 2H, H_9), 6.77 – 6.63 (m, 2H, H_1), 6.29 – 6.18 (m, 2H, H_2), 5.42 (dd, J = 9.1, 5.5 Hz, 2H, H_3), 2.71 (t, J = 5.5, 1.5 Hz, 1H, H_4). **^{13}C NMR** (151 MHz, $CDCl_3$) δ 162.4 (d, J_{CF} = 248.8 Hz, C_{10}), 133.7 (d, J_{CF} = 8.3 Hz, C_8), 132.0 (C_1), 125.0 (C_2), 123.0 (C_3), 120.0 (C_7), 115.6 (d, J_{CF} = 22.0 Hz, C_9), 90.8 (C_5), 79.7 (C_6), 32.3 (C_4). **^{19}F NMR** (376 MHz, $CDCl_3$) δ -114.9 (m, F_{11}). **HR-ASAP-MS** *m/z* = 209.0768 $[M-H]^+$ (calculated for $C_{15}H_{10}F^+$ = 209.0761).

Spectroscopic data were consistent with those published previously.[3,4]

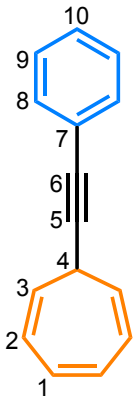

7-[2-Phenylethynyl)cyclohepta-1,3,5-triene: Phenylacetylene (255 mg, 2.5 mmol) was placed into an oven-dried round-bottomed flask fitted with a septum under a N_2 atmosphere. Anhydrous THF (15 mL) was added and the resulting solution was cooled to –78 °C before adding *n*-BuLi (1.0 mL, 2.56 mmol, 2.5 M in hexanes) and stirring for 40 min at this temperature. Tropylium tetrafluoroborate (455 mg, 2.5 mmol) was added, and the mixture was allowed to reach rt and stirred for 16 h. The reaction was quenched with a saturated aqueous solution of NH_4Cl (30 mL), then extracted with EtOAc (3 × 20 mL). The combined organic extracts were dried over $MgSO_4$, filtered and the solvent removed under reduced pressure. The crude residue was purified by column chromatography (Teledyne Isco CombiFlash Rf+ system, 24 g SiO_2, hexanes−EtOAc, gradient elution) to yield the title compound as a yellow oil (281 mg, 1.46 mmol, 58%). **^{1}H NMR** (700 MHz, $CDCl_3$) δ 7.50 – 7.47 (m, 2H, H_8), 7.34 – 7.321 (m, 3H, H_9 and H_{10}), 6.73 – 6.68 (m, 2H, H_1), 6.26 – 6.21 (m, 2H, H_2), 5.45 (dd, J = 8.7, 5.5 Hz, 2H, H_3), 2.73 (tt, J = 5.6, 1.5 Hz, 1H, H_4). **^{13}C NMR** (176 MHz, $CDCl_3$) 131.9 (C_8), 131.2 (C_1), 128.4 (C_9), 128.0 (C_{10}), 124.9 (C_2), 123.6 (C_7), 123.3 (C_3), 91.2 (C_5), 80.7 (C_6), 32.4 (C_4). **HR-ASAP-MS** *m/z* = 191.0857 $[M-H]^+$ (calculated for $C_{15}H_{11}^+$ = 191.0855).

Spectroscopic data were consistent with those published previously.[3,4]

In room temperature solutions, each of the barbaralones[5] and barbaralanes below exist as mixtures of two rapidly interconverting valence isomers. Based on our experimental observations, the structures bearing an aryl group at position 1 are the major species present in solution for all of the compounds investigated. The NMR spectroscopic assignments below, which have been made with the aid of two-dimensional NMR techniques, are labelled according to numbering of the major species. However, the species are in fast exchange on account of rapid strain-assisted Cope rearrangement. The chemical shifts of each nucleus are representative of the time-averaged chemical environment they experience as part of the two isomers.

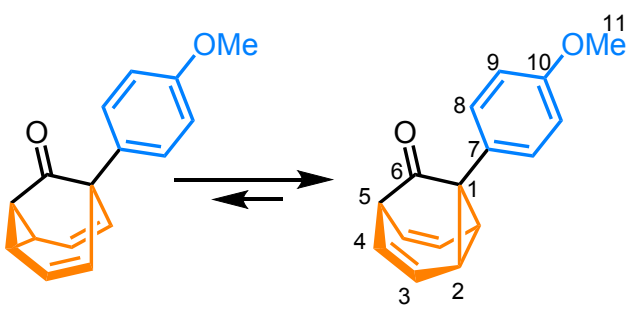

1-(4-Anisyl)tricyclo[3.3.1.0^{2,8}]nona-3,6-dien-9-one: 7-[2-(4-Anisyl)ethynyl]cyclohepta-1,3,5-triene (1.0 g, 4.5 mmol) and diphenyl sulfoxide (1.8 g, 9.0 mmol) were charged in a flask and dissolved in anhydrous CH_2Cl_2 (15 mL) at rt, with no particular precautions to exclude air. (Acetonitrile)[1,3-bis(2,6-diisopropylphenyl)imidazol-2-ylidene]gold(I) tetrafluoroborate (0.16 g, 0.23 mmol, 5 mol%) was added in one portion at the same temperature and the reaction mixture was stirred for 16 h. The reaction was quenched with Et_3N (10 drops) and the solvent was removed under reduced pressure. The crude residue was purified by column chromatography (Teledyne Isco CombiFlash Rf+ system, 24 g SiO_2, hexanes−EtOAc, gradient elution) to yield the title compound as a cream-coloured solid (0.81 g, 3.39 mmol, 75%). **M.P.** 78 – 80 °C (lit.[4] 79 – 81 °C). **^{1}H NMR** (600 MHz, $CDCl_3$) δ 7.16 (d, J = 8.8 Hz, 2H, H_8), 6.90 (d, J = 8.7 Hz, 2H, H_9), 5.93 – 5.89 (m, 2H, H_4), 5.88 –

5.84 (m, 2H, H_3), 3.80 (s, 3H, H_{11}), 3.34 – 3.17 (m, 2H, H_5), 3.10 – 2.98 (m, 2H, H_2). **^{13}C NMR** (151 MHz, $CDCl_3$) δ 208.5 (C_6), 159.2 (C_{10}), 130.8 (C_8), 128.9 (C_7), 125.0 (C_4), 121.5 (C_3), 114.2 (C_9), 55.4 (C_{11}), 49.1 (C_5), 42.2 (C_2), 39.1 (C_1). **HR-ASAP-MS** *m/z* = 239.1075 $[M+H]^+$ (calculated for $C_{16}H_{15}O_2^+$ = 239.1067).

Spectroscopic data were consistent with those published previously.[4]

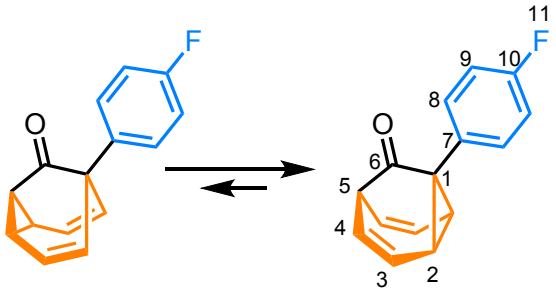

1-(4-Fluorophenyl)tricyclo[3.3.1.0^{2,8}]nona-3,6-dien-9-one: 7-[2-(4-Fluorophenyl)ethynyl]cyclohepta-1,3,5-triene (374 mg, 1.78 mmol) and diphenyl sulfoxide (720 mg, 3.56 mmol) were charged in a flask and dissolved in anhydrous CH_2Cl_2 (15 mL) at rt, with no particular precautions to exclude air. (Acetonitrile)[1,3-bis(2,6-diisopropylphenyl)-imidazol-2-ylidene]gold(I) tetrafluoroborate (63.5 mg, 0.09 mmol, 5 mol%) was added in one portion at the same temperature and the reaction mixture was stirred for 16 h. The reaction was quenched with Et_3N (4 drops) and the solvent was removed under reduced pressure. The crude residue was purified by column chromatography (Teledyne Isco CombiFlash Rf+ system, 24 g SiO_2, hexanes−EtOAc, gradient elution) to yield the title compound as a pale yellow crystalline solid (262 mg, 1.24 mmol, 65%). **M.P.** 111 – 113 °C (lit.[4] 112 – 115 °C). **^{1}H NMR** (600 MHz, $CDCl_3$) δ 7.24 – 7.19 (m, 2H, H_8), 7.04 (dd, J = 8.7, J_{HF} = 8.7 Hz, 2H, H_9), 5.96 – 5.88 (m, 2H, H_4), 5.88 – 5.84 (m, 2H, H_3), 3.23 (tt, J = 6.3, 1.2 Hz, 1H, H_5), 3.10 – 3.05 (m, 2H, H_2). **^{13}C NMR** (151 MHz, $CDCl_3$) δ 207.8 (C_6), 162.2 (d, J_{CF} = 246.3 Hz, C_{10}), 132.7 – 132.4 (m, C_7), 132.10 (d, J_{CF} = 8.2 Hz, C_8), 124.4 (C_4), 121.2 (C_3), 115.4 (d, J_{CF} = 21.5 Hz, C_9), 48.7 (C_5), 42.4 (C_2), 39.0 (C_1). **^{19}F NMR** (376 MHz, $CDCl_3$) δ -117.7 (tt, J_{FH} = 8.7, 5.3 Hz, F_{11}). **HR-ASAP-MS** *m/z* = 227.0876 $[M+H]^+$ (calculated for $C_{15}H_{12}OF^+$ = 227.0867).

Spectroscopic data were consistent with those published previously.[4]

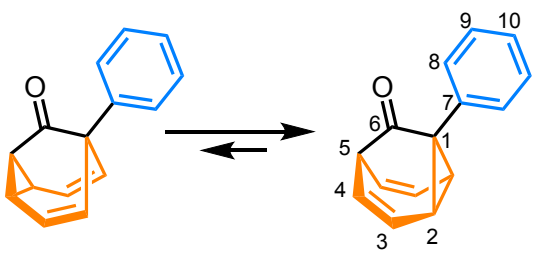

1-Phenyltricyclo[3.3.1.0.^{2,8}]nona-3,6-dien-9-one: 7-[2-Phenylethynyl)cyclohepta-1,3,5-triene (475 mg, 2.47 mmol) and diphenyl sulfoxide (1.0 g, 4.94 mmol) were charged in a flask and dissolved in anhydrous CH_2Cl_2 (15 mL) at rt, with no particular precautions to exclude air. (Acetonitrile)[1,3-bis(2,6-diisopropylphenyl)imidazol-2-ylidene]gold(I) tetrafluoroborate (88 mg, 0.12 mmol, 5 mol%) was added in one portion at the same temperature and the reaction mixture was stirred for 16 h. The reaction was quenched with Et_3N (5 drops) and the solvent was removed under reduced pressure. The crude residue was purified by column chromatography (Teledyne Isco CombiFlash Rf+ system, 24 g SiO_2, hexanes−EtOAc, gradient elution) to yield the title compound as a cream-coloured solid (297 mg, 1.43 mmol, 58%). **M.P.** 104 – 105 °C (lit.[4] 104 – 105 °C). **^{1}H NMR** (700 MHz, $CDCl_3$) δ 7.35 (dd, J = 8.2, 6.9 Hz, 2H, H_9), 7.31 – 7.27 (m, 1H, H_{10}), 7.24 (dd, J = 8.1, 1.4 Hz, 2H, H_8), 5.94 – 5.90 (m, 2H, H_4), 5.89 – 5.83 (m, 2H, H_3), 3.30 – 3.17 (m, 1H, H_5), 3.15 – 2.96 (m, 2H, H_2). **^{13}C NMR** (176 MHz, $CDCl_3$) δ 208.2 (C_6), 136.9 (C_7), 129.7 (C_8), 128.7 (C_9), 127.9 (C_{10}), 125.0 (C_4), 121.5 (C_3), 49.2 (C_5), 42.0 (C_2), 39.7 (C_1). **HR-ASAP-MS** *m/z* = 209.0952 $[M+H]^+$ (calculated for $C_{15}H_{13}O^+$ = 209.0961).

Spectroscopic data were consistent with those published previously.[4]

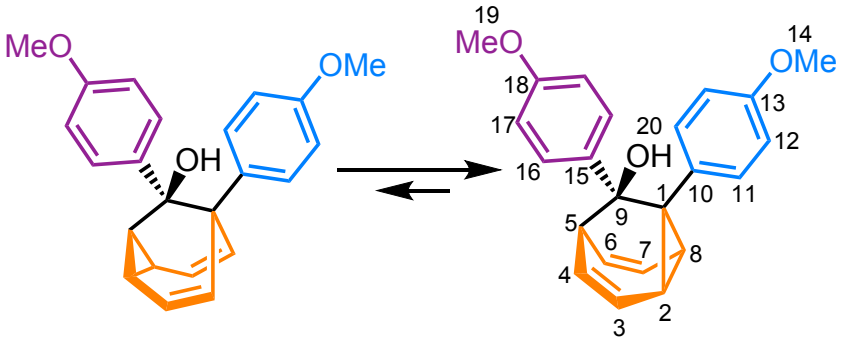

(±)1,9-Bis(4-anisyl)tricyclo-[3.3.1.0^{2,8}]nona-3,6-dien-9-ol (1a): Magnesium turnings (115 mg, 4.78 mmol) and I_2 (58.9 mg, 0.23 mmol, 5 mol%) were placed in an oven-dried two-necked round-bottomed flask fitted with a condenser and a septum under a N_2 atmosphere. The flask was gently heated with a heat gun until the I_2 started to sublime. The flask was cooled down to rt. A quarter of a solution of 4-bromoanisole (980 mg, 4.64 mmol) in anhydrous THF (10 mL) was added to the reaction mixture, which was heated until it reached reflux. Upon gentle reflux, the remaining solution of 4-bromoanisole in anhydrous THF was added dropwise over 30 min. The reaction mixture was heated at reflux for 30 min before cooling to rt. In an oven-dried round-bottomed flask, under an atmosphere of N_2, was added Bu_4NI (36.0 mg, 0.1 mmol), anhydrous diglyme (0.21 mL, 201 mg, 1.5 mmol), and the Grignard solution (prepared above).[6] Anhydrous THF (15 mL) was added and the solution was cooled to 0 °C for 30 min with stirring. 1-(4-Anisyl)tricyclo[3.3.1.0^{2,8}]nona-3,6-dien-9-one (225 mg, 0.94 mg) was added dropwise over 30 min at the same temperature. The reaction mixture was stirred for 16 h, where the temperature was raised from 0 °C to rt, following removal of the ice bath. The reaction was quenched with a saturated aqueous solution of NH_4Cl (10 mL), then extracted with EtOAc (3 × 20 mL). The combined organic extracts were dried over $MgSO_4$, filtered and the solvent removed under reduced pressure. The crude residue was purified by column chromatography (Teledyne Isco CombiFlash Rf+ system, 24 g Al_2O_3, hexanes−CH_2Cl_2, gradient elution) to yield **1a** as a white solid (158 mg, 0.46 mmol, 43%). **M.P.** 128 – 130 °C. **^{1}H NMR** (700 MHz, $CDCl_3$) δ 7.20 (d, J = 9.0 Hz, 2H, H_{16}), 7.18 (d, J = 9.5 Hz, 2H, H_{11}), 6.70 (d, J = 8.7 Hz, 2H, H_{12}), 6.68 (d,

J = 8.9 Hz, 2H, H_{17}), 6.07 – 6.00 (m, 1H, H_3), 5.84 – 5.79 (m, 1H, H_7), 5.59 – 5.53 (m, 1H, H_4), 5.50 – 5.46 (m, 1H, H_6), 3.73 (s, 6H, H_{19} and H_{14}), 3.50 – 3.45 (m, 1H, H_8), 3.17 – 3.10 (m, 1H, H_2), 2.80 (t, J = 6.8 Hz, 1H, H_5), 2.14 (s, 1H, H_{20}). **^{13}C NMR** (176 MHz, $CDCl_3$) δ 158.3 (C_{13}), 158.2 (C_{18}), 135.0 (C_{15}), 132.6 (C_{10}), 131.4 (C_{11}), 128.5 (C_{16}), 123.9 (C_3), 121.8 (C_7), 113.1 (C_{12}), 112.6 (C_{17}), 111.9 (C_6), 110.6 (C_4), 69.7 (C_9), 55.3 (C_{14} or C_{19}), 55.2 (C_{14} or C_{19}), 51.0 (C_8), 49.6 (C_2), 45.2 (C_5), 44.1 (C_1). **HR-ASAP-MS** *m/z* = 346.1568 $[M]^+$ (calculated for $C_{23}H_{22}O_3^+$ = 346.1564).

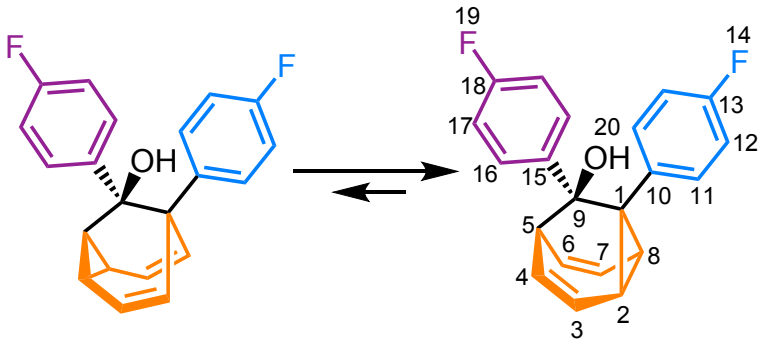

(±)1,9-Bis(4-fluorophenyl)tricyclo-[3.3.1.0^{2,8}]nona-3,6-dien-9-ol (1b): Magnesium turnings (118 mg, 4.9 mmol) and I_2 (62 mg, 0.24 mmol, 5 mol%) were placed in an oven-dried two-necked round-bottomed flask fitted with a condenser and a septum under a N_2 atmosphere. The flask was gently heated with a heat gun until the I_2 started to sublime. The flask was cooled down to rt. A quarter of a solution of 1-bromo-4-fluorobenzene (0.52 mL, 823 mg, 4.7 mmol) in anhydrous THF (10 mL) was added to the reaction mixture, which was heated until it reached reflux. Upon gentle reflux, the remaining solution of 1-bromo-4-fluorobenzene in anhydrous THF was added dropwise over 30 min. The reaction mixture was heated at reflux for 30 min before cooling to rt. 1-(4-Fluorophenyl)tricyclo[3.3.1.0^{2,8}]nona-3,6-dien-9-one (162 mg, 0.72 mmol) was transferred to an oven-dried round-bottomed flask, and the flask was purged with N_2. Anhydrous THF (10 mL) was added and the solution was cooled to 0 °C. The Grignard solution (prepared above) was added dropwise over 30 min to the barbaralone. The reaction mixture was

stirred for 16 h, and the temperature was raised from 0 °C to rt, following removal of the ice bath. The reaction was quenched with a saturated aqueous solution of NH_4Cl (10 mL), then extracted with EtOAc (3 × 20 mL). The combined organic extracts were dried over $MgSO_4$, filtered and the solvent removed under reduced pressure. The crude residue was purified by column chromatography (Teledyne Isco CombiFlash Rf+ system, 24 g SiO_2, hexanes−CH_2Cl_2, gradient elution) to yield **1b** as an off-white powder (215 mg, 0.67 mmol, 93%). **M.P.** 116 – 118 °C. **^{1}H NMR (**700 MHz, $CDCl_3$) δ 7.28 (ddd, J = 8.6, 5.4, 2.7 Hz, 2H, H_{16}), 7.23 (ddd, J = 8.5, 5.4, 2.6 Hz, 2H, H_{11}), 6.90 – 6.84 (m, 4H, H_{12} and H_{17}), 6.07 (ddd, J = 8.7, 7.0, 0.8 Hz, 1H, H_3), 5.87 (dd, J = 8.6, 7.0 Hz, 1H, H_7), 5.46 (dddd, J = 8.2, 7.0, 1.3, 1.5 Hz, 1H, H_4), 5.43 (dddd, J = 8.5, 6.9, 1.5, 1.5 Hz, 1H, H_6), 3.63 (ddd, J = 6.7, 6.7, 1.5 Hz, 1H, H_8), 3.31 (ddd, J = 7.1, 7.1, 1.4 Hz, 1H, H_2), 2.84 (t, J = 6.8 Hz, 1H, H_5), 2.28 (s, 1H, H_{20}). **^{13}C NMR** (176 MHz, $CDCl_3$) δ 161.7 (d, J_{CF} = 245.5 Hz, C_{13}), 160.6 (d, J_{CF} = 245.0 Hz, C_{18}), 138.2 (d, J_{CF} = 3.1 Hz, C_{15}), 136.0 (d, J_{CF} = 3.2 Hz, C_{10}), 131.8 (d, J_{CF} = 7.9 Hz, C_{11}), 128.9 (d, J_{CF} = 7.8 Hz, C_{16}), 123.9 (C_3), 121.7 (C_7), 114.4 (d, J_{CF} = 21.1 Hz, C_{12}), 113.9 (d, J_{CF} = 20.9 Hz, C_{17}), 108.3 (C_6), 106.7 (C_4), 69.5 (C_9), 54.3 (C_8), 53.1 (C_2), 44.7 (C_1), 44.3 (C_5). **^{19}F NMR** (376 MHz, $CDCl_3$) δ -119.3 (tt, J_{FH} = 8.6, 5.5 Hz, F_{14} or F_{19}), -120.0 (tt, J_{FH} = 8.6, 5.5 Hz, F_{14} or F_{19}). **HR-ASAP-MS** *m/z* = 322.1176 $[M]^+$ (calculated for $C_{21}H_{16}OF_2^+$ = 322.1168).

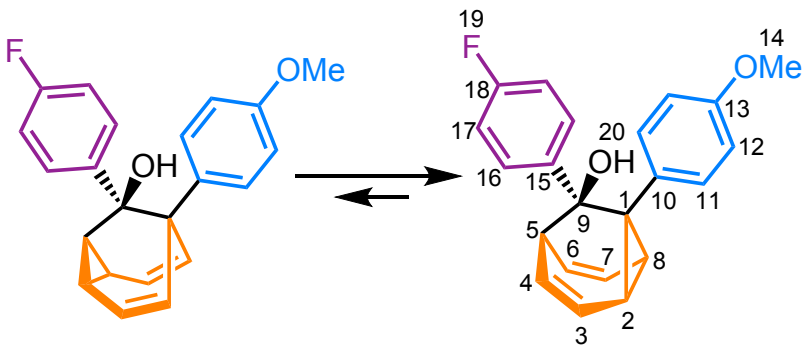

(±)9-(4-Fluorophenyl)-1-(4-anisyl)tricyclo[3.3.1.0^{2,8}]nona-3,6-dien-9-ol (1c): Magnesium turnings (57 mg, 2.38 mg) and I_2 (29.9 mg, 0.12 mmol, 5 mol%)

were placed in an oven-dried two-necked round-bottomed flask fitted with a condenser and a septum under a N_2 atmosphere. The flask was gently heated with a heat gun until the I_2 started to sublime. The flask was cooled down to rt. A quarter of a solution of 1-bromo-4-fluorobenzene (410 mg, 2.36 mmol) in anhydrous THF (10 mL) was added to the reaction mixture, which was heated until it reached reflux. Upon gentle reflux, the remaining solution of 1-bromo-4-fluorobenzene in anhydrous THF was added dropwise over 30 min. The reaction mixture was heated at reflux for 30 min before cooling to rt. 1-(4-Anisyl)tricyclo[3.3.1.$0^{2,8}$]nona-3,6-dien-9-one (94 mg, 0.40 mmol) was transferred to an oven-dried round-bottomed flask, and the flask was purged with N_2. Anhydrous THF (10 mL) was added and the solution was cooled to 0 °C. The Grignard solution (prepared above) was added dropwise over 30 min to the barbaralone. The reaction mixture was stirred for 16 h, and the temperature was raised from 0 °C to rt, following removal of the ice bath. The reaction was quenched with a saturated aqueous solution of NH_4Cl (10 mL), then extracted with EtOAc (3 × 20 mL). The combined organic extracts were dried over $MgSO_4$, filtered and the solvent removed under reduced pressure. The crude residue was purified by column chromatography (Teledyne Isco CombiFlash Rf+ system, 24 g SiO_2, hexanes−CH_2Cl_2, gradient elution including 0.5% Et_3N in the elution) to yield **1c** as a light yellow solid (73 mg, 0.23 mmol, 59%). **M.P.** 122 – 124 °C. **^{1}H NMR** (700 MHz, $CDCl_3$) δ 7.25 – 7.23 (m, 2H, H_{16}), 7.19 – 7.09 (m, 2H, H_{11}), 6.81 (d, J = 8.8 Hz, 2H, H_{17}), 6.70 (d, J = 8.8 Hz, 2H, H_{12}), 6.05 (ddd, J = 8.6, 6.9, 0.8 Hz, 1H, H_3), 5.83 (ddd, J = 8.8, 6.9, 0.6 Hz, 1H, H_7), 5.51 (ddd, J = 8.2, 6.7, 1.4 Hz, 1H, H_4), 5.45 (ddd, J = 8.4, 6.8, 1.4 Hz, 1H, H_6), 3.73 (s, 3H, H_{14}), 3.53 (dd, J = 6.7, 1.5 Hz, 1H, H_8), 3.19 (dd, J = 6.7, 1.4 Hz, 1H, H_2), 2.79 (ddd, J = 6.7, 1.4 Hz, 1H, H_5), 2.19 (s, 1H, H_{20}). **^{13}C NMR** (176 MHz, $CDCl_3$) δ 161.6 (d, J_{CF} = 244.6 Hz, C_{18}), 158.4 (C_{13}), 138.5 (d, J_{CF} = 3.2 Hz, C_{15}), 132.2 (C_{10}), 131.4 (C_{11}), 129.1 (d, J_{CF} = 7.8 Hz, C_{16}), 124.1 (C_3), 121.9 (C_7), 113.9 (d, J_{CF} = 21.0

Hz, C_{17}), 113.2 (C_{12}), 110.4 (C_6), 109.0 (C_4), 69.7 (C_9), 55.3 (C_{14}), 52.4 (C_8), 51.1 (C_2), 44.9 (C_5), 44.5 (C_1). **^{19}F NMR** (376 MHz, $CDCl_3$) δ -120.2 – 120.4 (m, F_{19}). **HR-ASAP-MS** *m/z* = 317.1330 $[M\text{-}OH]^+$ (calculated for $C_{22}H_{18}OF^+$ = 317.1336).

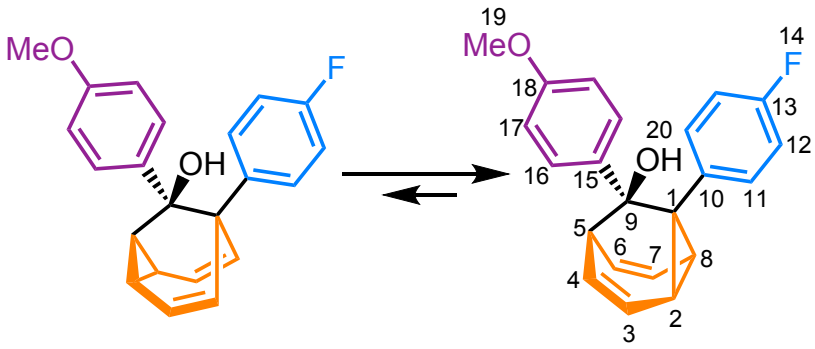

(±)9-(4-Anisyl)-1-(4-fluoro-phenyltricyclo[3.3.1.0^{2,8}]nona-3,6-dien-9-ol (1d): Magnesium turnings (120 mg, 5.30 mg) and I_2 (66.7 mg, 0.26 mmol, 5 mol%) were placed in an oven-dried two-necked round-bottomed flask fitted with a condenser and a septum under a N_2 atmosphere. The flask was gently heated with a heat gun until the I_2 started to sublime. The flask was cooled down to rt. A quarter of a solution of 4-bromoanisole (980 mg, 5.26 mmol) in anhydrous THF (10 mL) was added to the reaction mixture, which was heated until it reached reflux. Upon gentle reflux, the remaining solution of 4-bromoanisole in anhydrous THF was added dropwise over 30 min. The reaction mixture was heated at reflux for 30 min before cooling to rt. 1-(4-Fluorophenyl)tricyclo[3.3.1.0^{2,8}]nona-3,6-dien-9-one (200 mg, 0.88 mmol) was transferred to an oven-dried round-bottomed flask, and the flask was purged with N_2. Anhydrous THF (10 mL) was added and the solution was cooled to 0 °C. The Grignard solution (prepared above) was added dropwise over 30 min to the barbaralone. The reaction mixture was stirred for 16 h, and the temperature was raised from 0 °C to rt, following removal of the ice bath. The reaction was quenched with a saturated aqueous solution of NH_4Cl (10 mL), then extracted with EtOAc (3 × 20 mL). The combined organic extracts were dried over $MgSO_4$, filtered and the solvent removed

under reduced pressure. The crude residue was purified by column chromatography (Teledyne Isco CombiFlash Rf+ system, 24 g SiO_2, hexanes−CH_2Cl_2, gradient elution including 0.5% Et_3N in the elution) to yield **1d** as a colourless sticky residue (284 mg, 0.85 mmol, 96%). **^{1}H NMR** (700 MHz, $CDCl_3$) δ 7.24 – 7.18 (m, 2H, H_{11}), 7.19 – 7.10 (m, 2H, H_{16}), 6.91 – 6.78 (m, 2H, H_{12}), 6.75 – 6.57 (m, 2H, H_{17}), 6.04 (ddd, J = 8.7, 6.9, 0.8 Hz, 1H, H_3), 5.83 (ddd, J = 8.6, 6.9, 0.6 Hz, 1H, H_7), 5.54 – 5.46 (m, 1H, H_4), 5.43 (ddd, J = 8.4, 6.9, 1.5 Hz, 1H, H_6), 3.73 (s, 3H, H_{19}), 3.63 – 3.46 (m, 1H, H_8), 3.36 – 3.10 (m, 1H, H_2), 2.81 (tt, J = 6.8, 0.7 Hz, 1H, H_5), 2.15 (s, 1H, H_{20}). **^{13}C NMR** (176 MHz, $CDCl_3$) δ 161.7 (d, J_{CF} = 245.3 Hz, C_{13}), 158.2 (C_{18}), 136.4 (d, J_{CF} = 3.1 Hz, C_{10}), 134.6 (C_{15}), 131.9 (d, J_{CF} = 7.9 Hz, C_{11}), 128.4 (C_{16}), 123.9 (C_3), 121.6 (C_7), 114.4 (d, J_{CF} = 21.1 Hz, C_{12}), 112.6 (C_{17}), 109.7 (C_6), 108.2 (C_4), 69.6 (C_9), 55.2 (C_{19}), 53.2 (C_8), 51.9 (C_2), 44.8 (C_5), 44.5 (C_1). **^{19}F NMR** (376 MHz, $CDCl_3$) δ -119.5 – 119.7 (m, F_{14}). **HR-ASAP-MS** *m/z* = 317.1346 [M-OH]$^+$ (calculated for $C_{22}H_{18}FO^+$ = 317.1336).

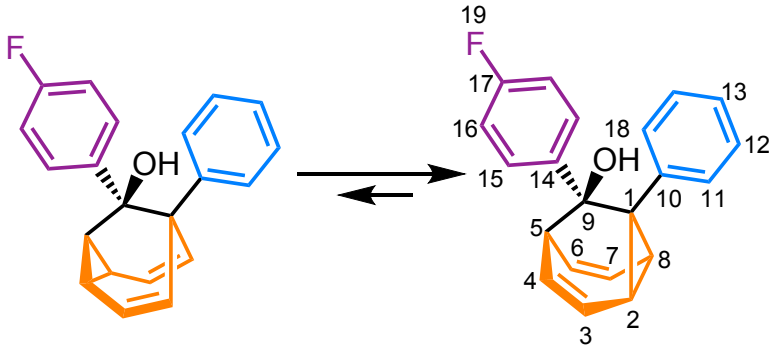

(±)9-(4-Fluorophenyl)-1-phenyl-tricyclo[3.3.1.0^{2,8}]nona-3,6-dien-9-ol (1e): Magnesium turnings (203 mg, 8.4 mmol) and I_2 (9 mg, 0.07 mmol, 5 mol%) were placed in an oven-dried two-necked round-bottomed flask fitted with a condenser and a septum under a N_2 atmosphere. The flask was gently heated with a heat gun until the I_2 started to sublime. The flask was cooled down to rt. A quarter of a solution of 1-bromo-4-fluorobenzene (1.46 g, 8.37 mmol) in anhydrous THF (10 mL) was added to the reaction mixture, which was heated until it reached reflux. Upon gentle reflux, the remaining solution of 1-bromo-4-fluorobenzene in anhydrous THF

was added dropwise over 30 min. The reaction mixture was heated at reflux for 30 min before cooling to rt. 1-Phenyltricyclo-[3.3.1.0.^{2,8}]nona-3,6-dien-9-one (293 mg, 1.4 mmol) was transferred to an oven-dried round-bottomed flask, and the flask was purged with N_2. Anhydrous THF (5 mL) was added and the solution was cooled to 0 °C. The Grignard solution (prepared above) was added dropwise over 30 min to the barbaralone. The reaction mixture was stirred for 16 h, and the temperature was raised from 0 °C to rt, following removal of the ice bath. The reaction was quenched with a saturated aqueous solution of NH_4Cl (10 mL), then extracted with EtOAc (3 × 20 mL). The combined organic extracts were dried over $MgSO_4$, filtered and the solvent removed under reduced pressure. The crude residue was purified by column chromatography (Teledyne Isco CombiFlash Rf+ system, 24 g SiO_2, hexanes−CH_2Cl_2, gradient elution including 0.5% Et_3N in the elution) to yield **1e** as a white solid (315 mg, 1.04 mmol, 74%). **M.P.** 122 – 123 °C. **^{1}H NMR** (600 MHz, $CDCl_3$) δ 7.27 – 7.22 (m, 4H, H_{11} and H_{15}), 7.19 – 7.12 (m, 3H, H_{12} and H_{13}), 6.84 – 6.77 (m, 2H, H_{16}), 6.09 – 6.03 (m, 1H, H_3), 5.88 – 5.82 (m, 1H, H_7), 5.55 – 5.49 (m, 1H, H_4), 5.48 – 5.42 (m, 1H, H_6), 3.59 (dd, J = 6.8 Hz, 1H, H_8), 3.25 (dd, J = 6.8 Hz, 1H, H_2), 2.81 (dd, J = 6.8 Hz, 1H, H_5), 2.23 (s, 1H, H_{18}). **^{13}C NMR** (151 MHz, $CDCl_3$) δ 161.7 (d, J = 244.8 Hz, C_{17}), 140.3 (C_{10}), 138.4 (d, J = 3.2 Hz, C_{14}), 130.3 (C_{11}), 129.0 (d, J = 7.8 Hz, C_{15}), 127.7 (C_{12}), 126.8 (C_{13}), 124.0 (C_3), 121.8 (C_7), 113.9 (d, J = 20.9 Hz, C_{16}), 110.3 (C_6), 108.9 (C_4), 69.8 (C_9), 52.5 (C_8), 51.3 (C_2), 44.9 (C_1), 44.9 (C_5). **^{19}F NMR** (376 MHz, $CDCl_3$) δ -120.23 (tt, J_{FH} = 8.7, 5.5 Hz, F_{19}). **HR-ESI-MS** *m/z* = 287.1246 $[M–OH]^+$ (calculated for $C_{21}H_{16}F^+$ = 287.1231).

3. ^{1}H, ^{13}C and ^{19}F NMR Spectroscopic Characterisation of Synthesised Compounds

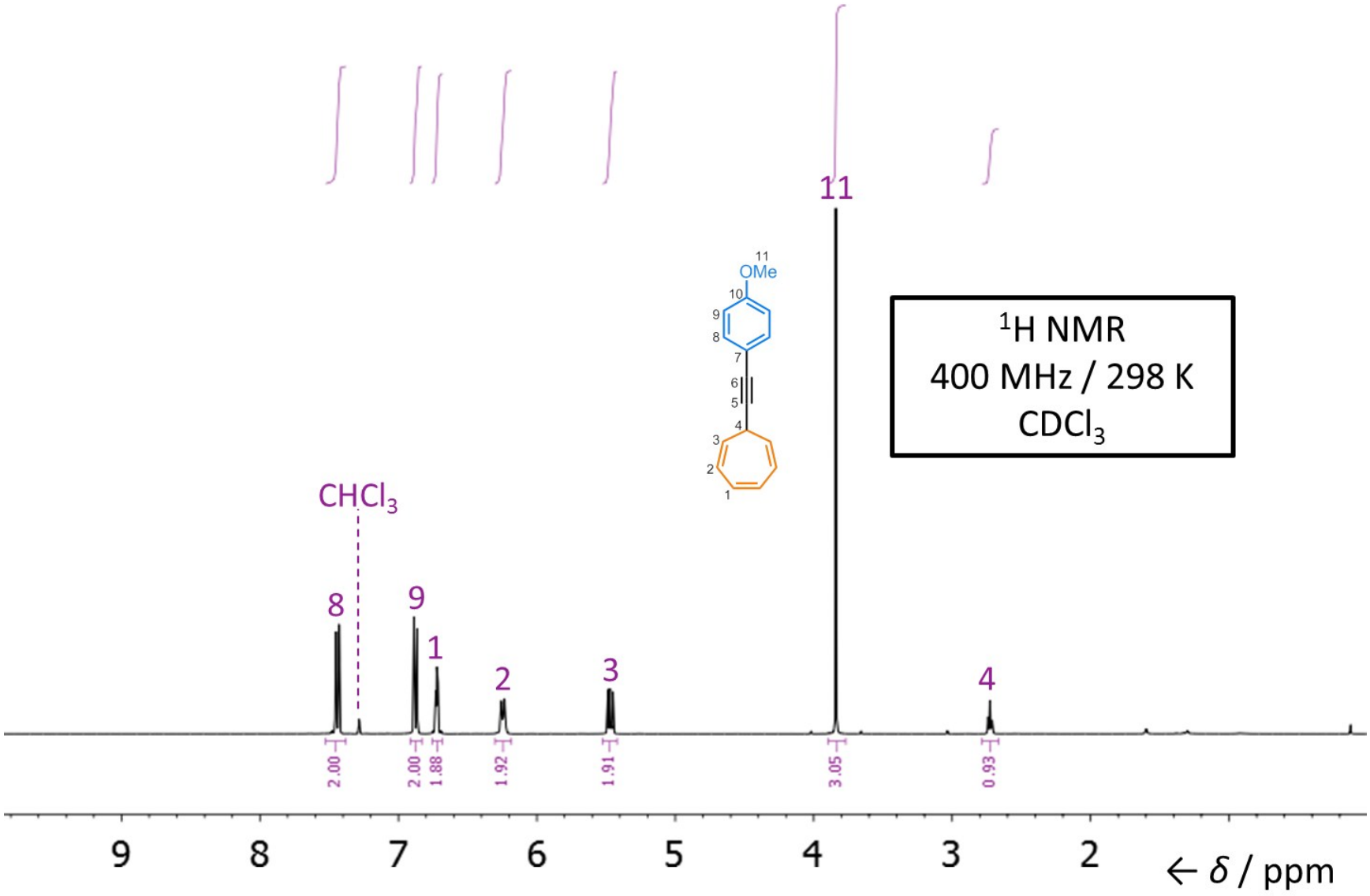

Figure S1. ^{1}H NMR Spectrum of 7-[2-(4-anisyl)ethynyl]cyclohepta-1,3,5-triene.

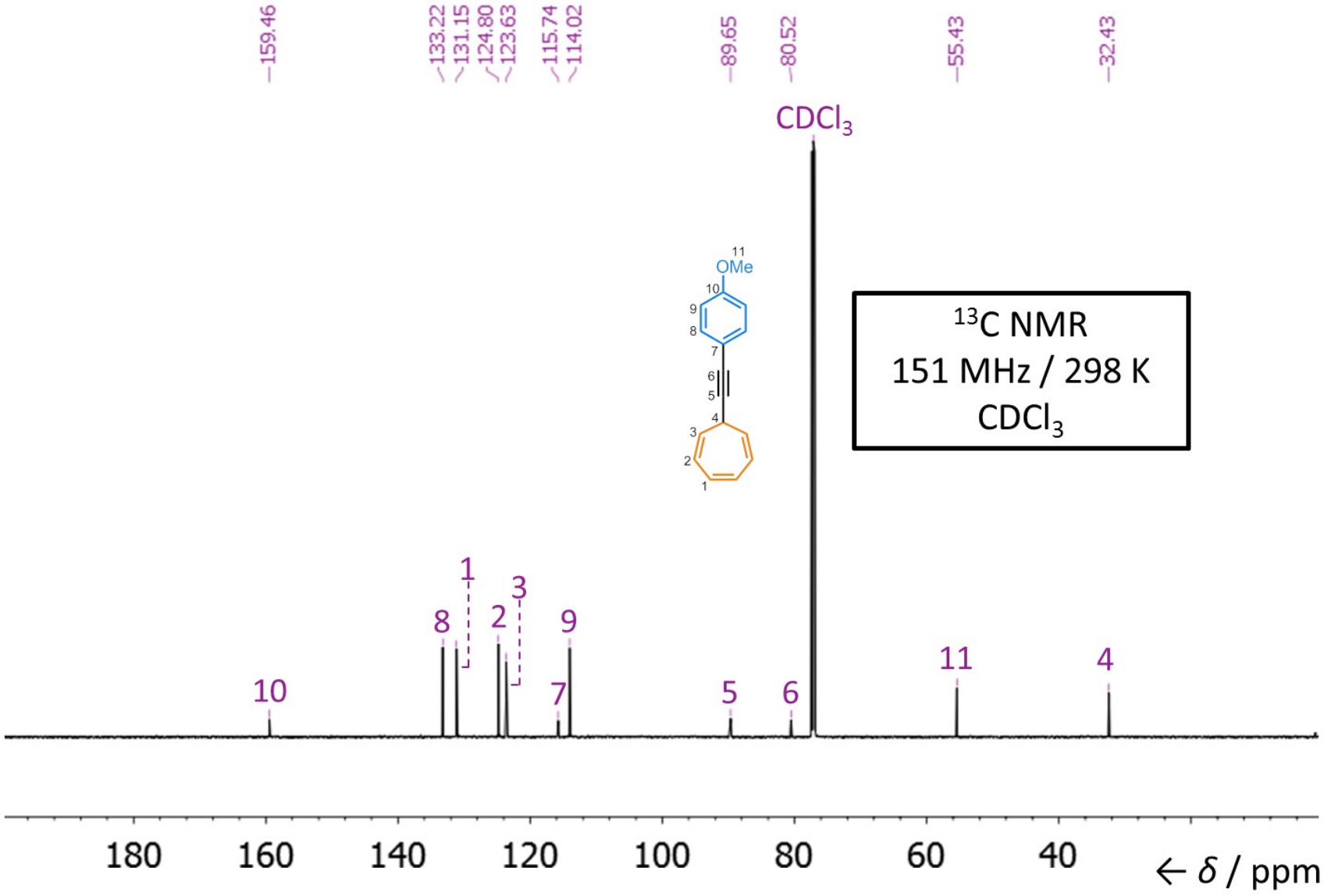

Figure S2. ^{13}C NMR Spectrum of 7-[2-(4-anisyl)ethynyl]cyclohepta-1,3,5-triene.

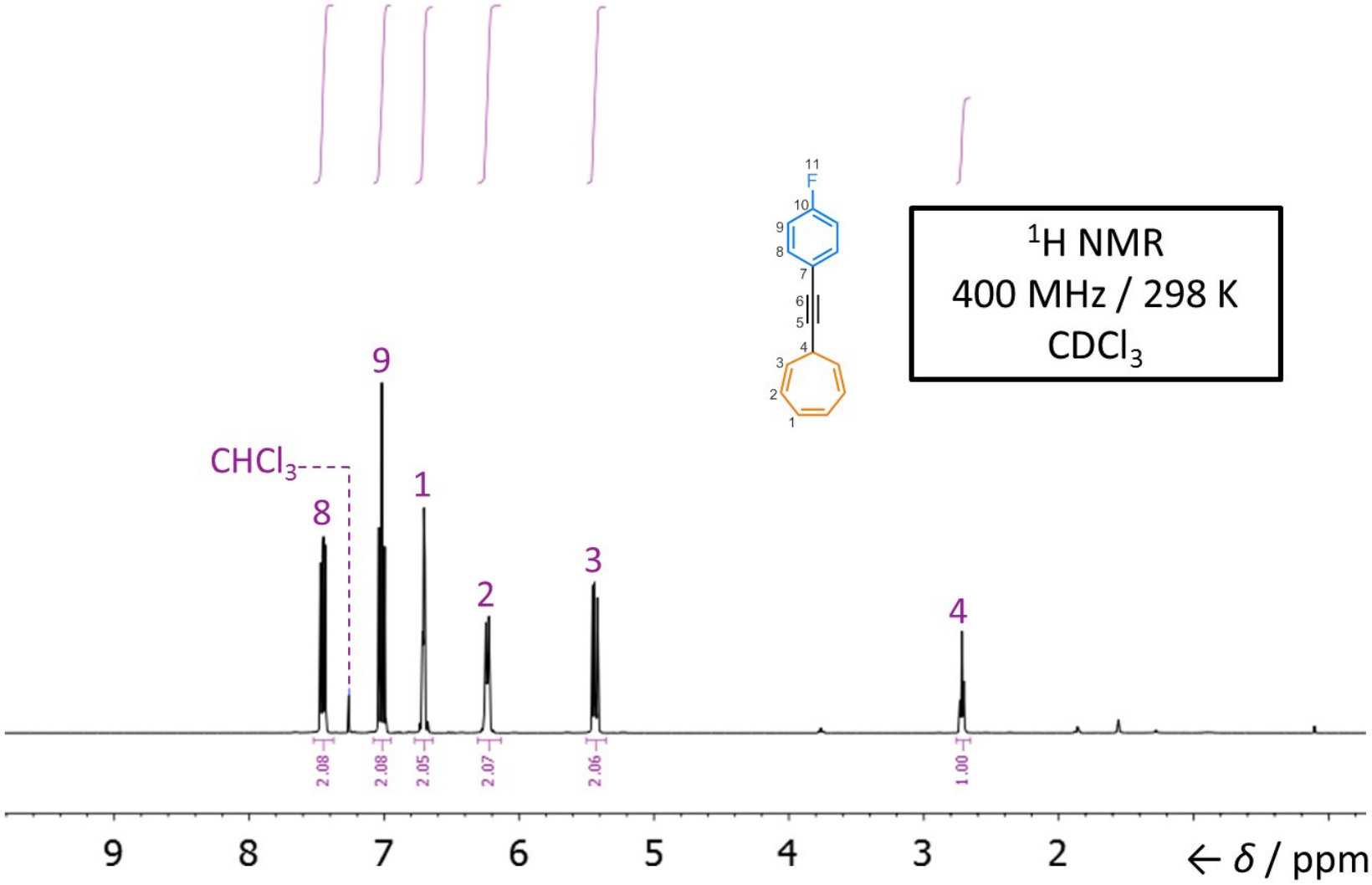

Figure S3. ^{1}H NMR Spectrum of 7-[2-(4-fluorophenyl)ethynyl]cyclohepta-1,3,5-triene.

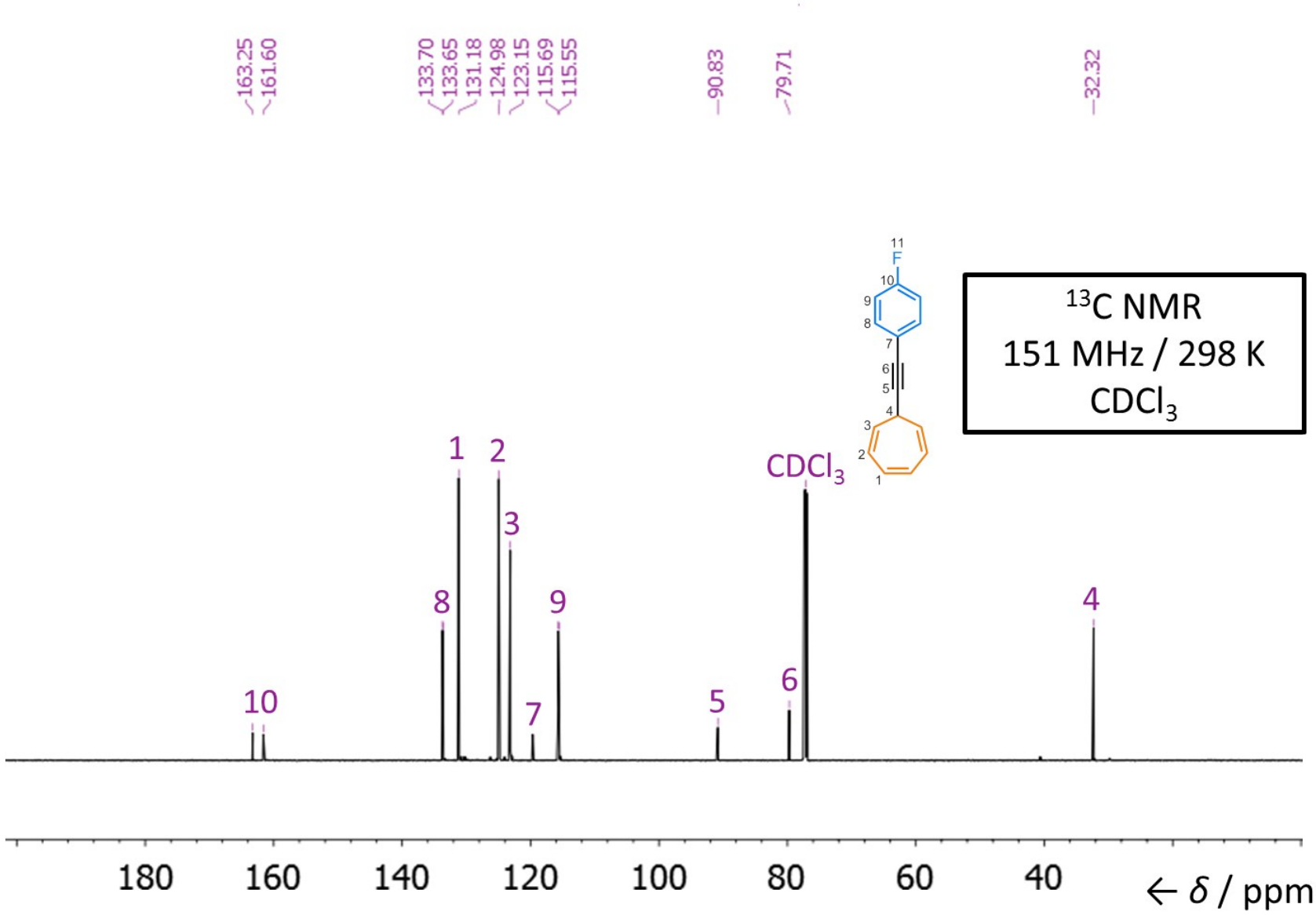

Figure S4. ^{13}C NMR Spectrum of 7-[2-(4-fluorophenyl)ethynyl]cyclohepta-1,3,5-triene.

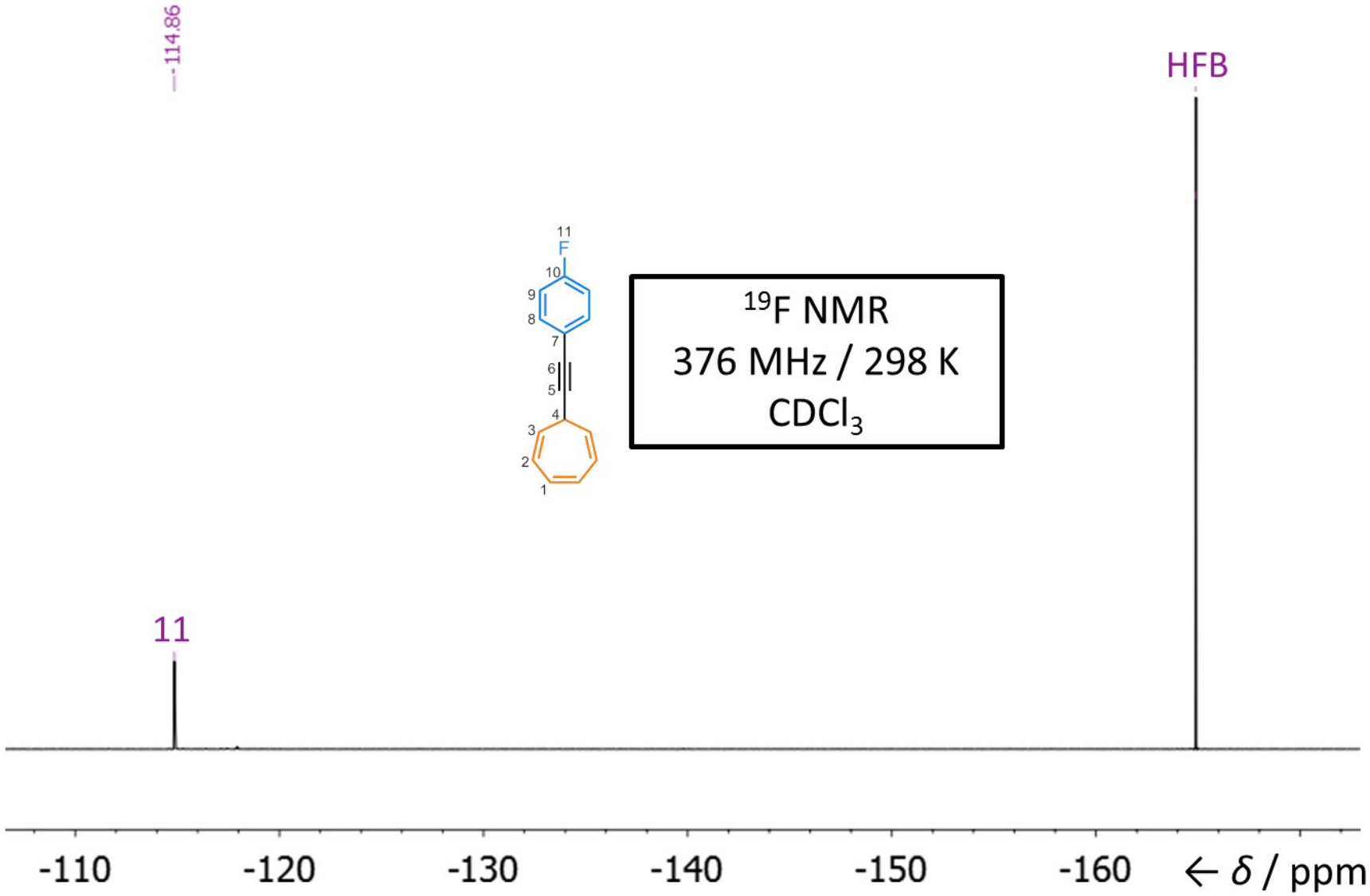

Figure S5. ^{19}F NMR Spectrum of 7-[2-(4-fluorophenyl)ethynyl]cyclohepta-1,3,5-triene.

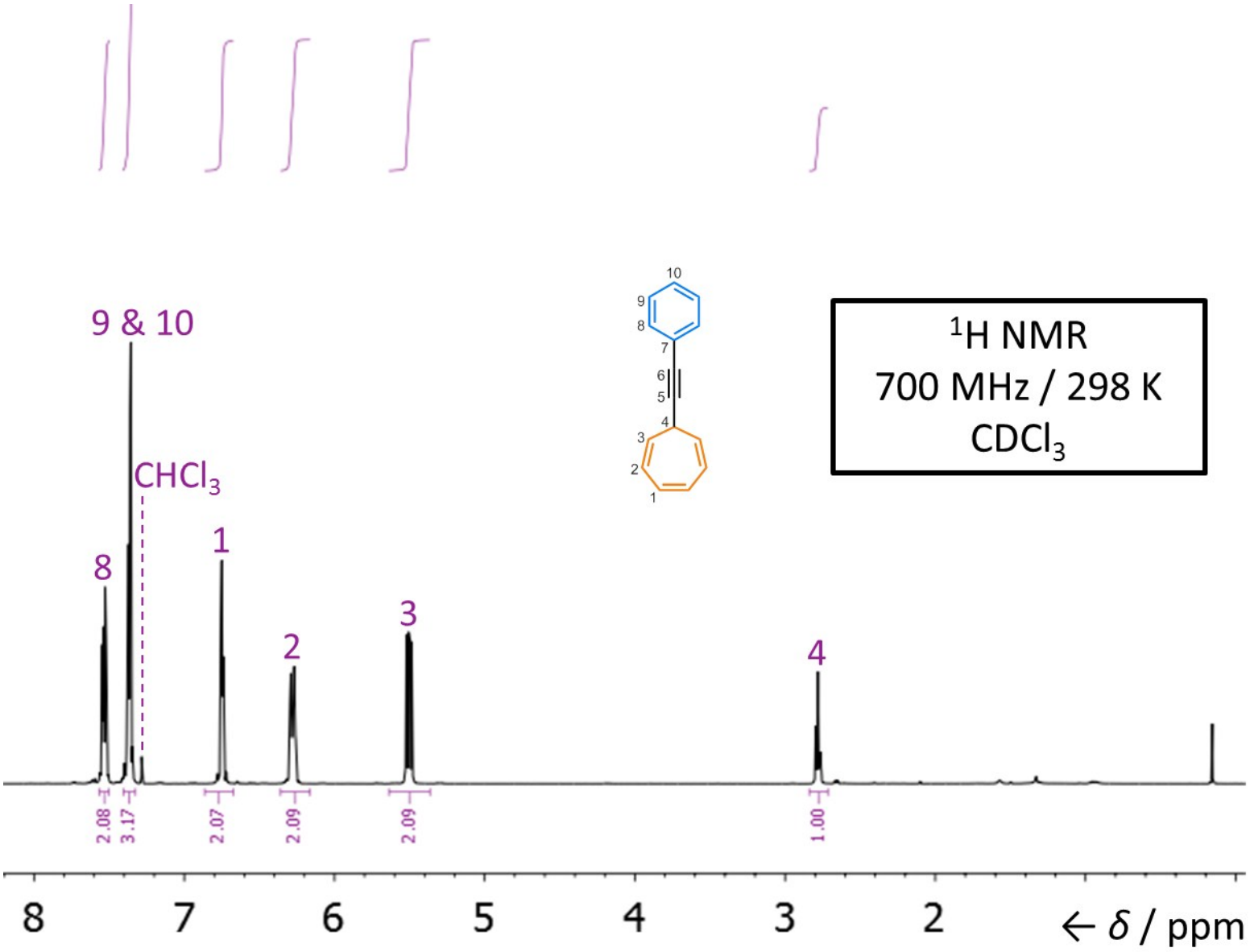

Figure S6. ^{1}H NMR Spectrum of 7-[2-phenylethynyl]cyclohepta-1,3,5-triene.

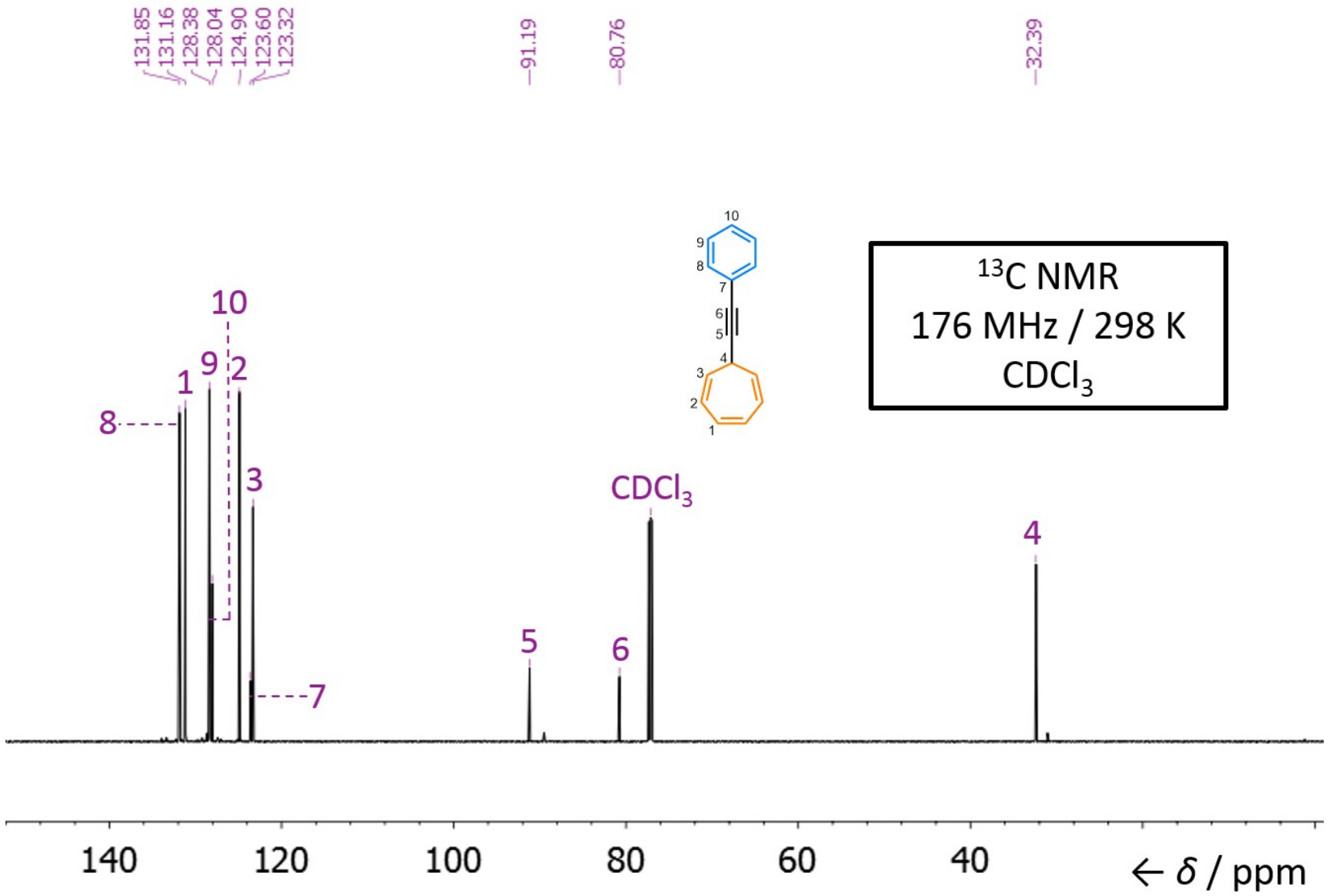

Figure S7. ^{13}C NMR Spectrum of 7-[2-phenylethynyl]cyclohepta-1,3,5-triene.

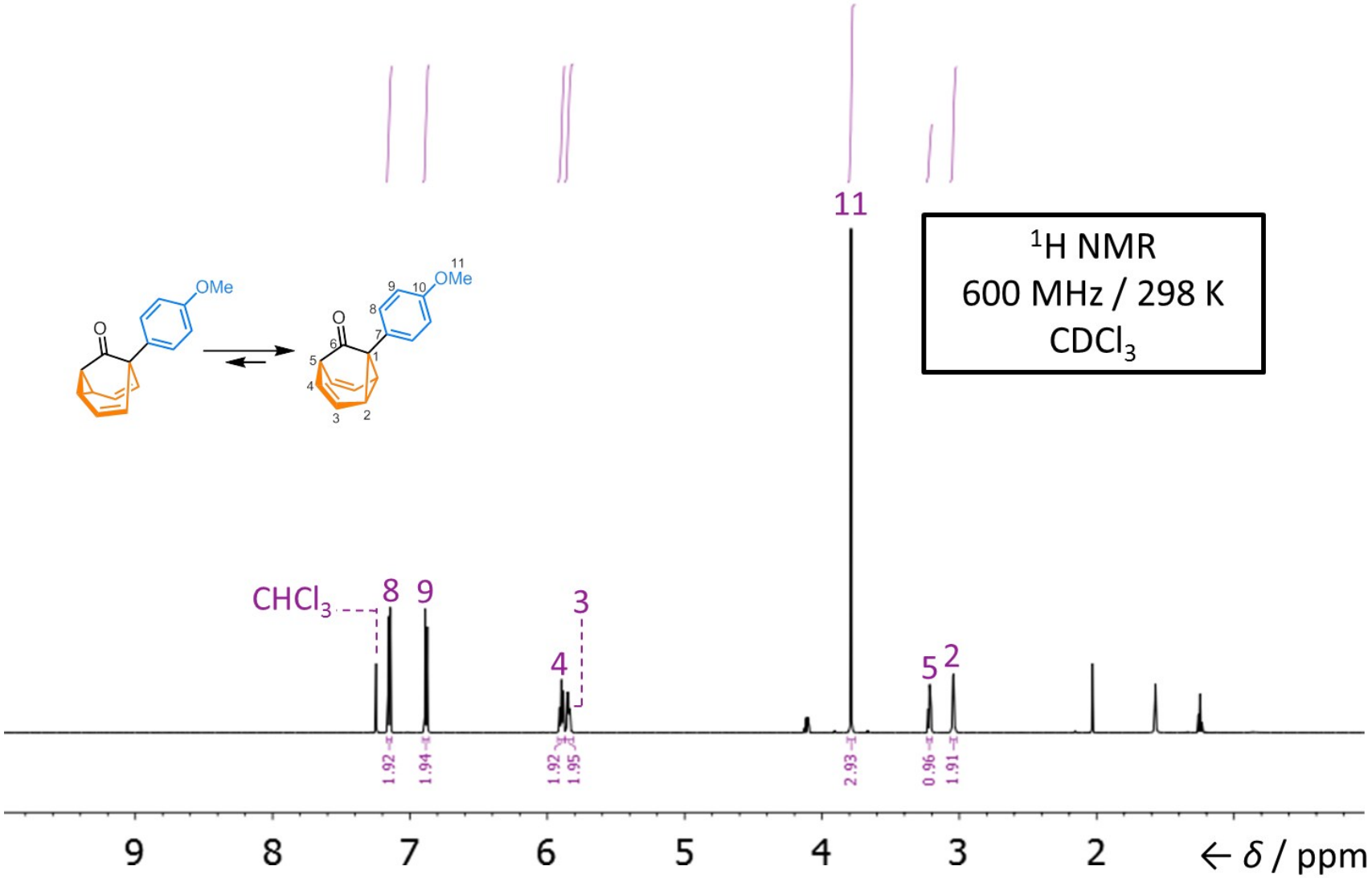

Figure S8. ^{1}H NMR Spectrum of 1-(4-anisyl)tricyclo[3.3.1.0^{2,8}]nona-3,6-dien-9-one.

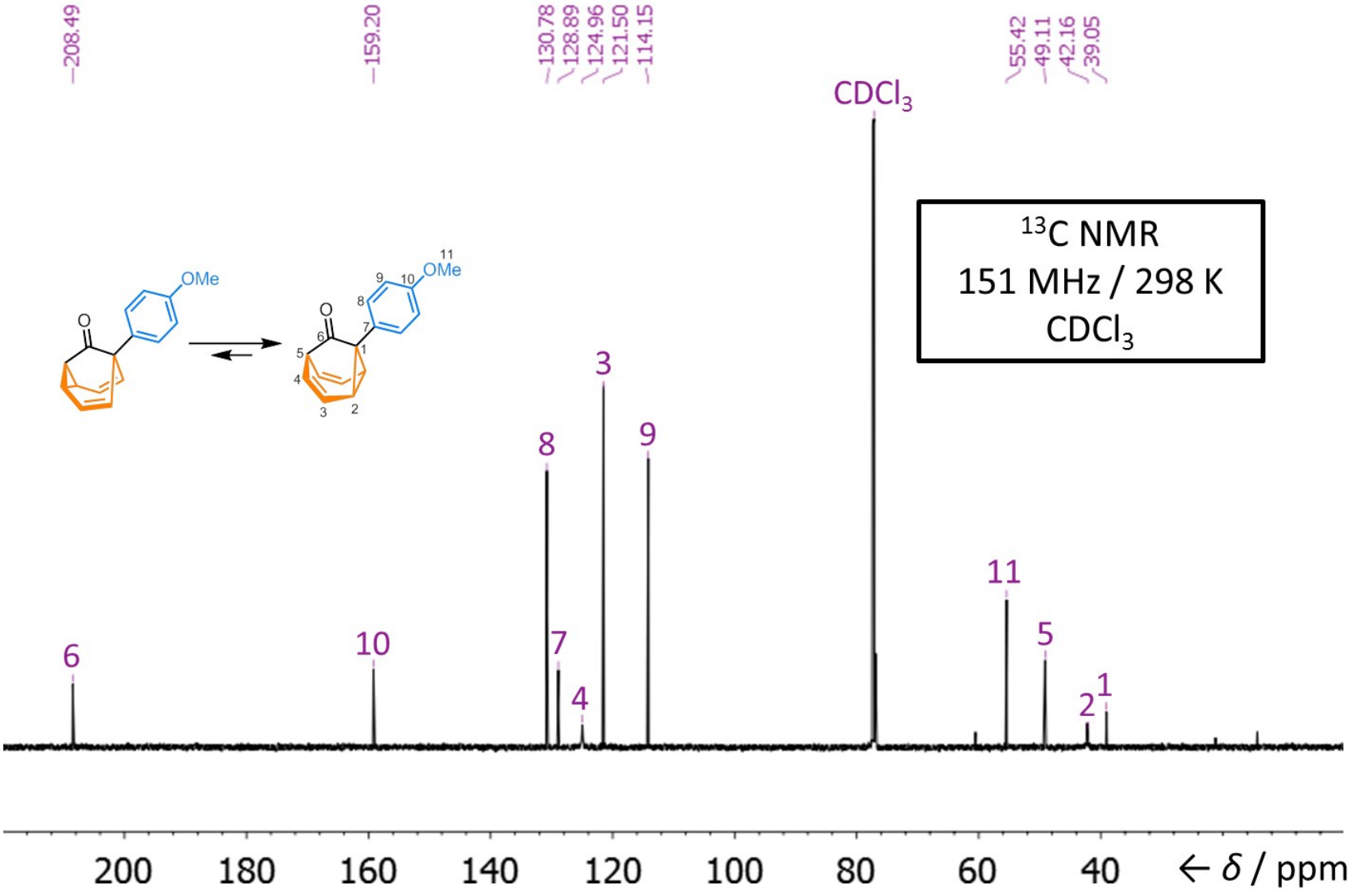

Figure S9. ^{13}C NMR Spectrum of 1-(4-anisyl)tricyclo[3.3.1.0^{2,8}]nona-3,6-dien-9-one.

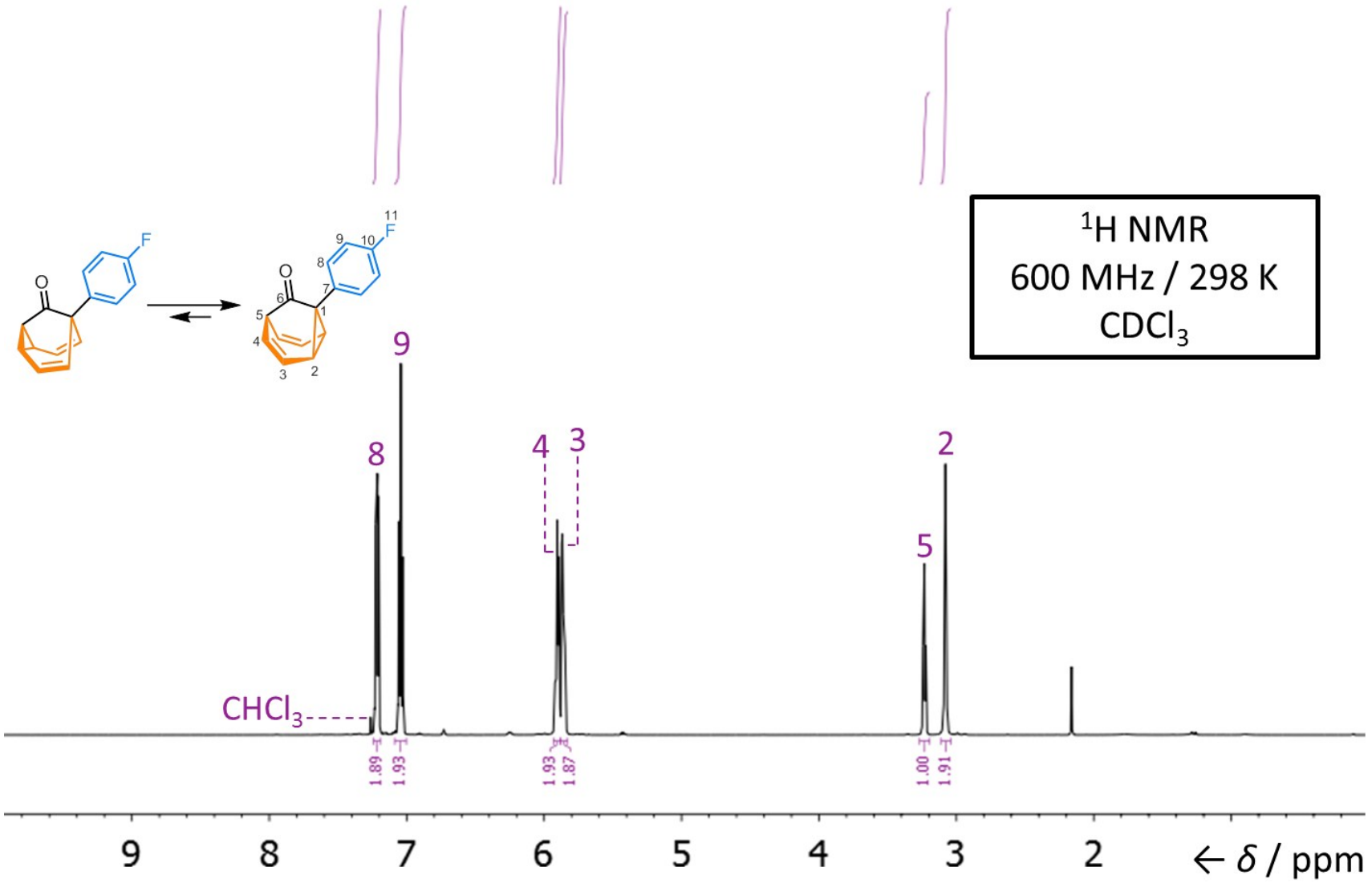

Figure S10. ^{1}H NMR Spectrum of 1-(4-fluorophenyl)tricyclo[3.3.1.0^{2,8}]nona-3,6-dien-9-one.

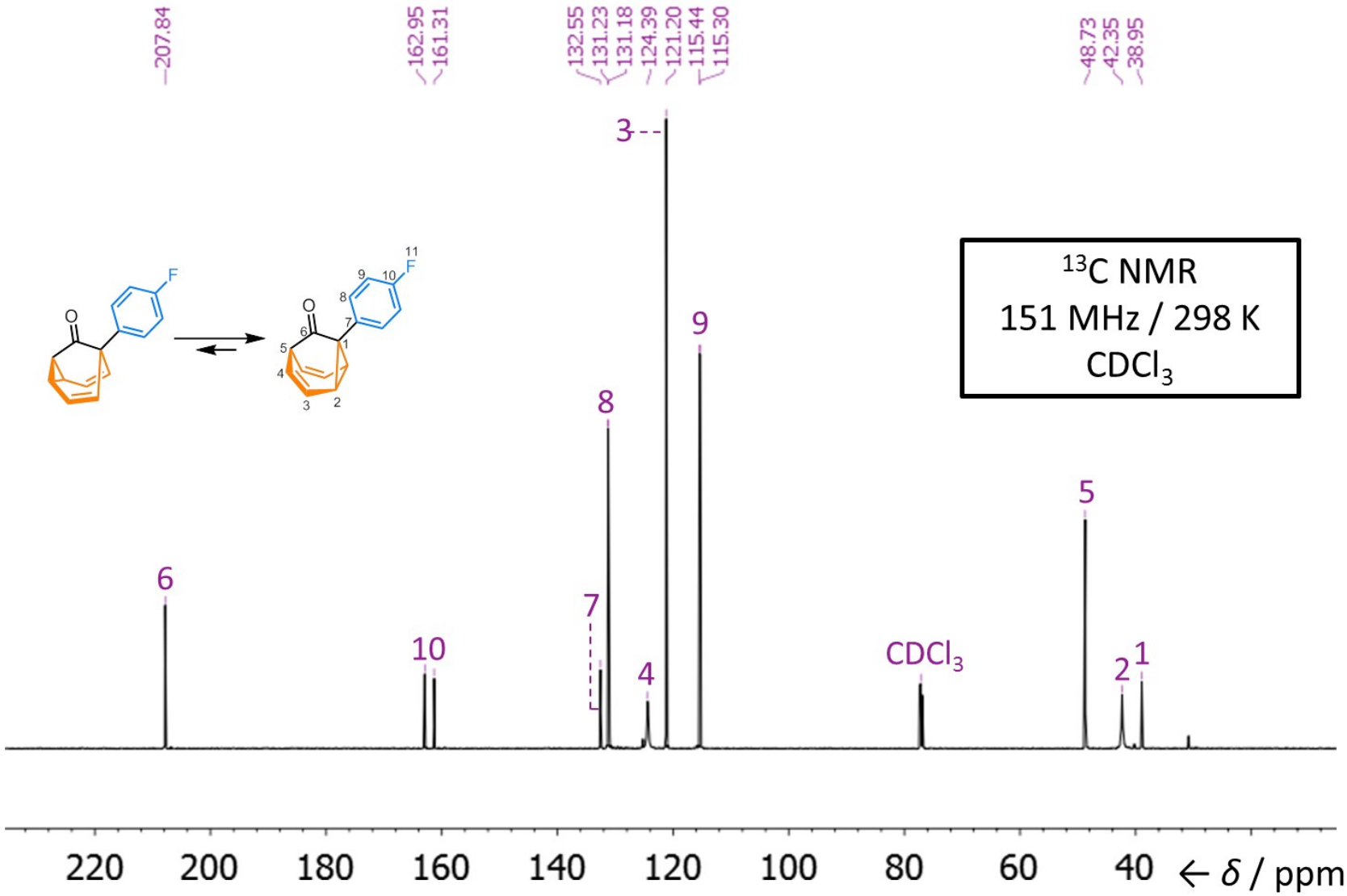

Figure S11. ^{13}C NMR Spectrum of 1-(4-fluorophenyl)tricyclo[3.3.1.0^{2,8}]nona-3,6-dien-9-one.

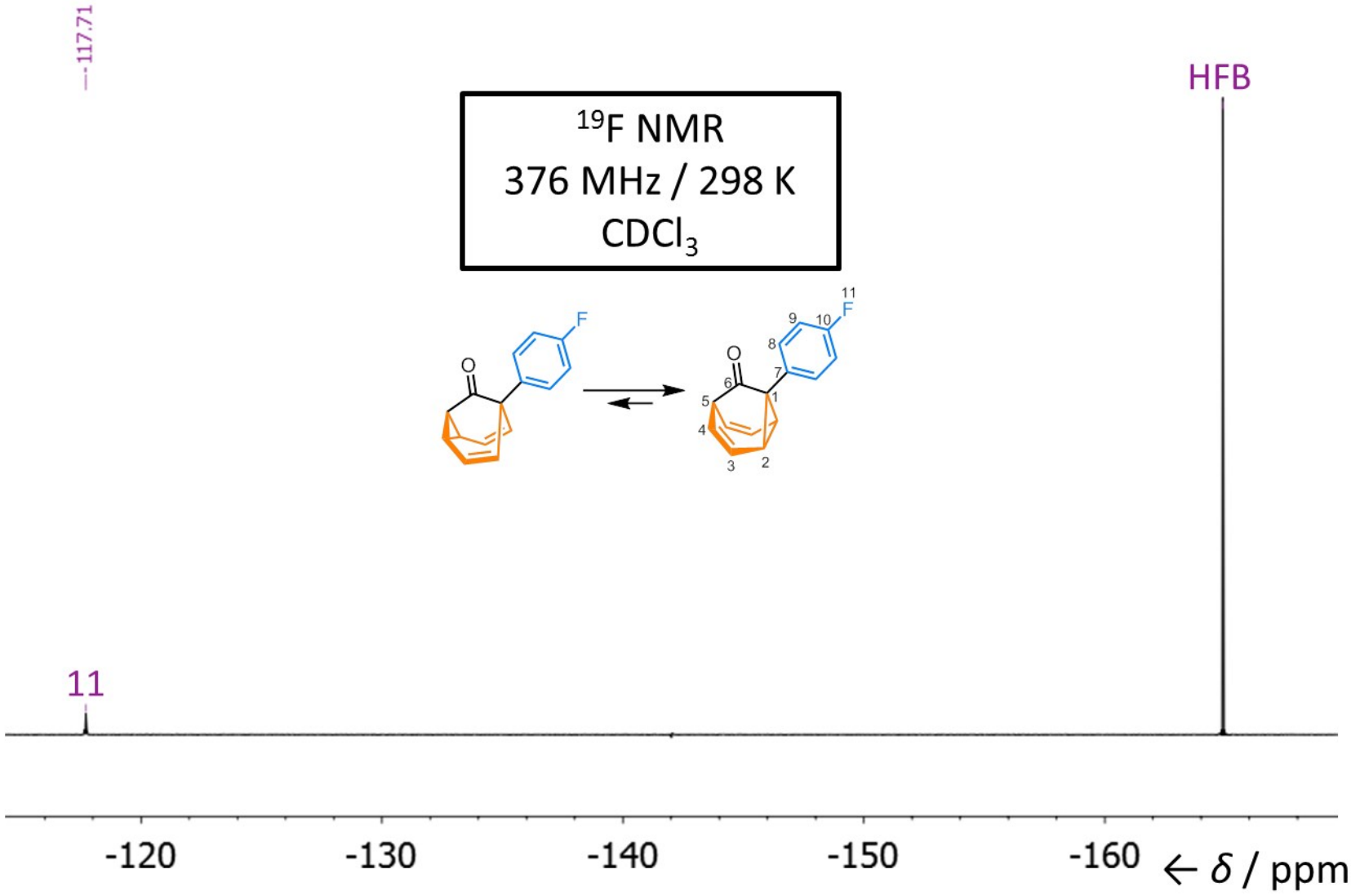

Figure S12. ^{19}F NMR Spectrum of 1-(4-fluorophenyl)tricyclo[3.3.1.$0^{2,8}$]nona-3,6-dien-9-one.

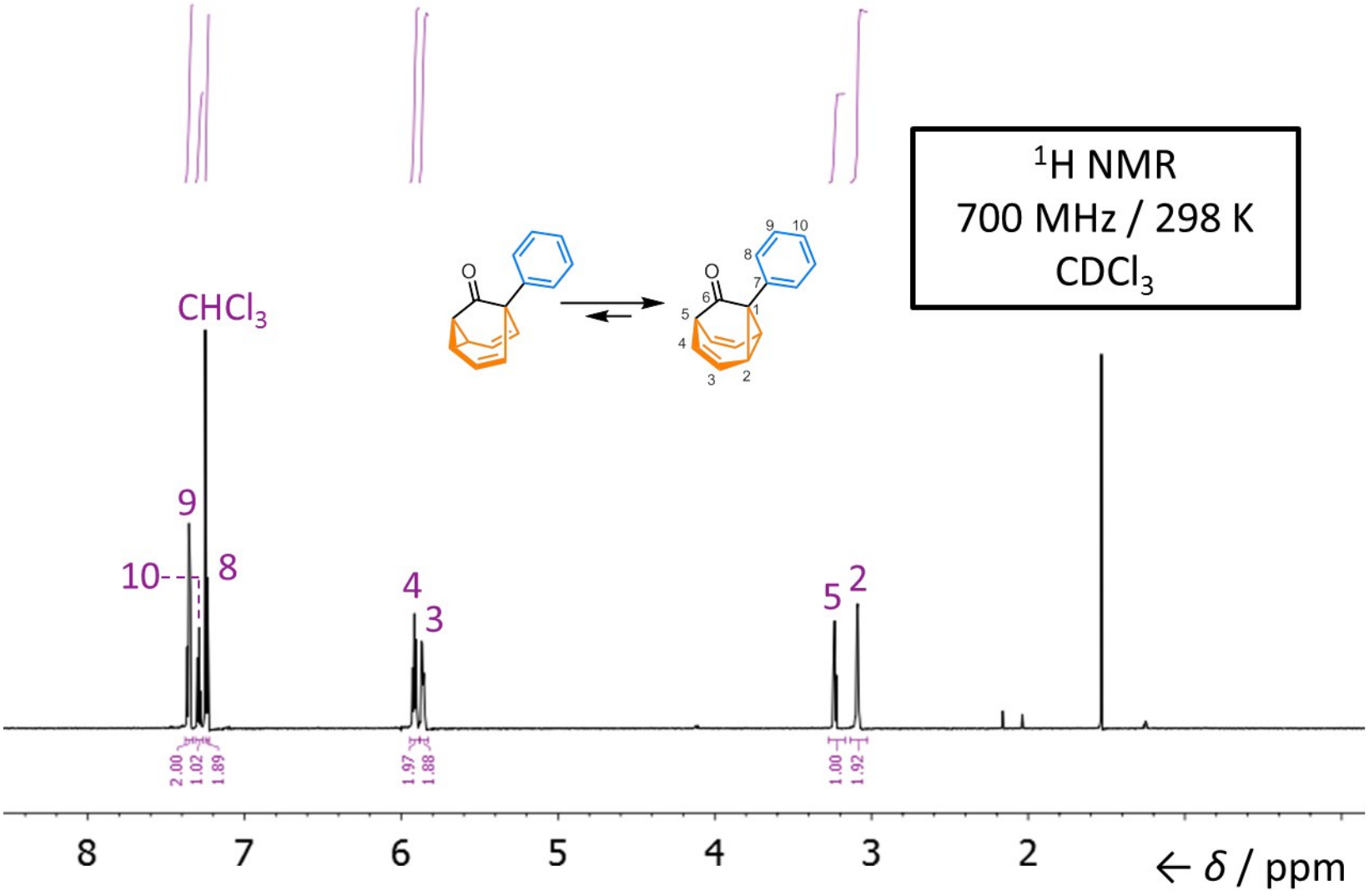

Figure S13. ^{1}H NMR Spectrum of 1-phenyltricyclo[3.3.1.0^{2,8}]nona-3,6-dien-9-one.

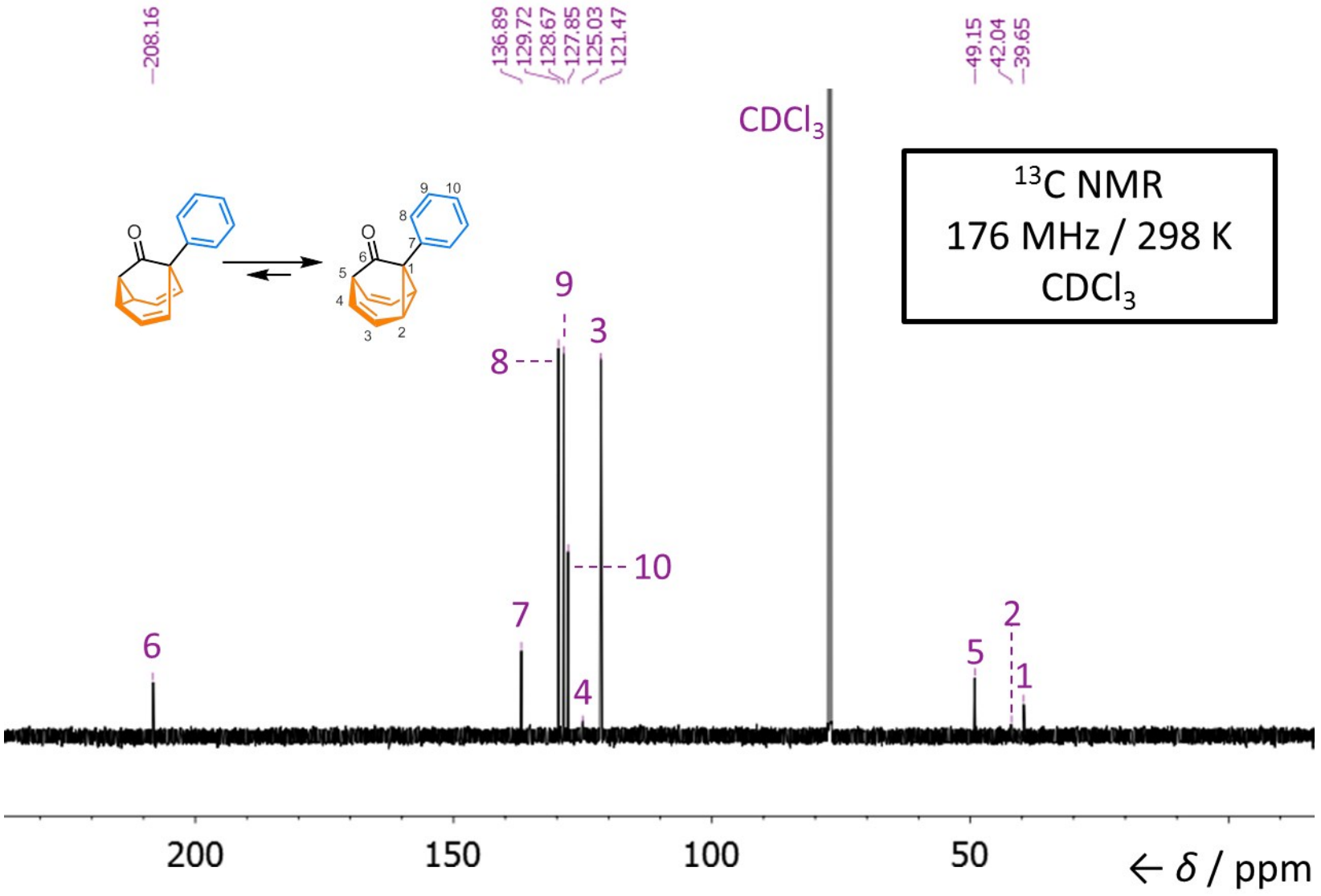

Figure S14. ^{13}C NMR Spectrum of 1-phenyltricyclo[3.3.1.$0^{2,8}$]nona-3,6-dien-9-one.

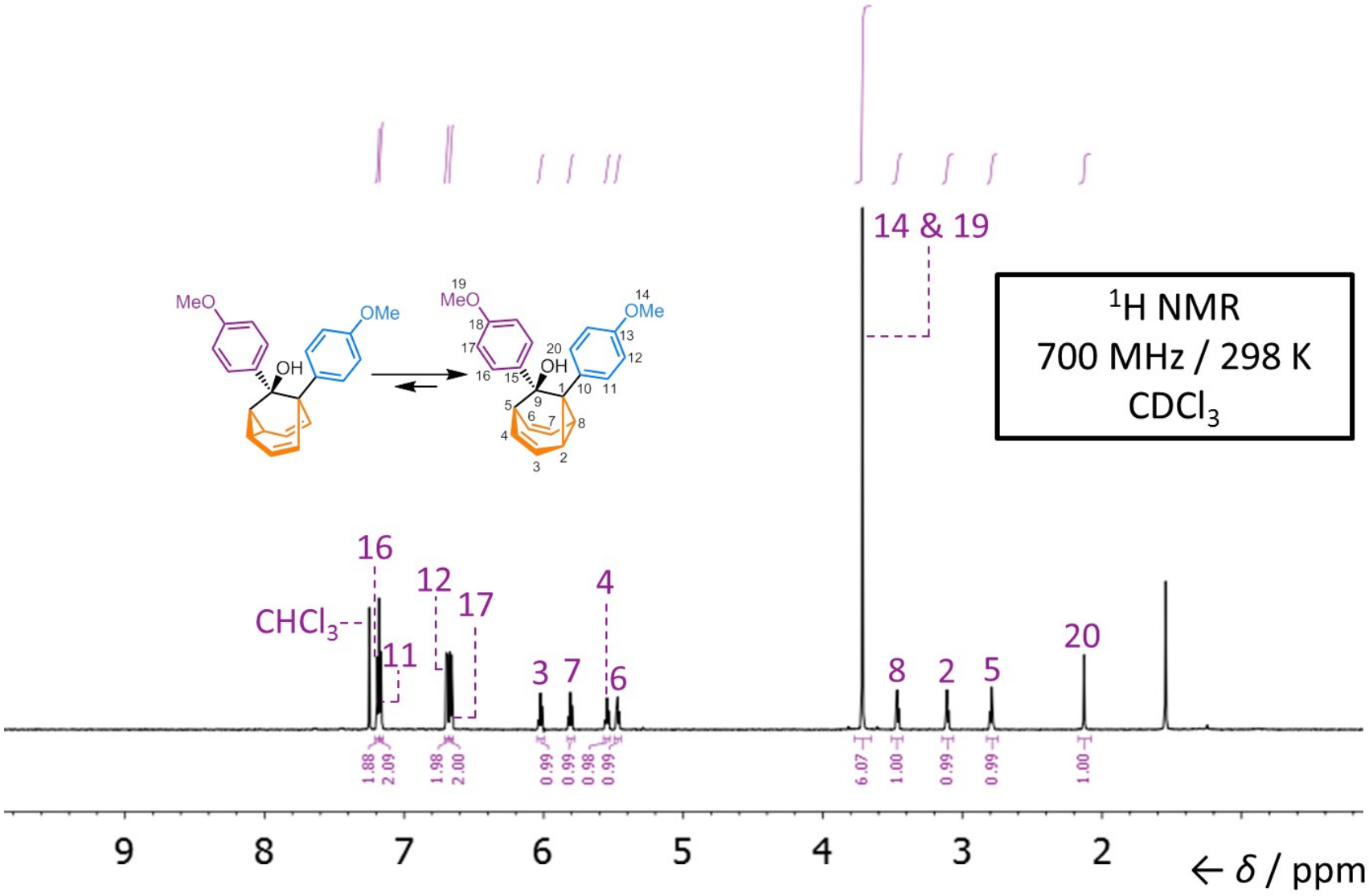

Figure S15. ^{1}H NMR Spectrum of **1a**.

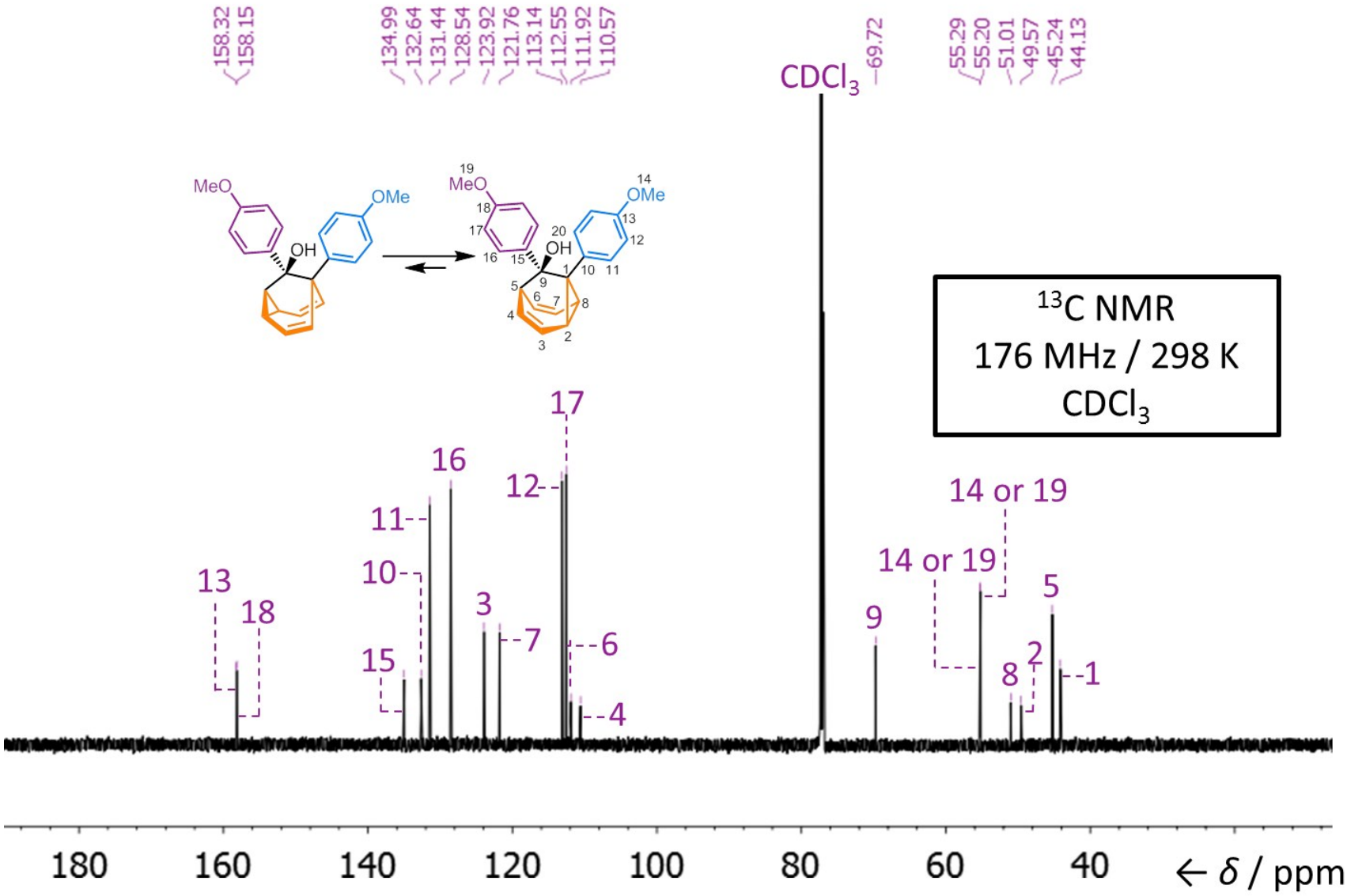

Figure S16. ^{13}C NMR Spectrum of **1a**.

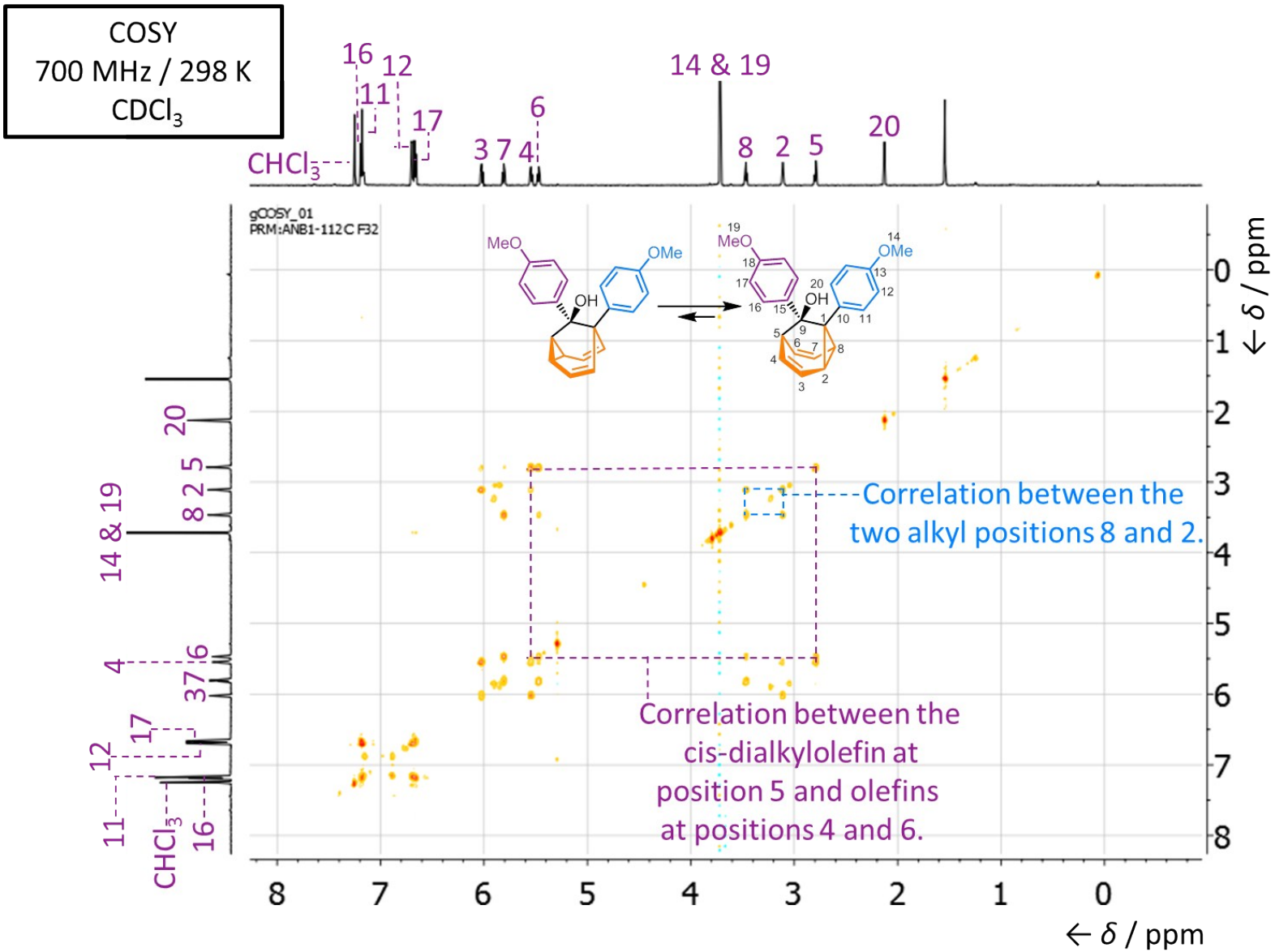

Figure S17. COSY Spectrum of **1a**.

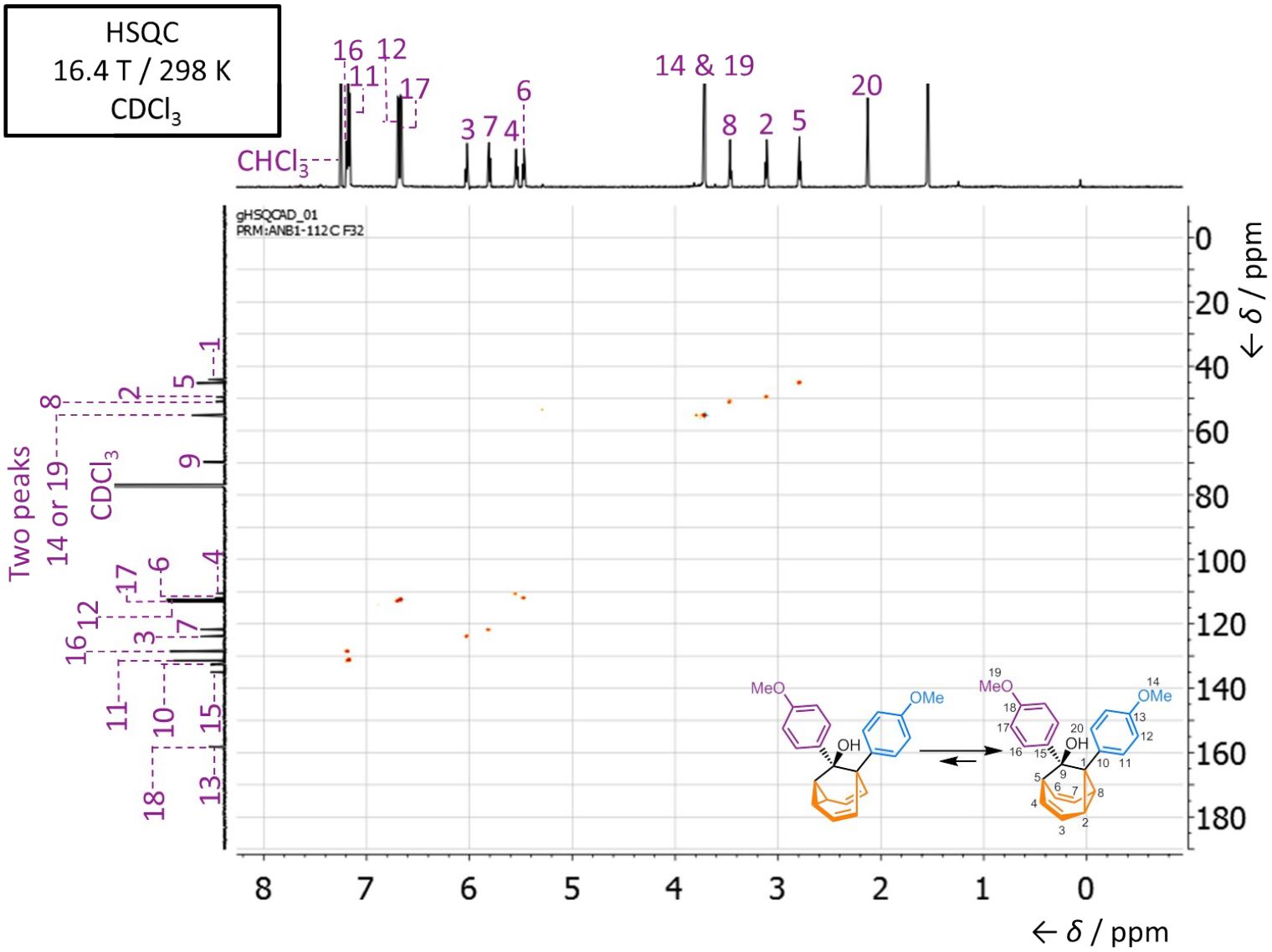

Figure S18. HSQC Spectrum of **1a**.

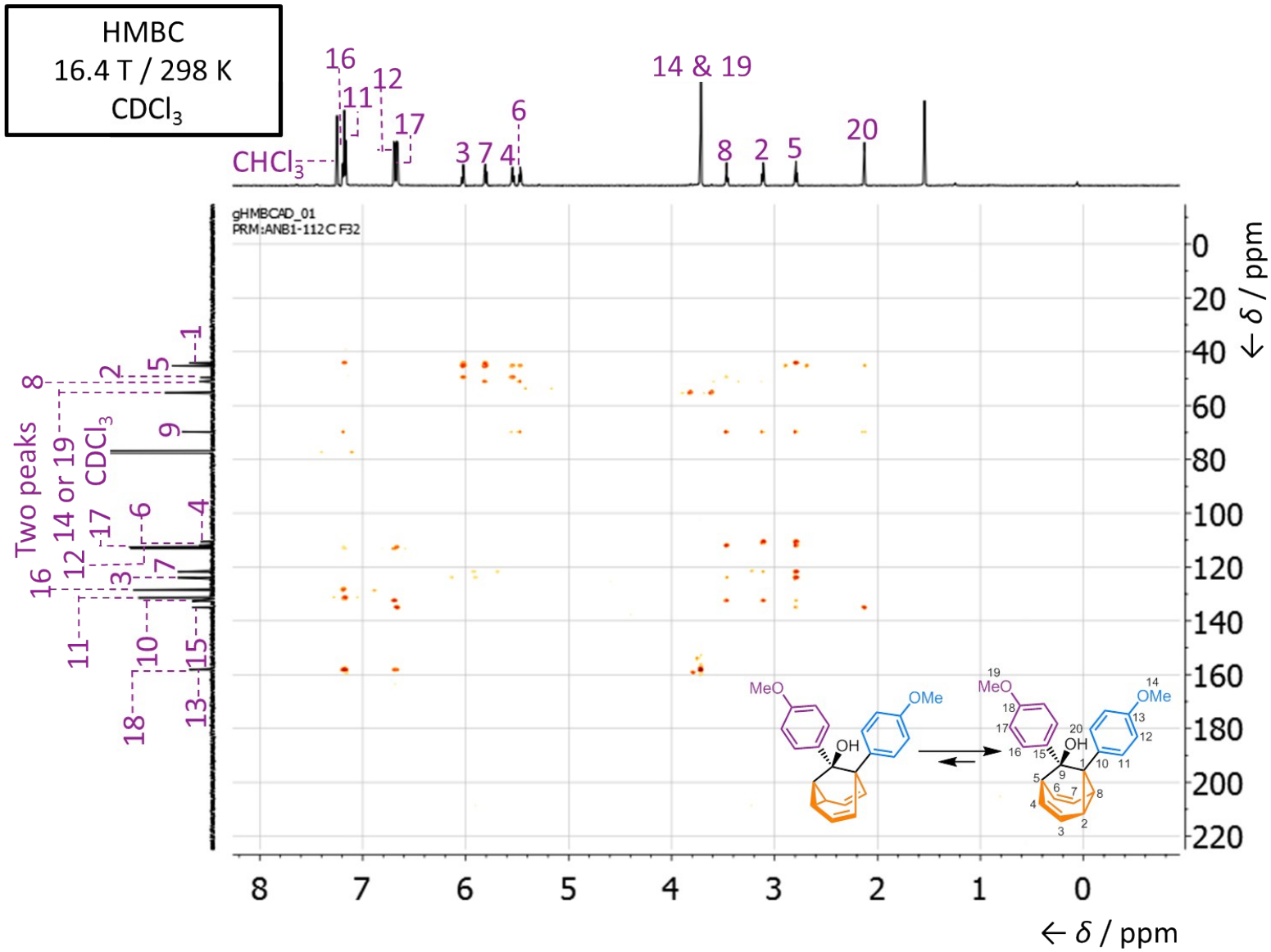

Figure S19. HMBC Spectrum of **1a**.

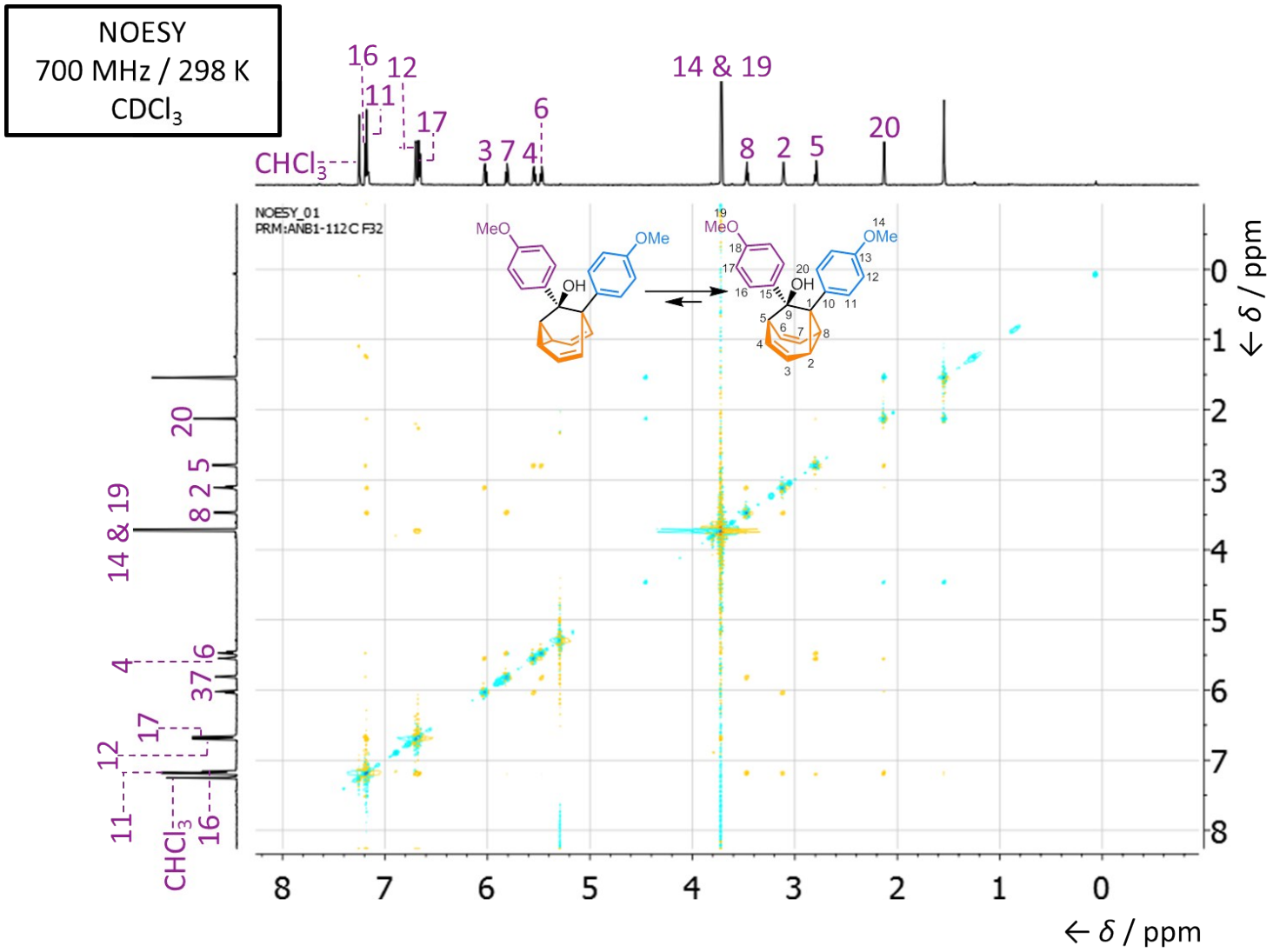

Figure S20. NOESY Spectrum of **1a**.

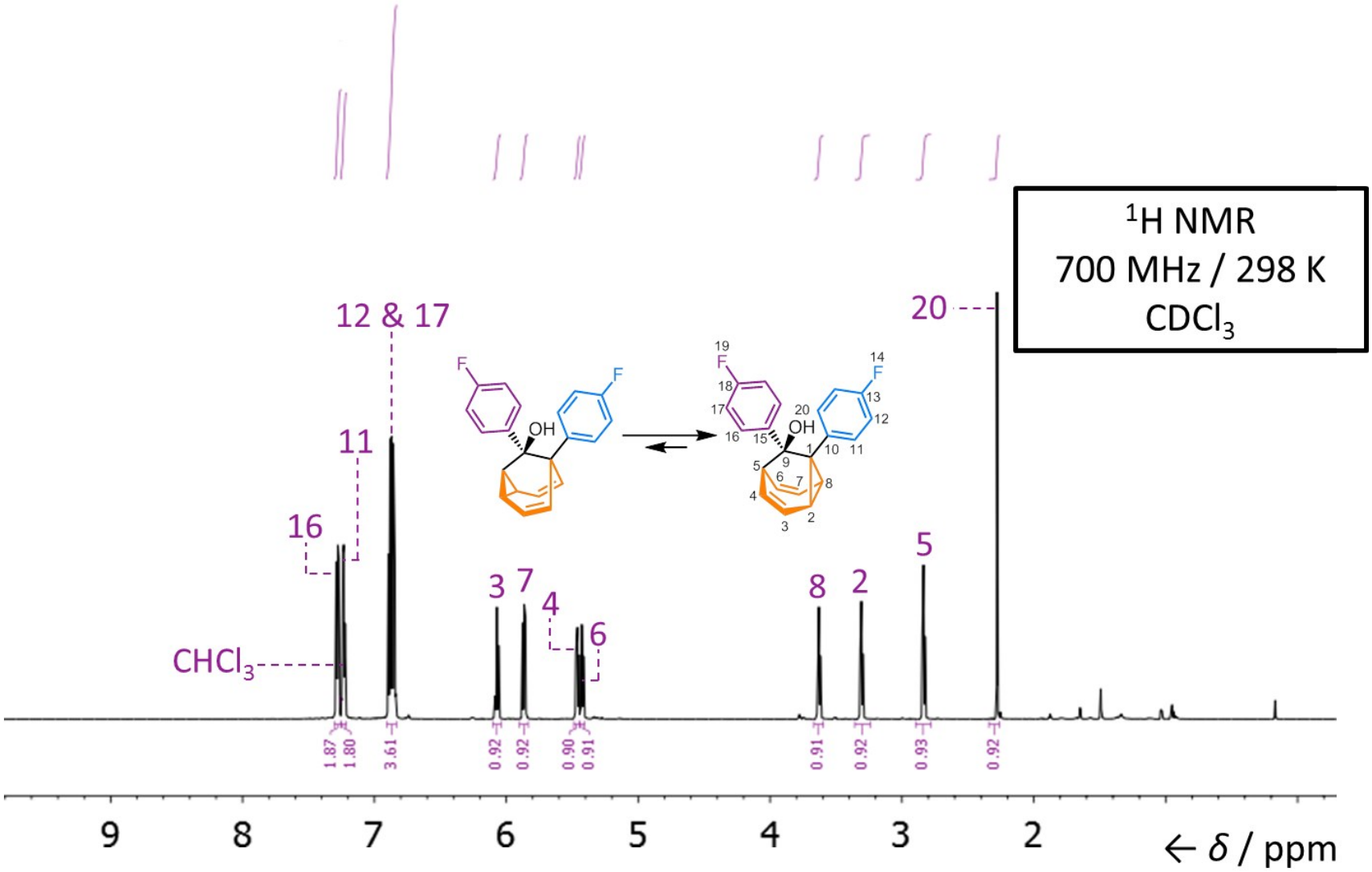

Figure S21. ^{1}H NMR Spectrum of **1b**.

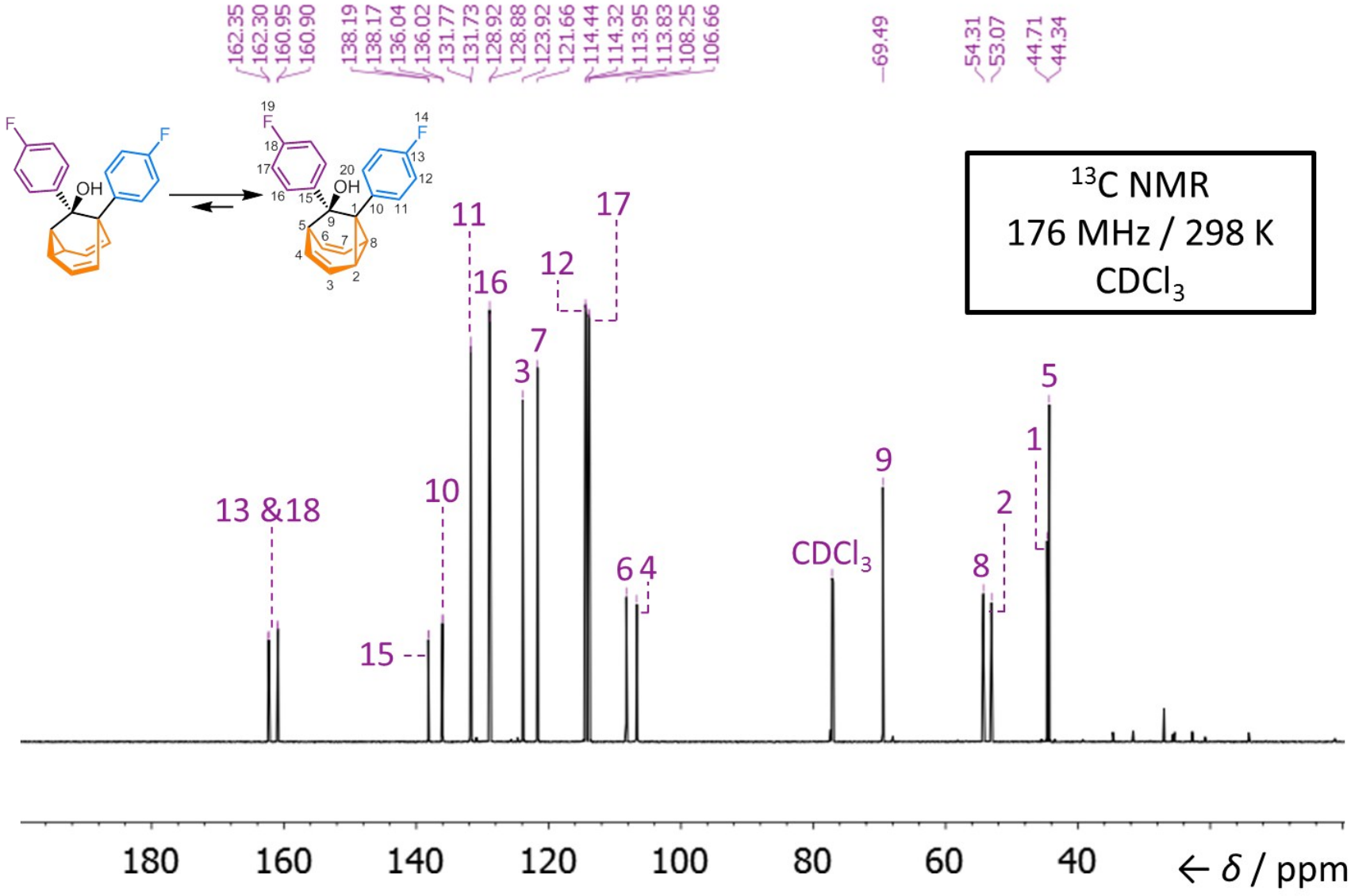

Figure S22. ^{13}C NMR Spectrum of **1b**.

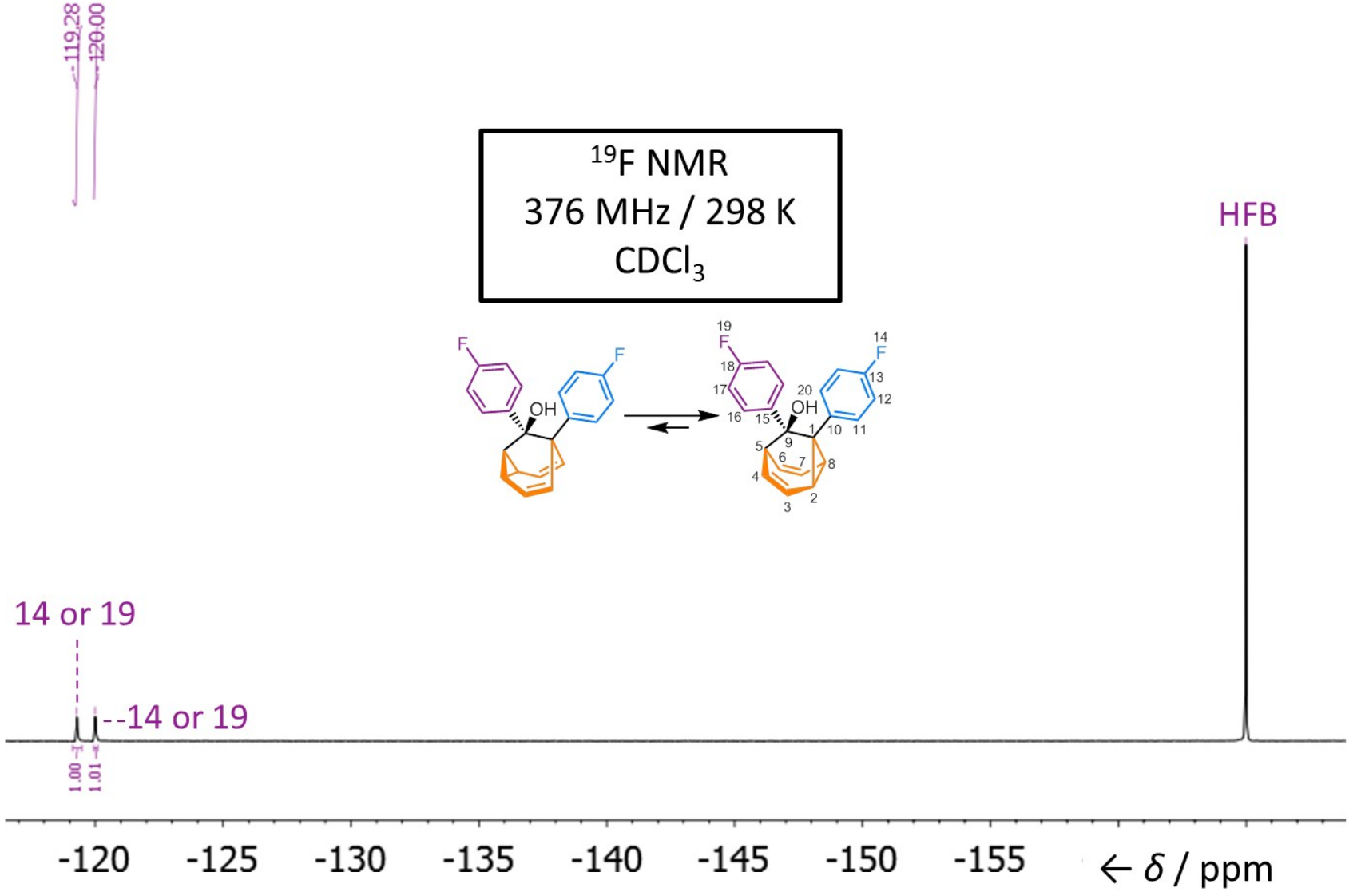

Figure S23. ^{19}F NMR Spectrum of **1b**.

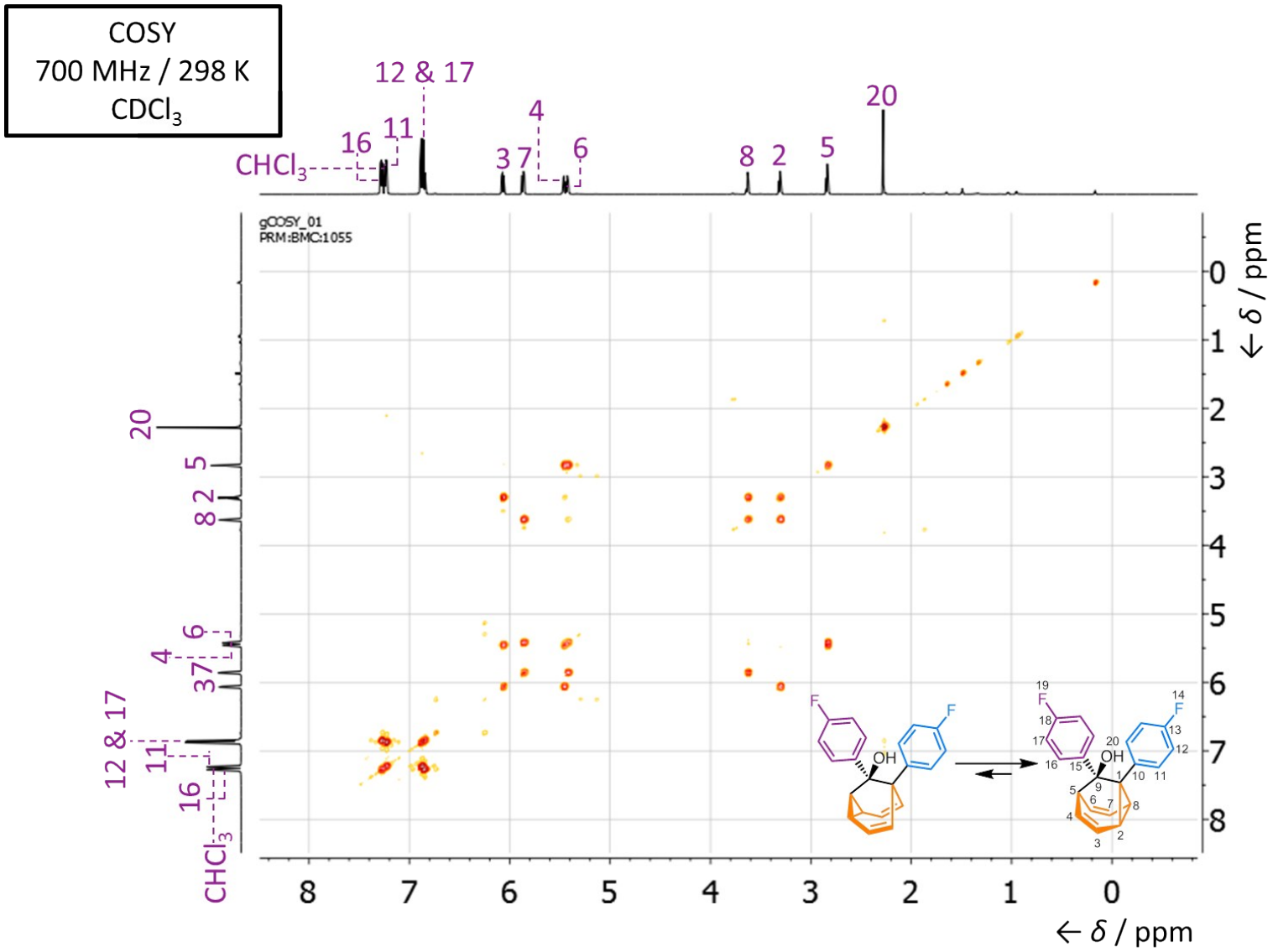

Figure S24. COSY Spectrum of **1b**.

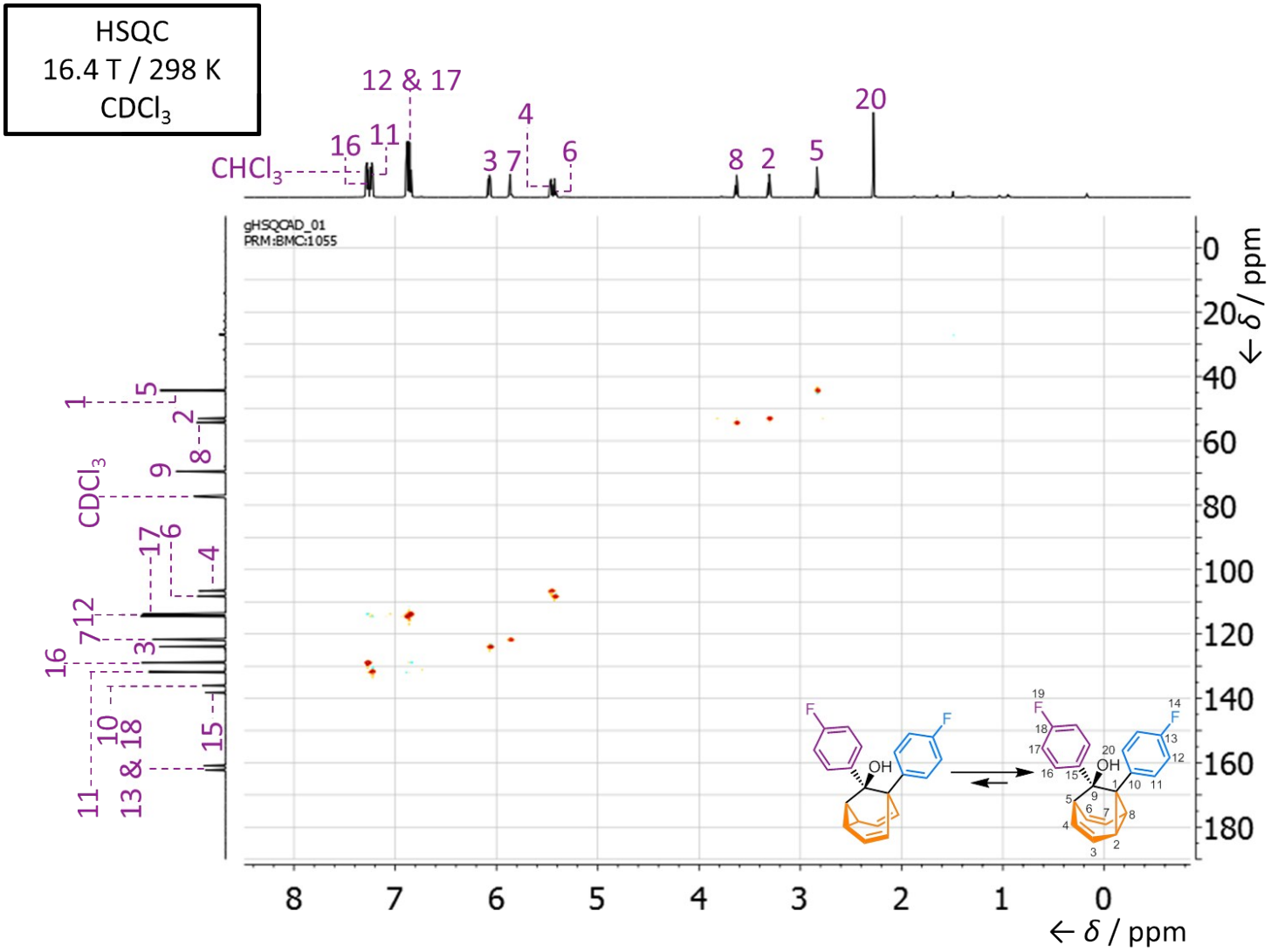

Figure S25. HSCQ Spectrum of **1b**.

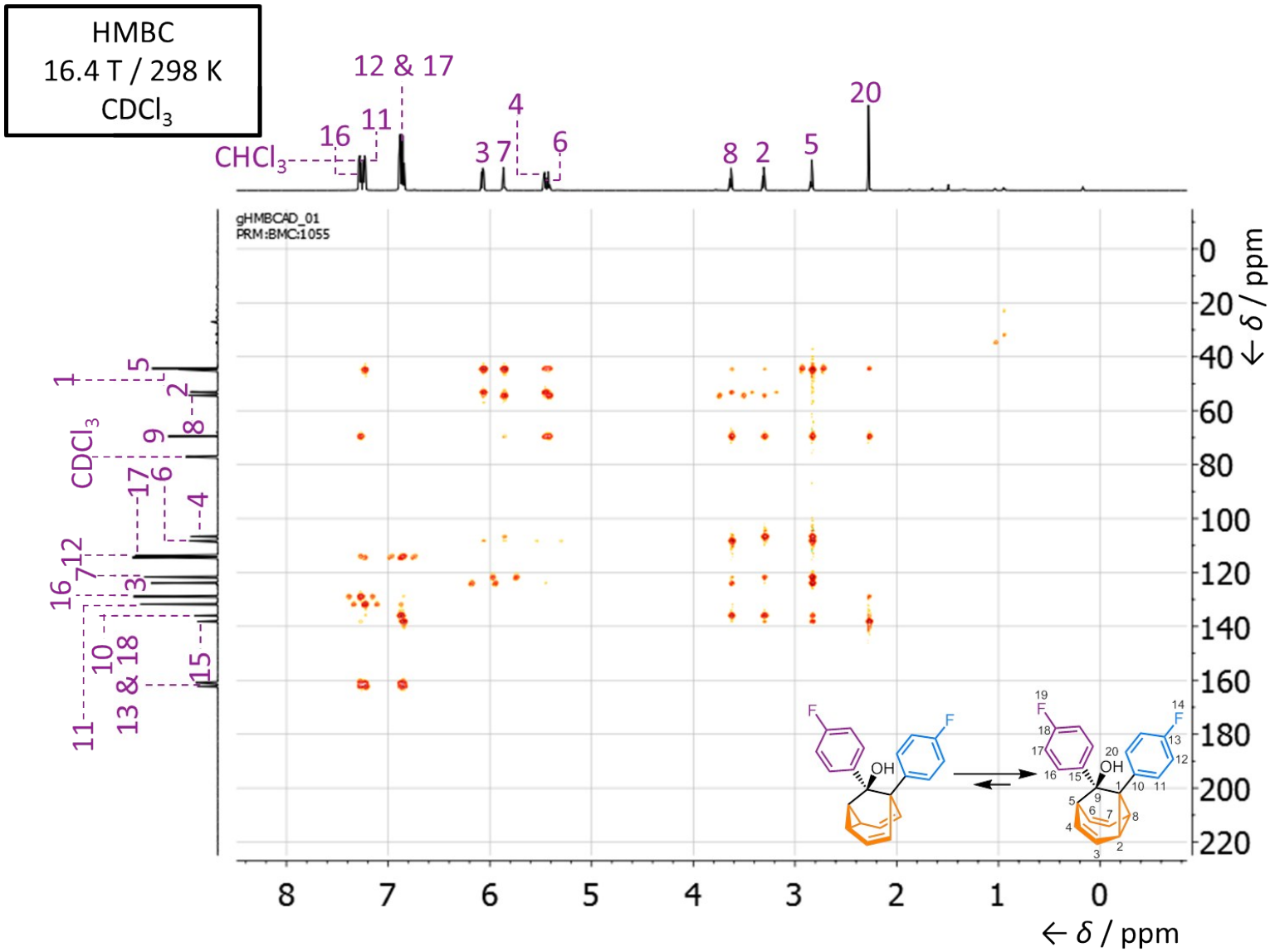

Figure S26. HMBC Spectrum of **1b**.

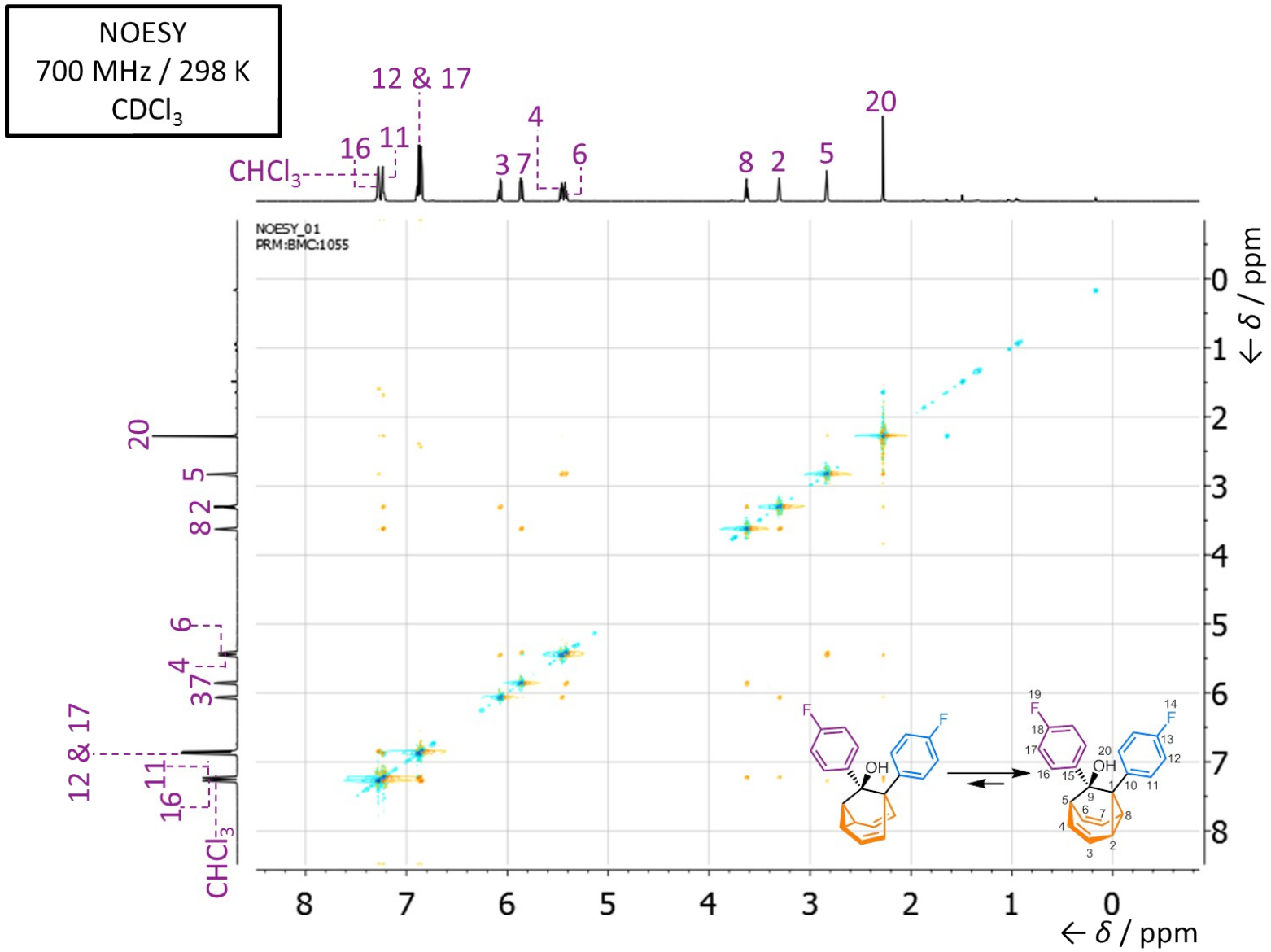

Figure S27. NOESY Spectrum of **1b**.

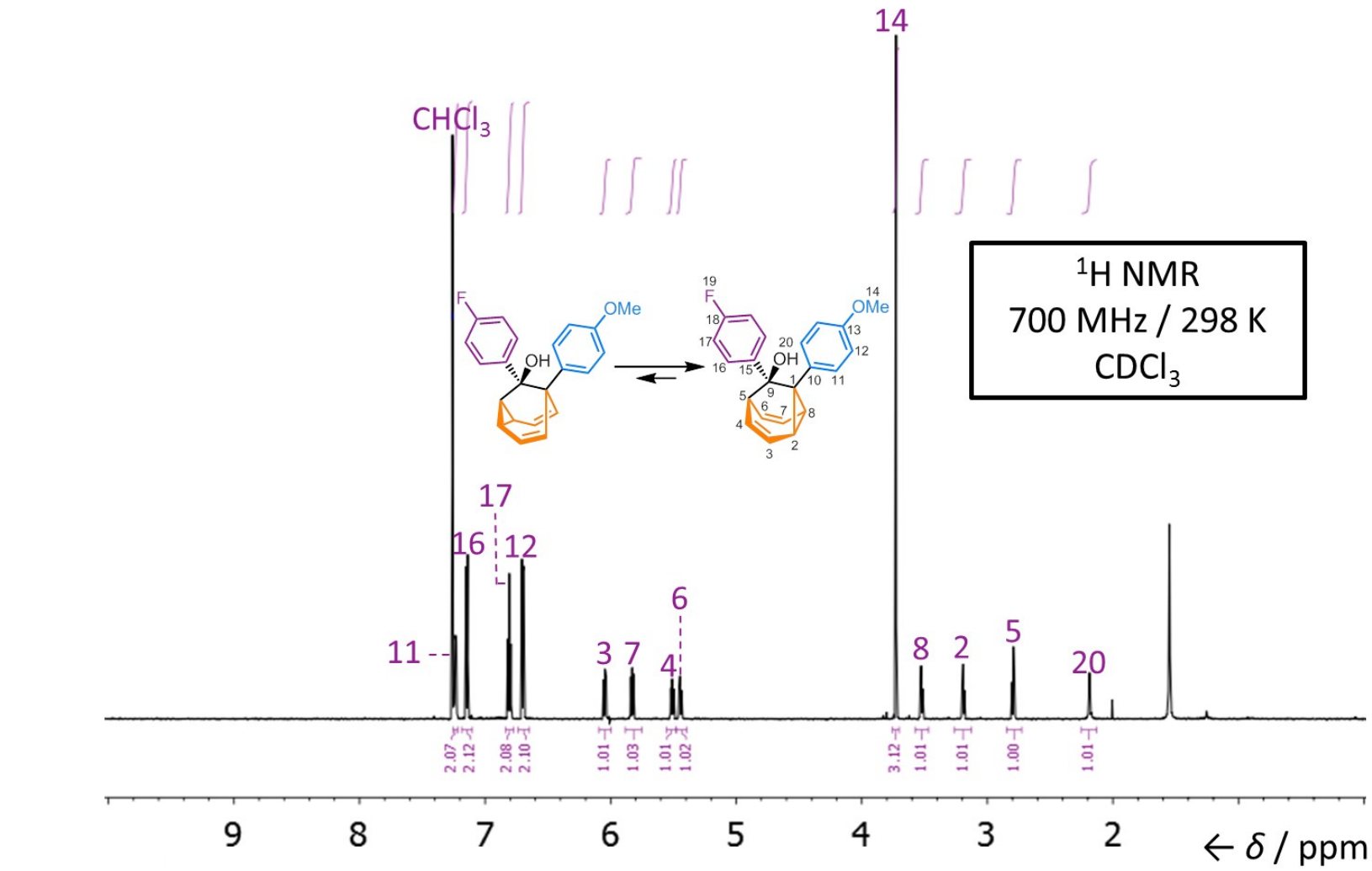

Figure S28. ^{1}H NMR Spectrum of **1c**.

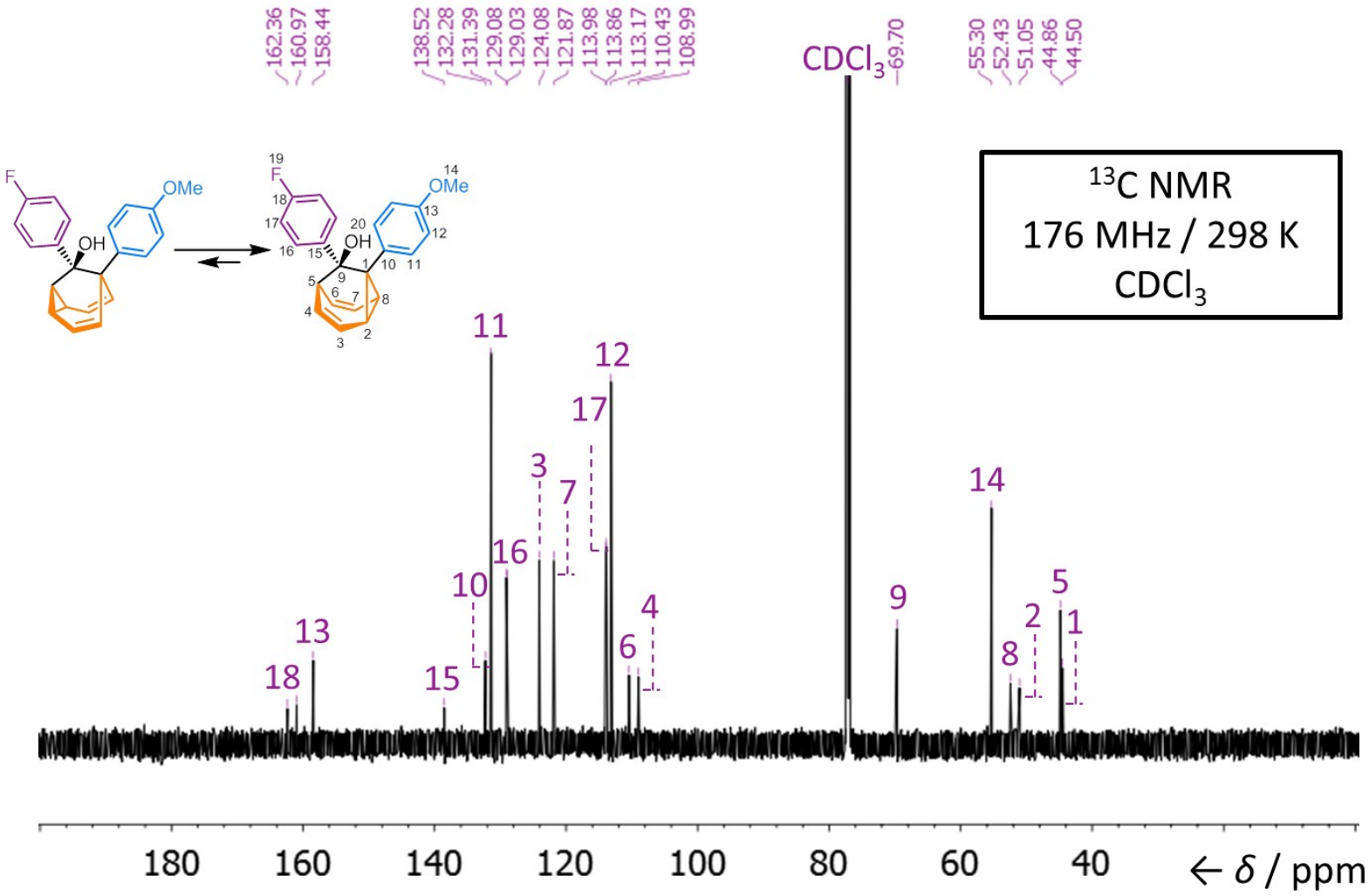

Figure S29. ^{13}C NMR Spectrum of **1c**.

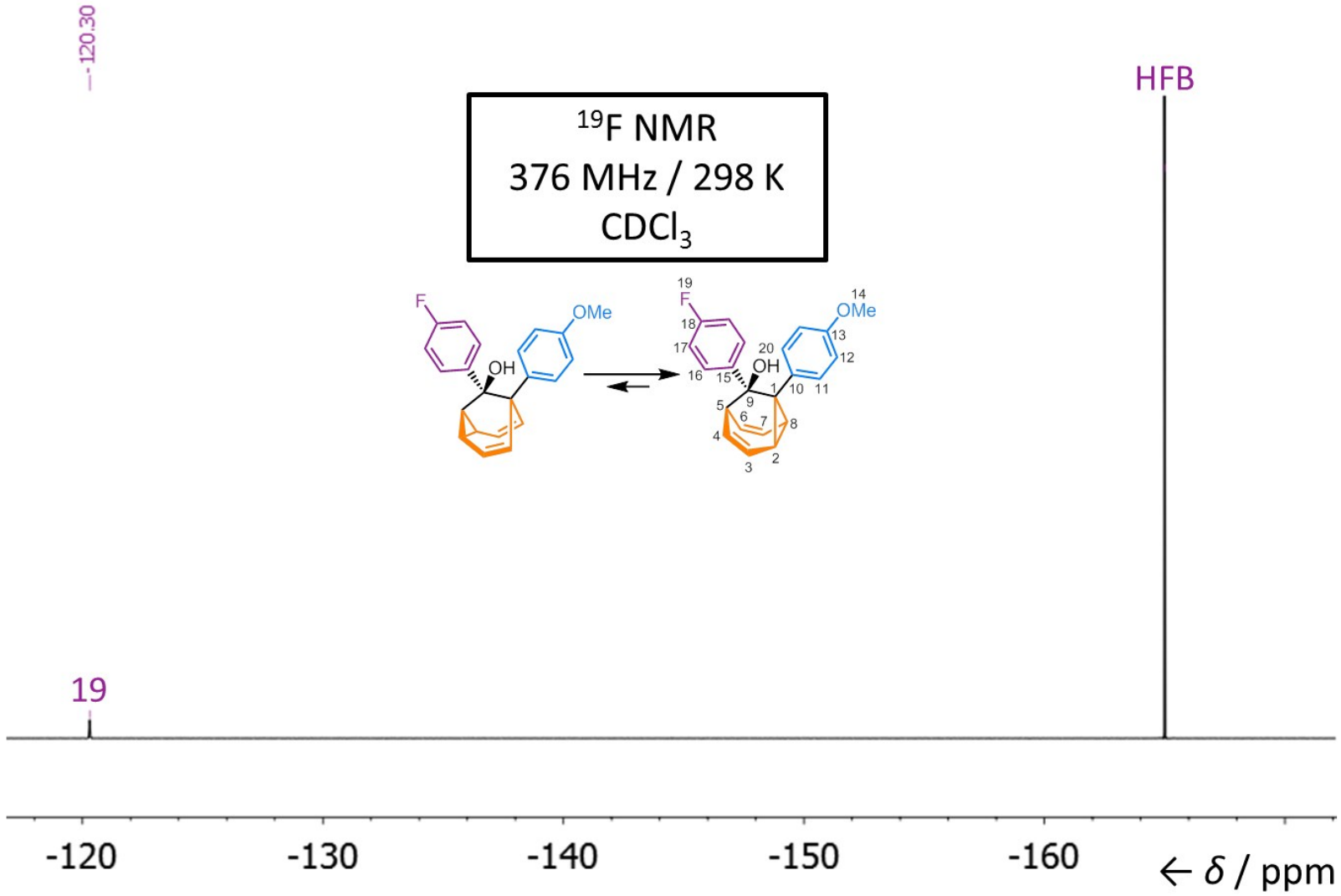

Figure S30. ^{19}F NMR Spectrum of **1c**.

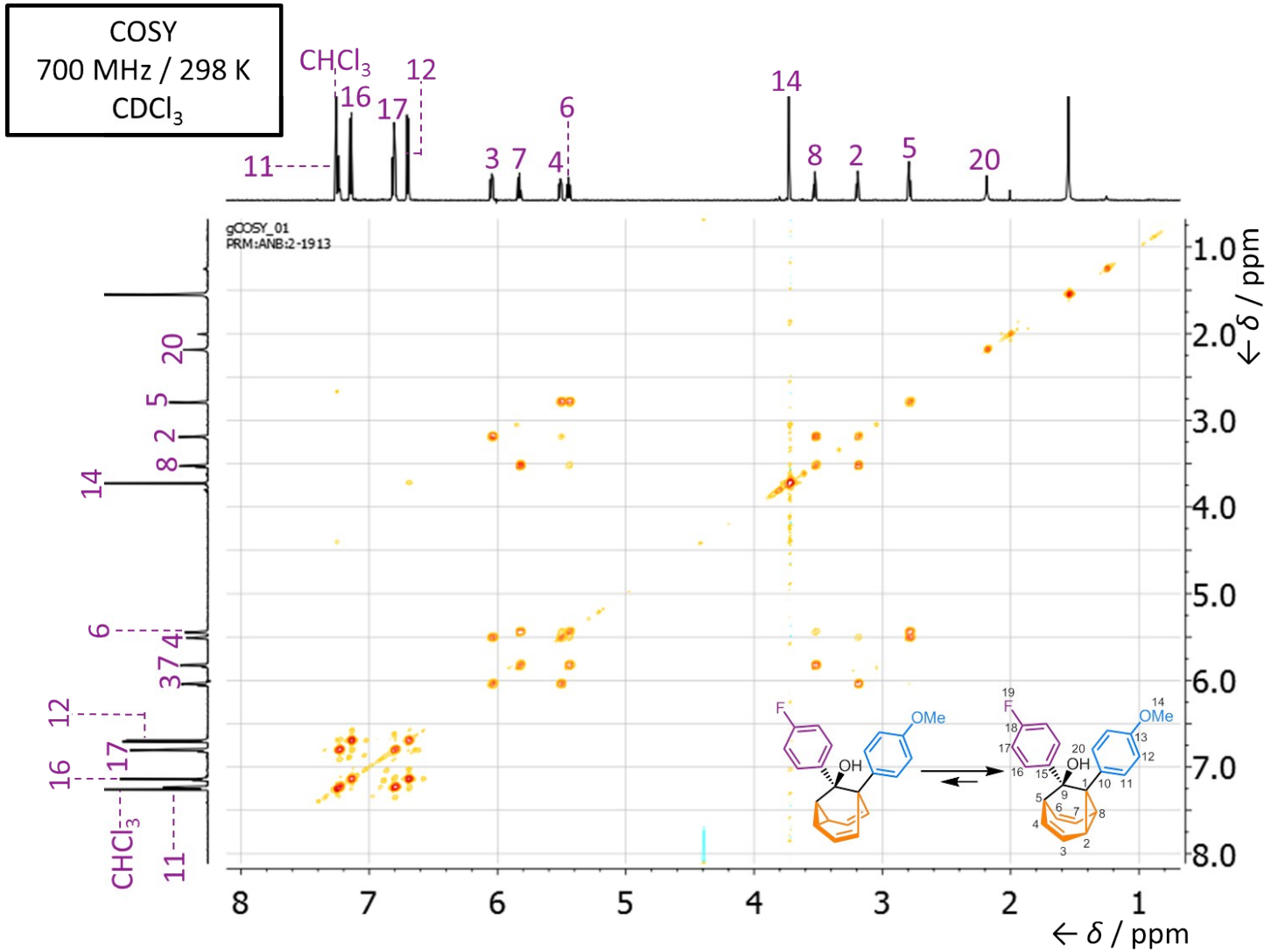

Figure S31. COSY Spectrum of **1c**.

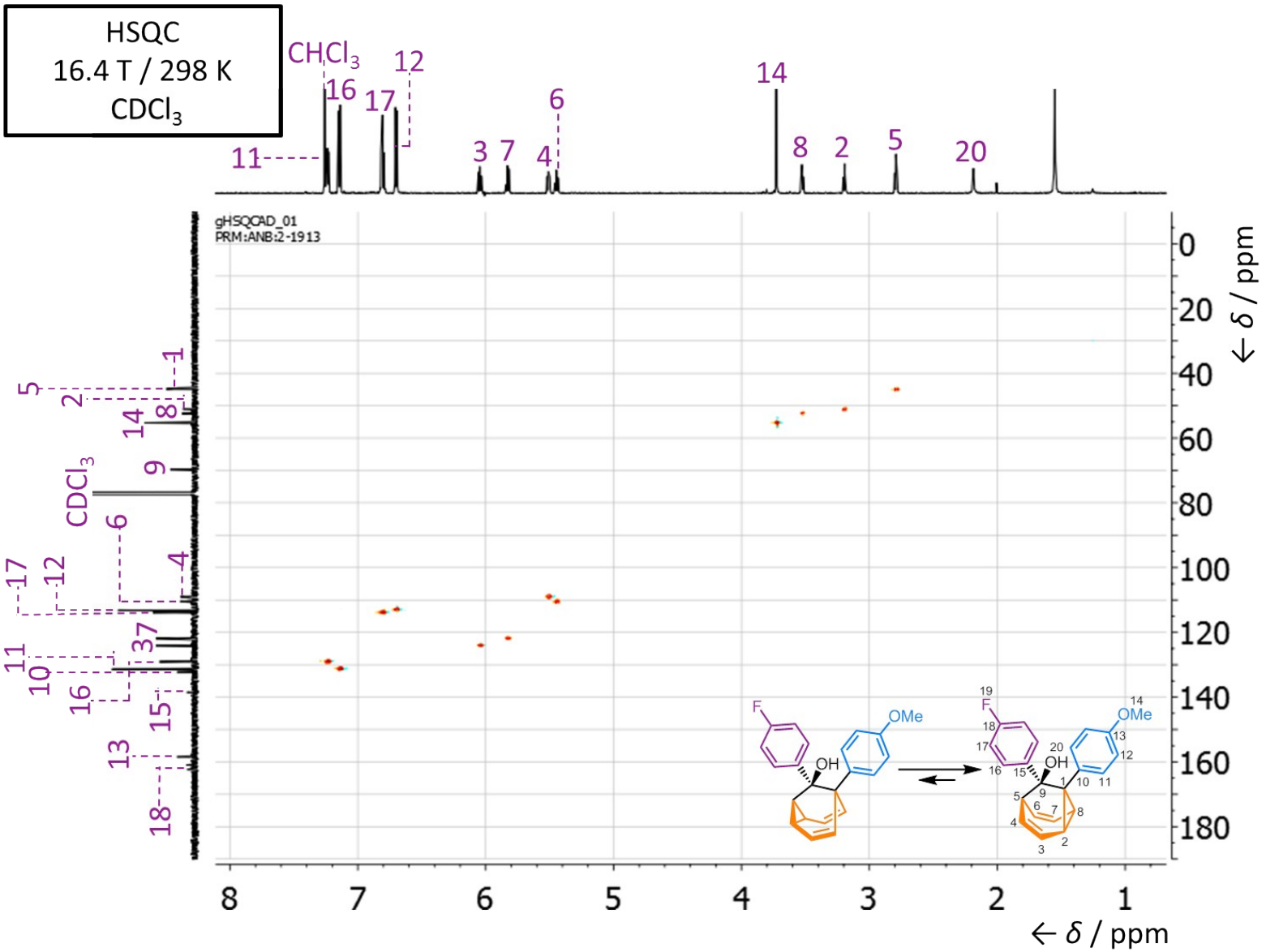

Figure S32. HSQC Spectrum of **1c**.

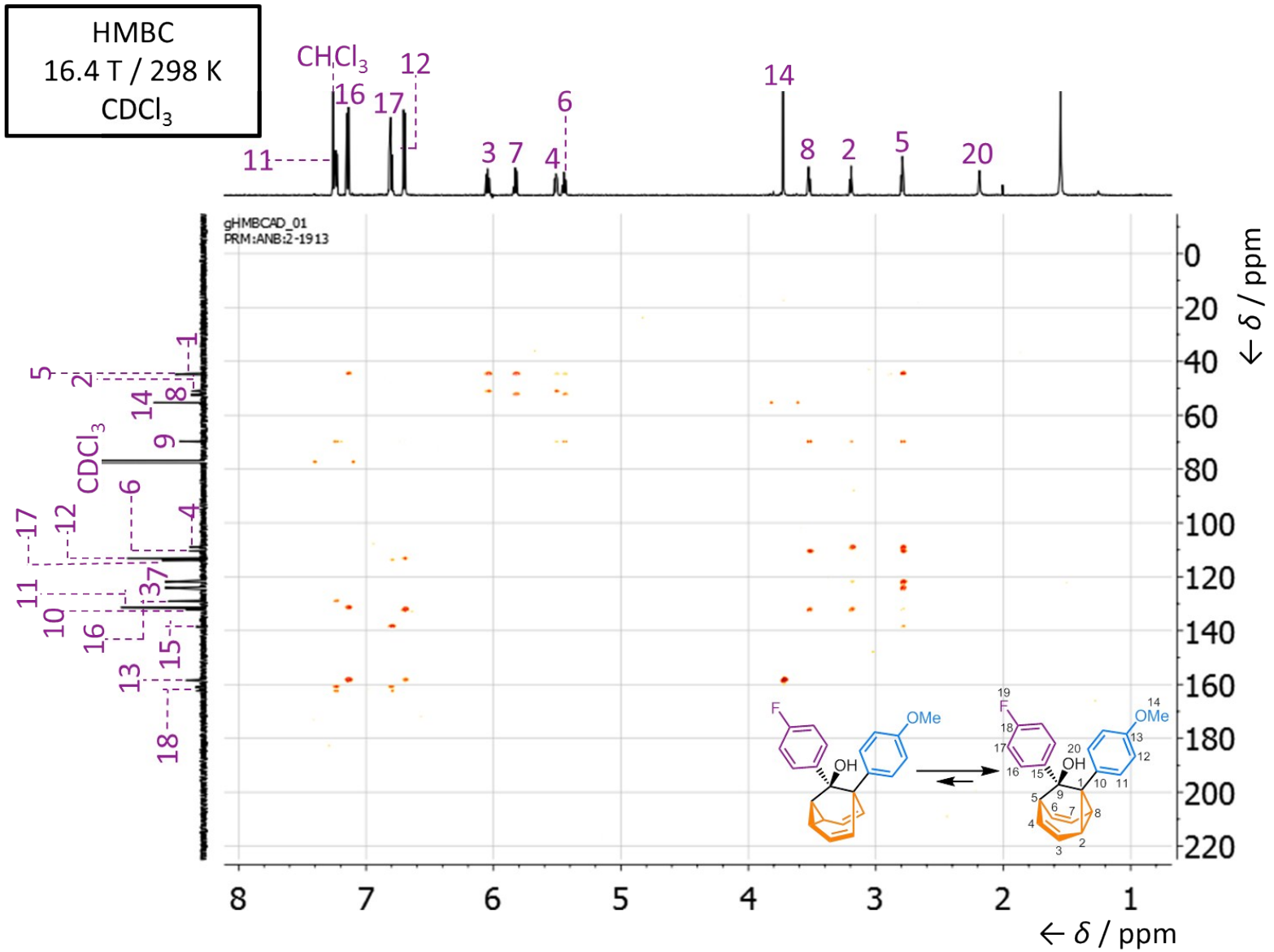

Figure S33. HMBC Spectrum of **1c**.

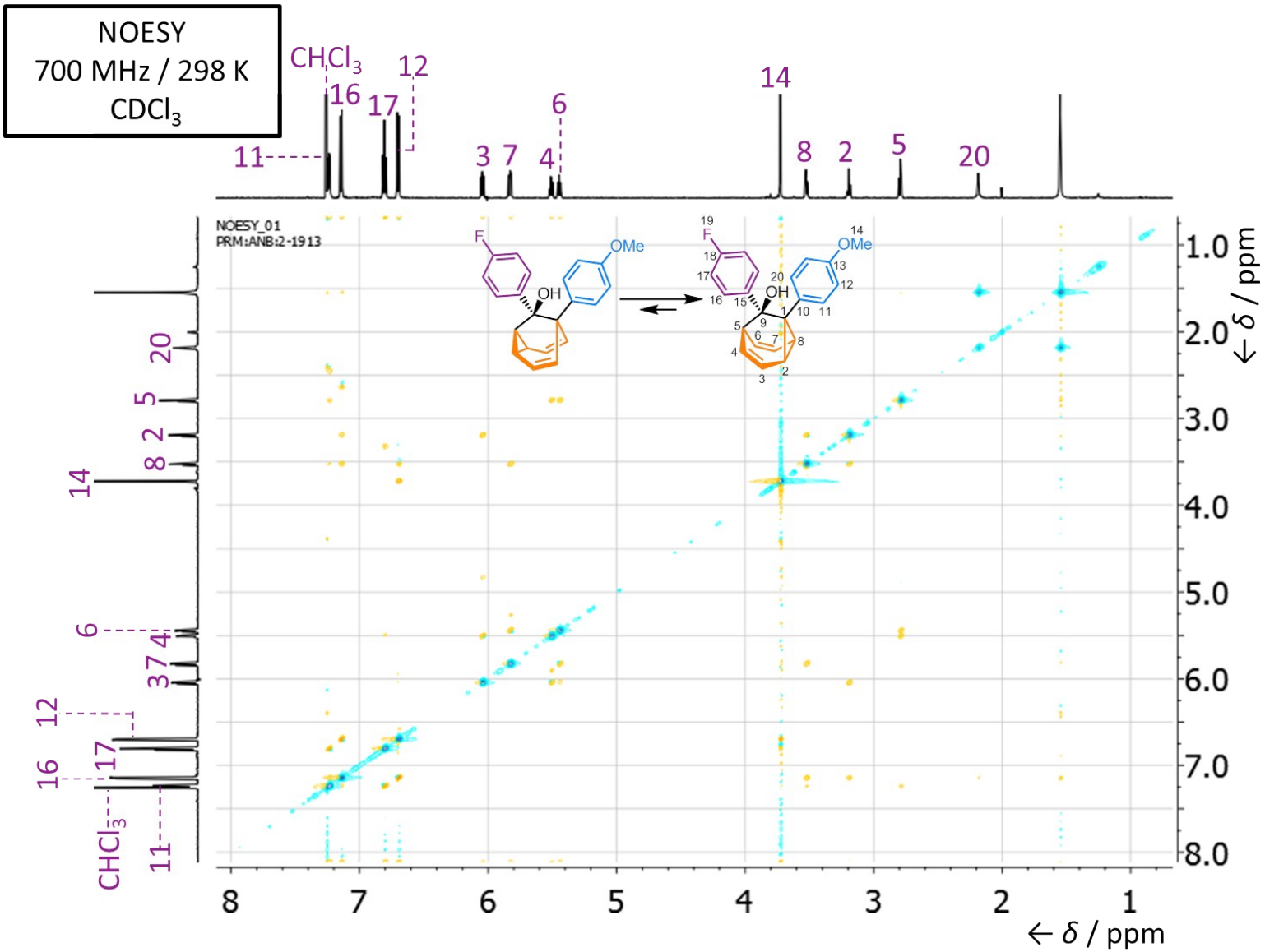

Figure S34. NOESY Spectrum of **1c**.

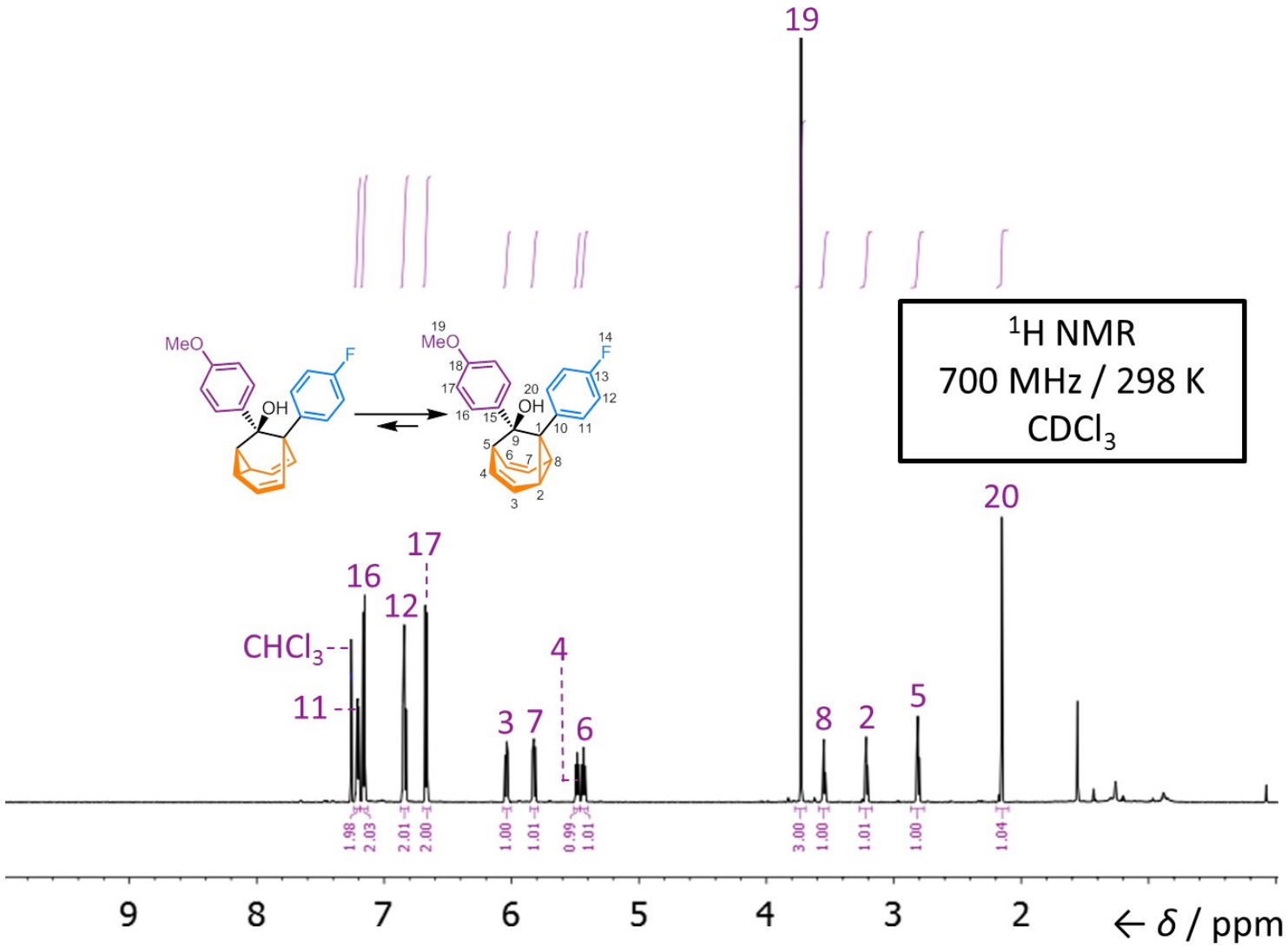

Figure S35. ^{1}H NMR Spectrum of **1d**.

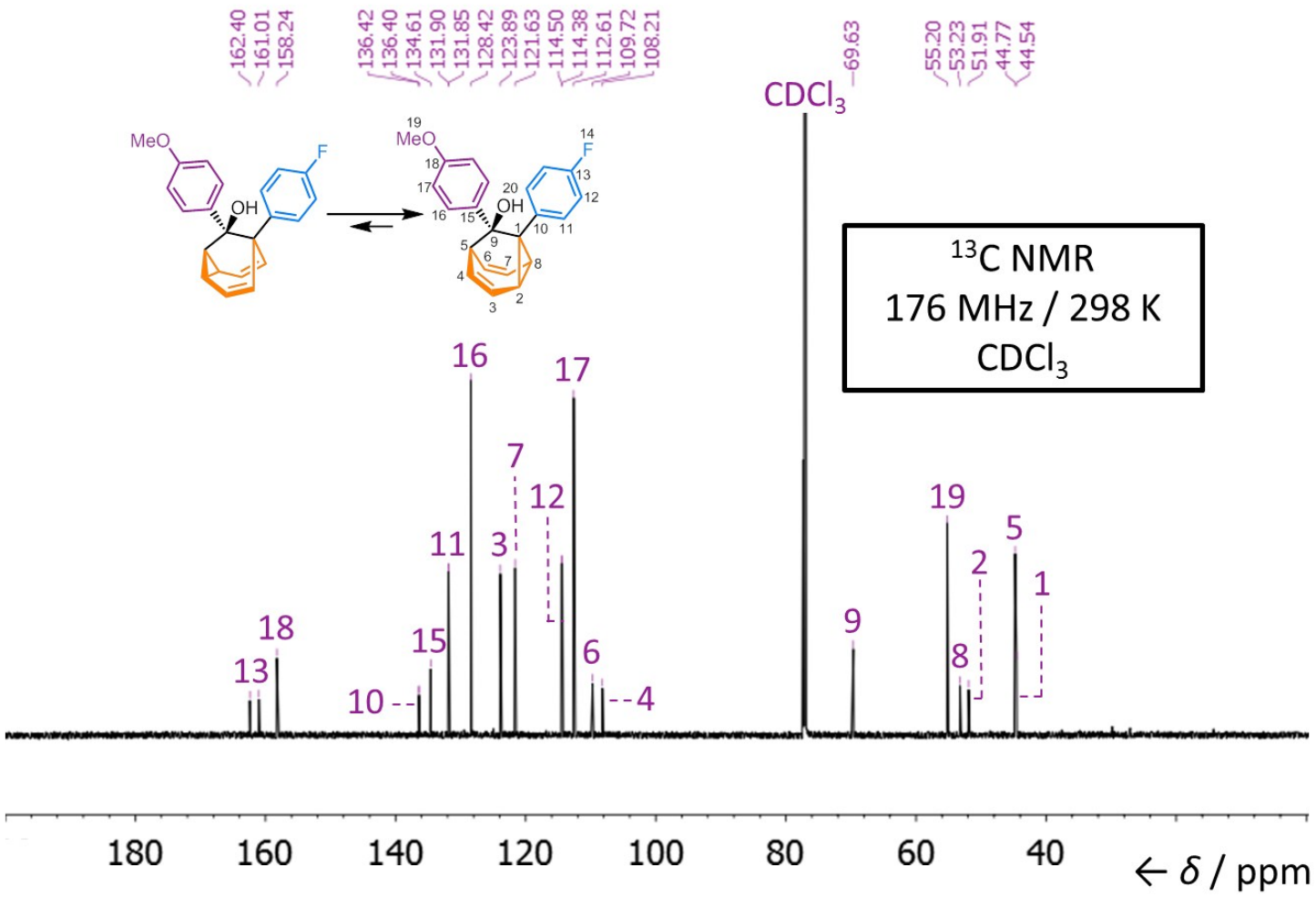

Figure S36. ^{13}C NMR Spectrum of **1d**.

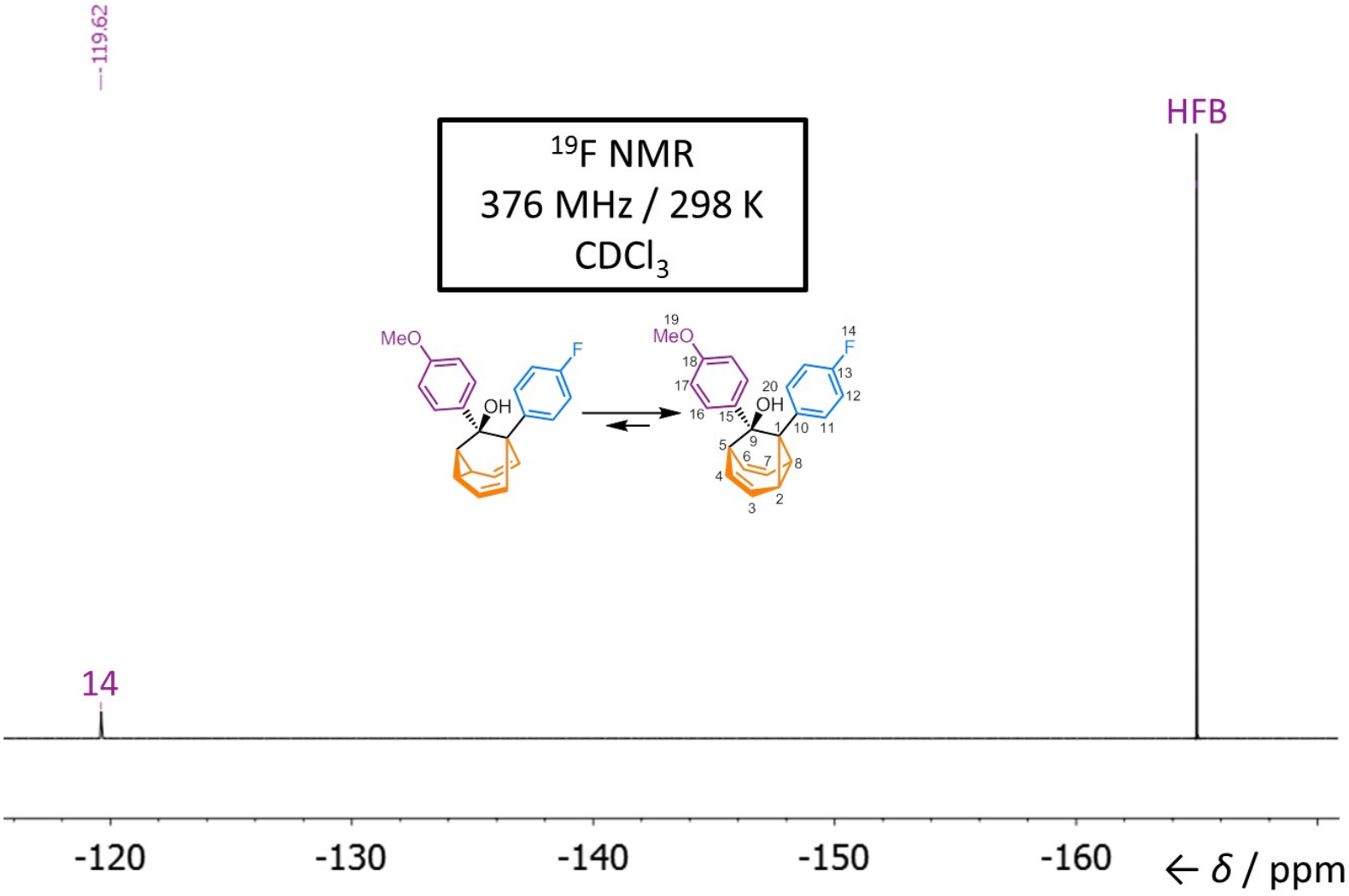

Figure S37. ^{19}F NMR Spectrum of **1d**.

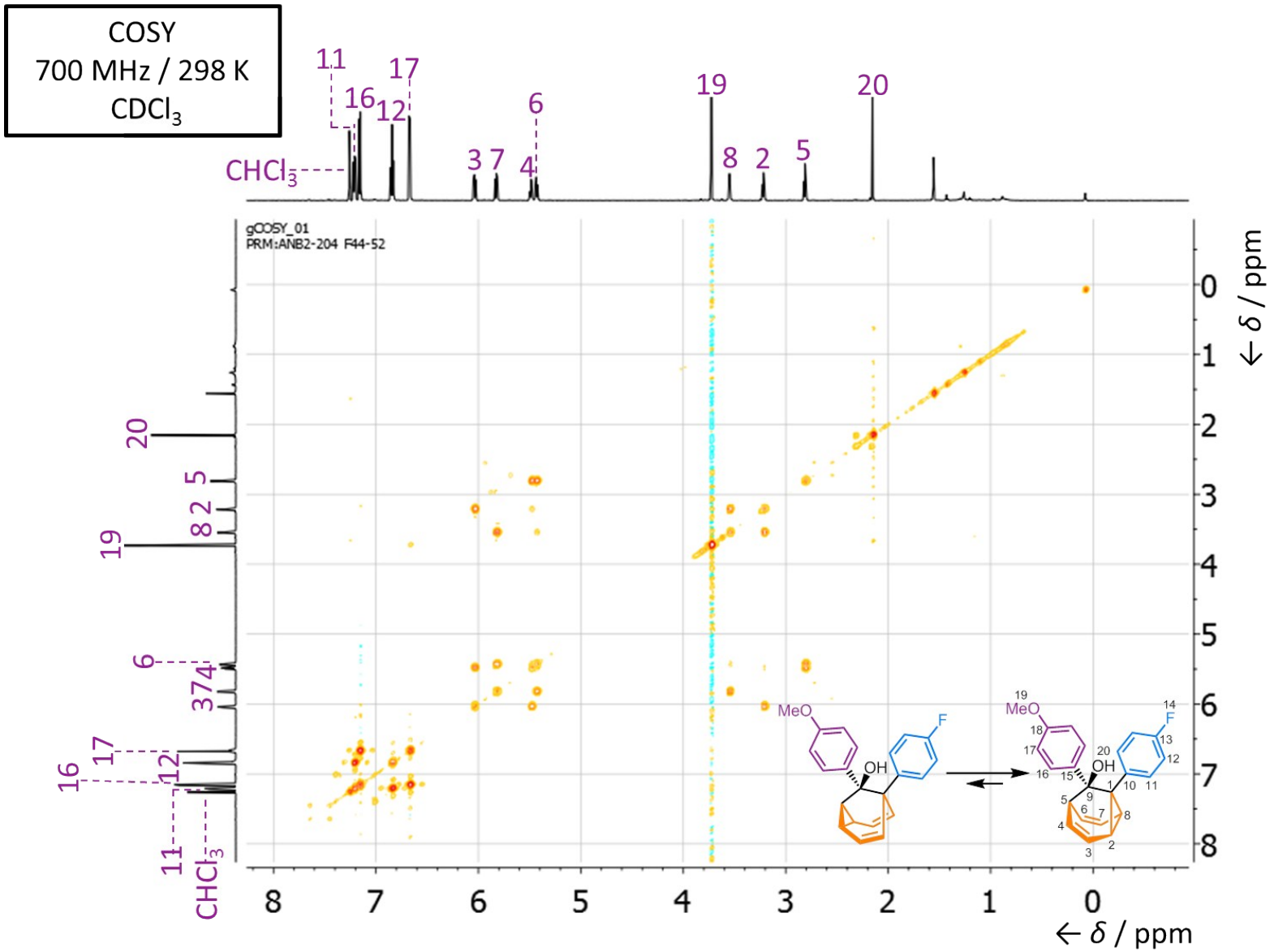

Figure S38. COSY Spectrum of **1d**.

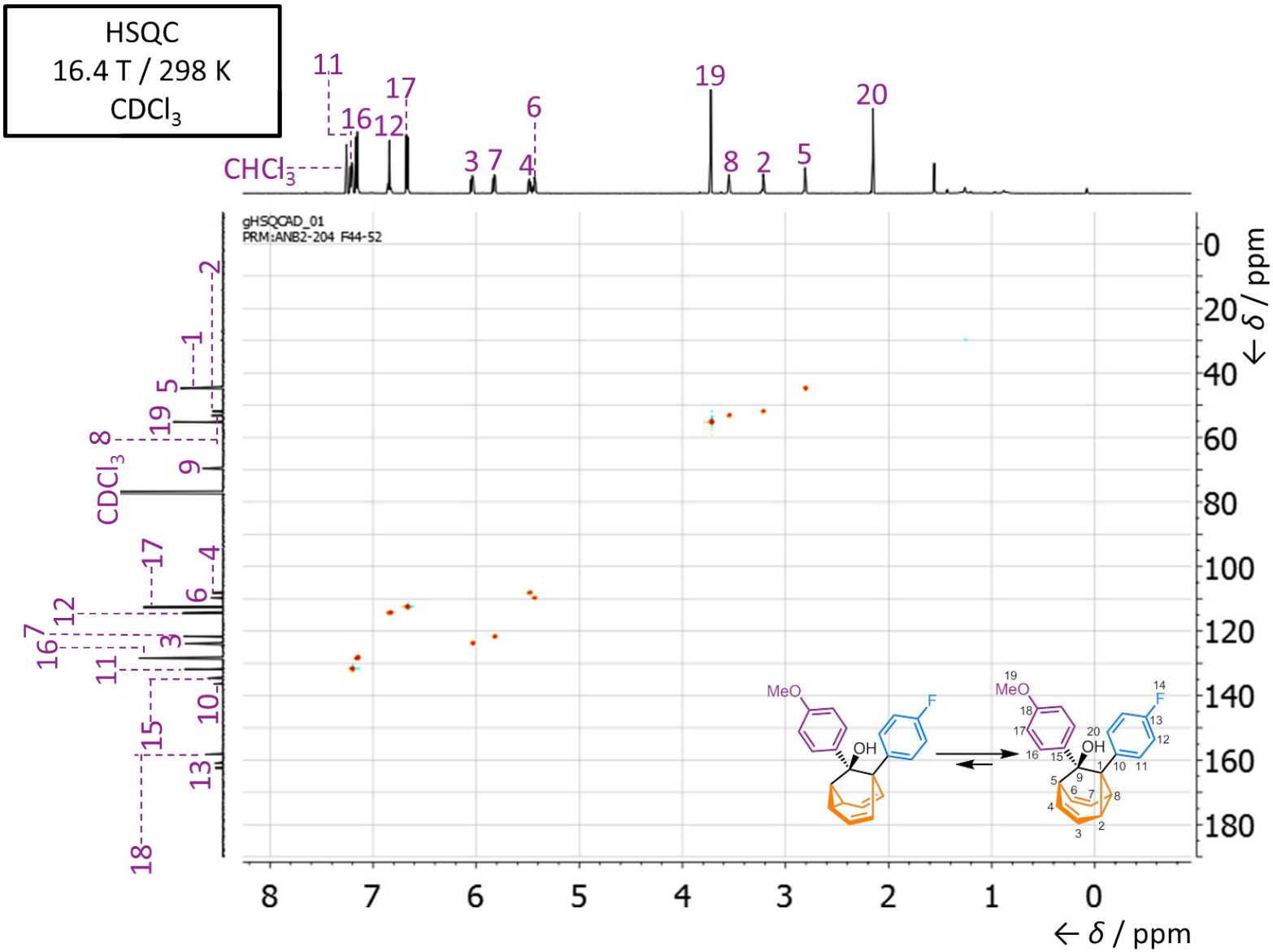

Figure S39. HSQC Spectrum of **1d**.

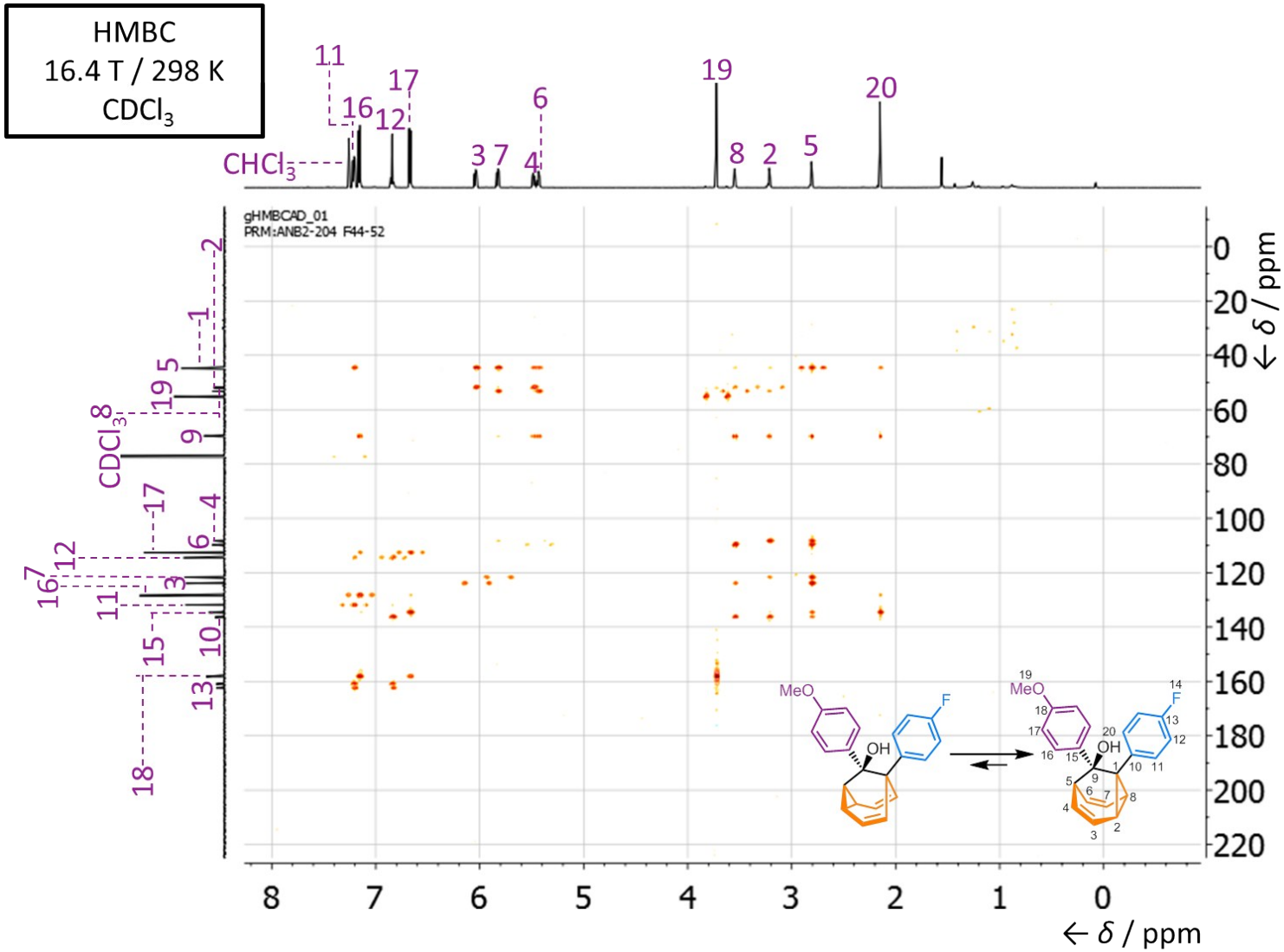

Figure S40. HMBC Spectrum of **1d**.

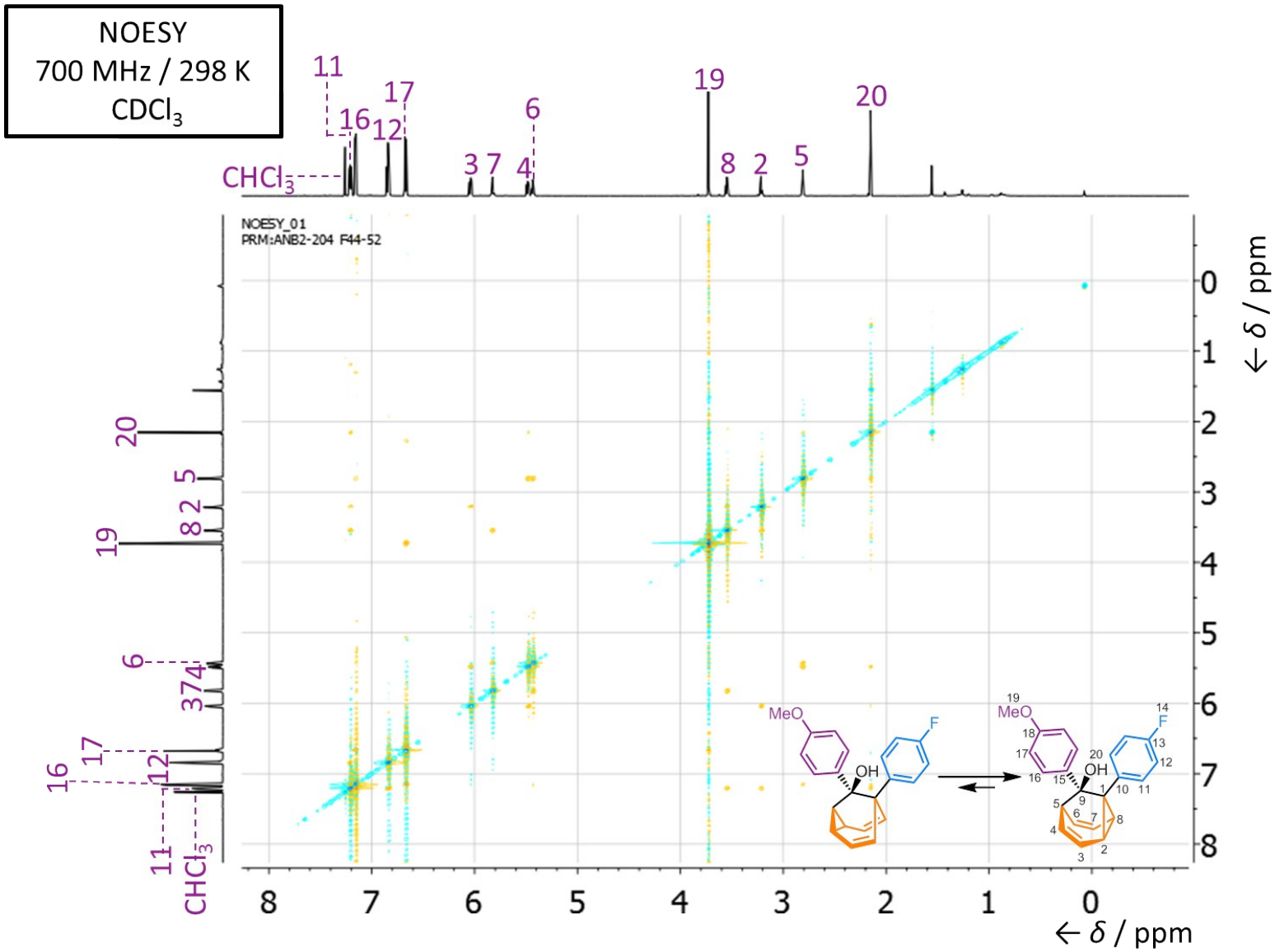

Figure S41. NOESY Spectrum of **1d**.

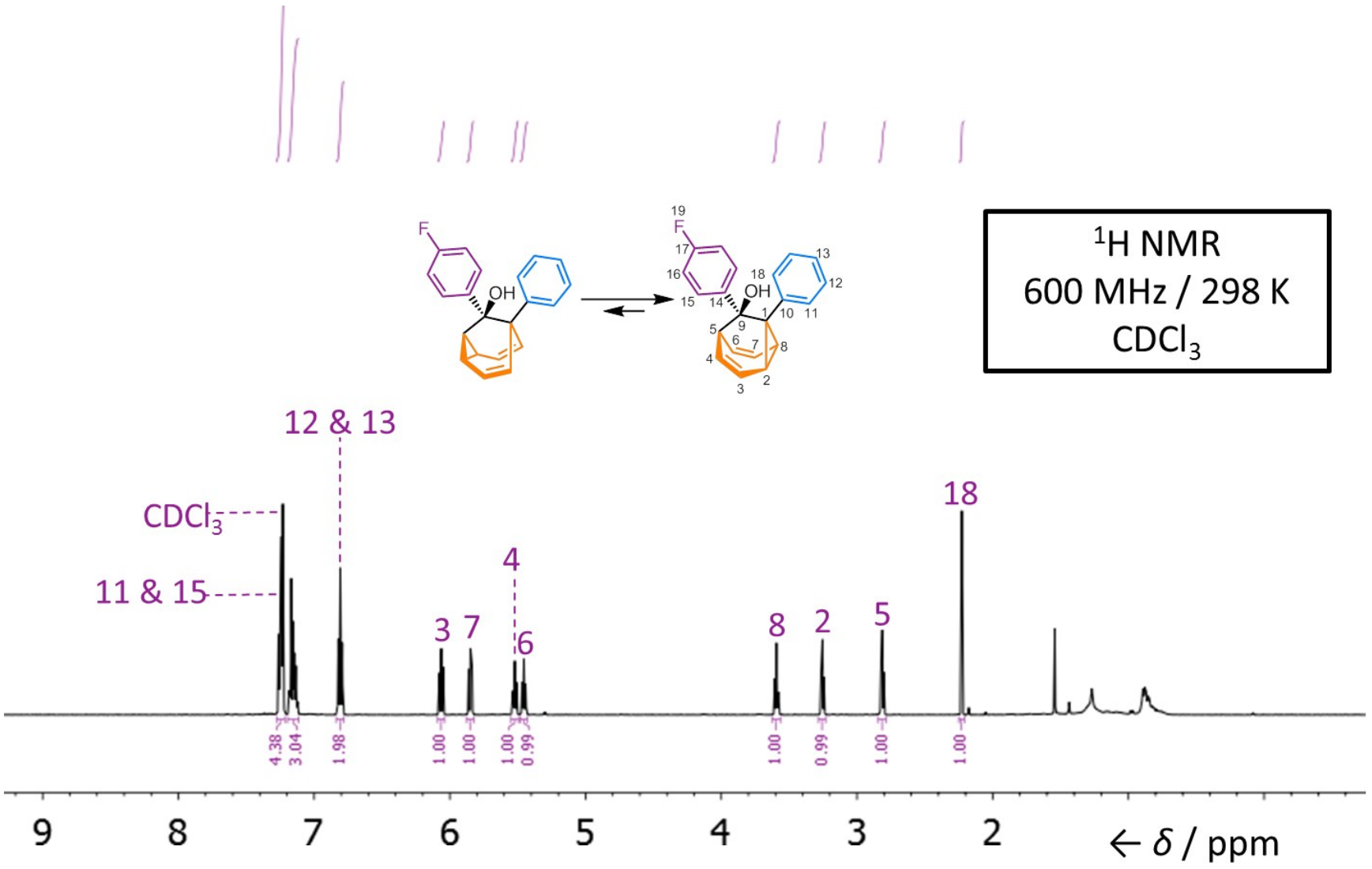

Figure S42. ^{1}H NMR Spectrum of **1e**.

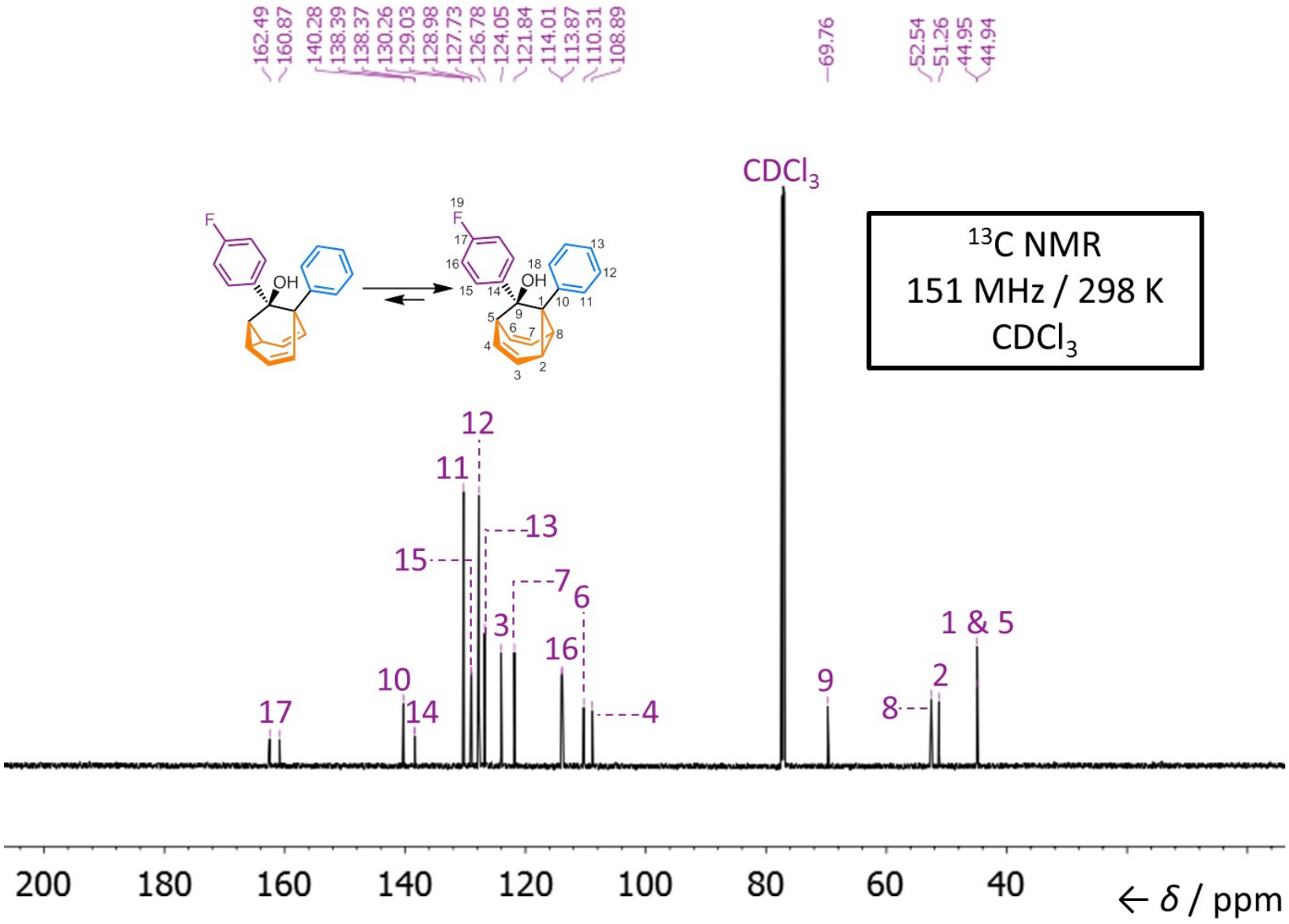

Figure S43. ^{13}C NMR Spectrum of **1e**.

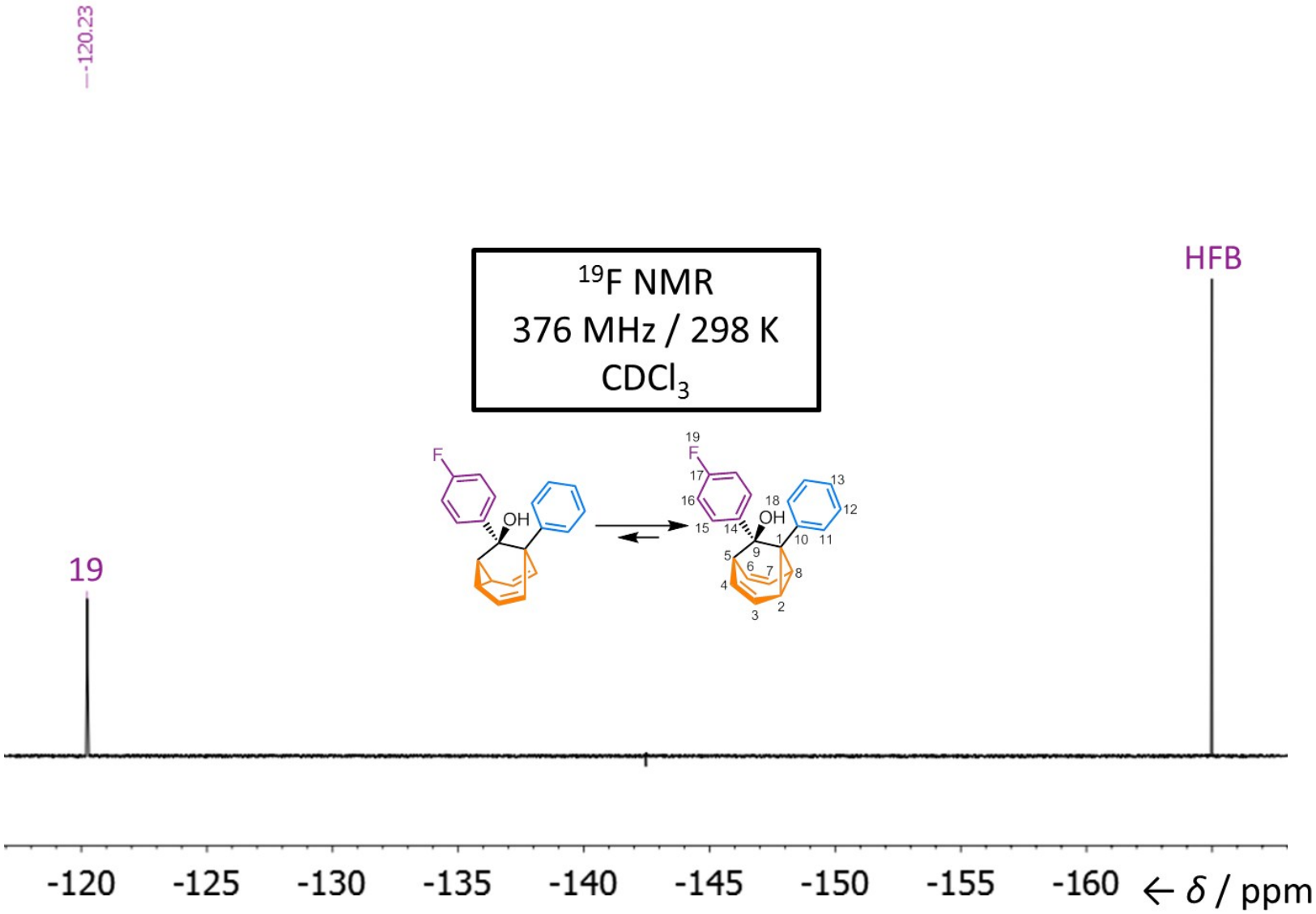

Figure S44. ^{19}F NMR Spectrum of **1e**.

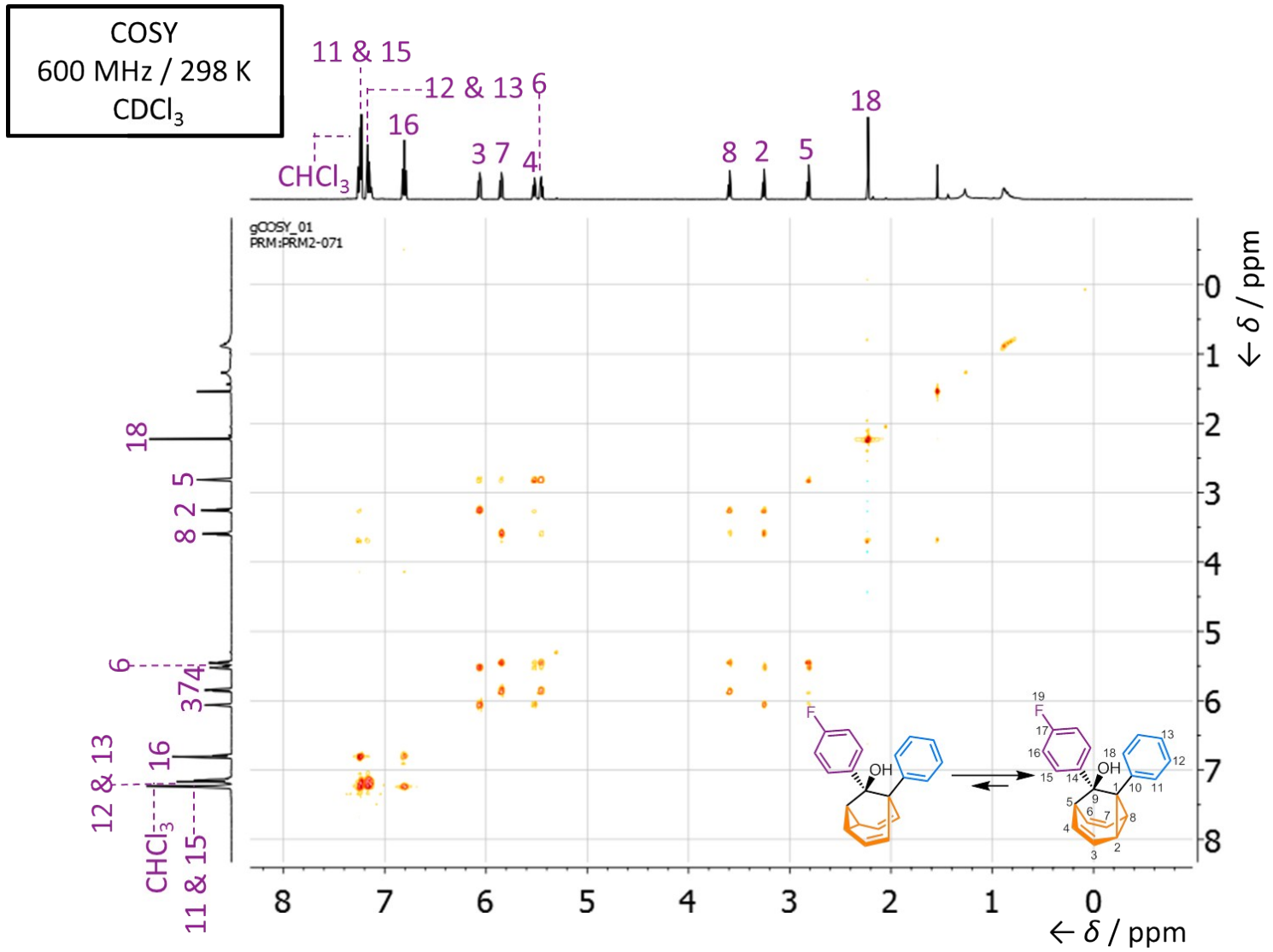

Figure S45. COSY Spectrum of **1e**.

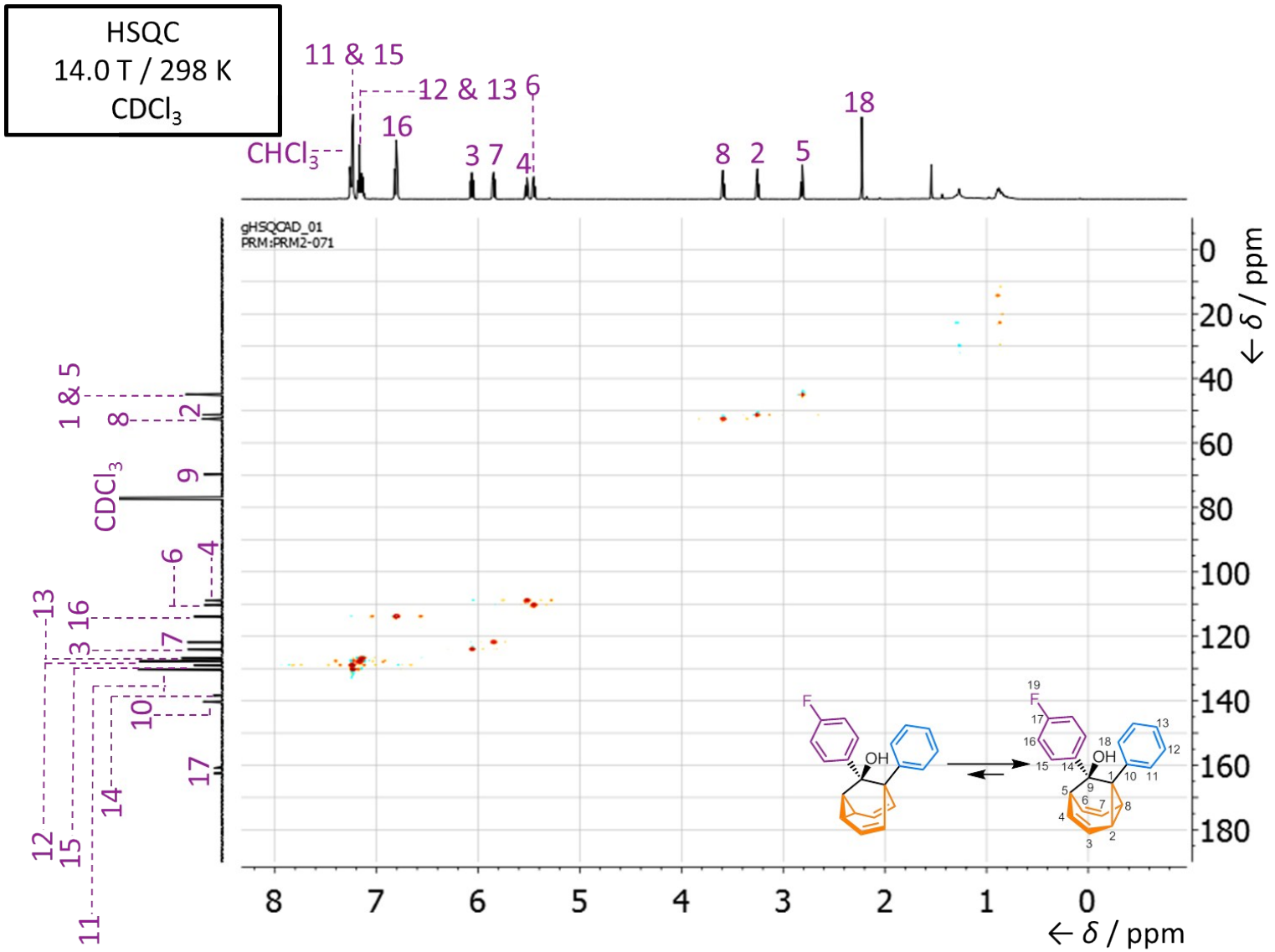

Figure S46. HSQC Spectrum of **1e**.

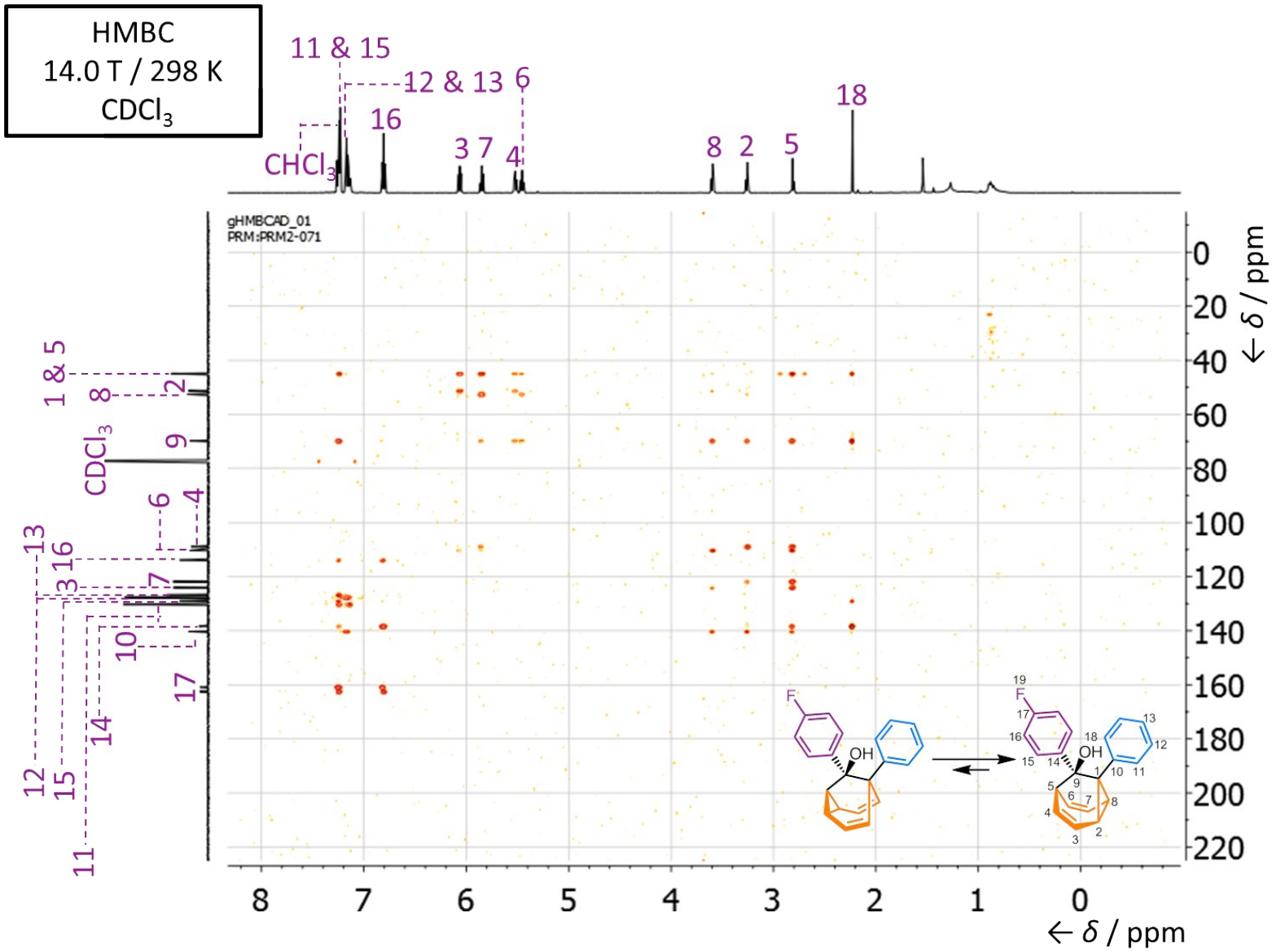

Figure S47. HMBC Spectrum of **1e**.

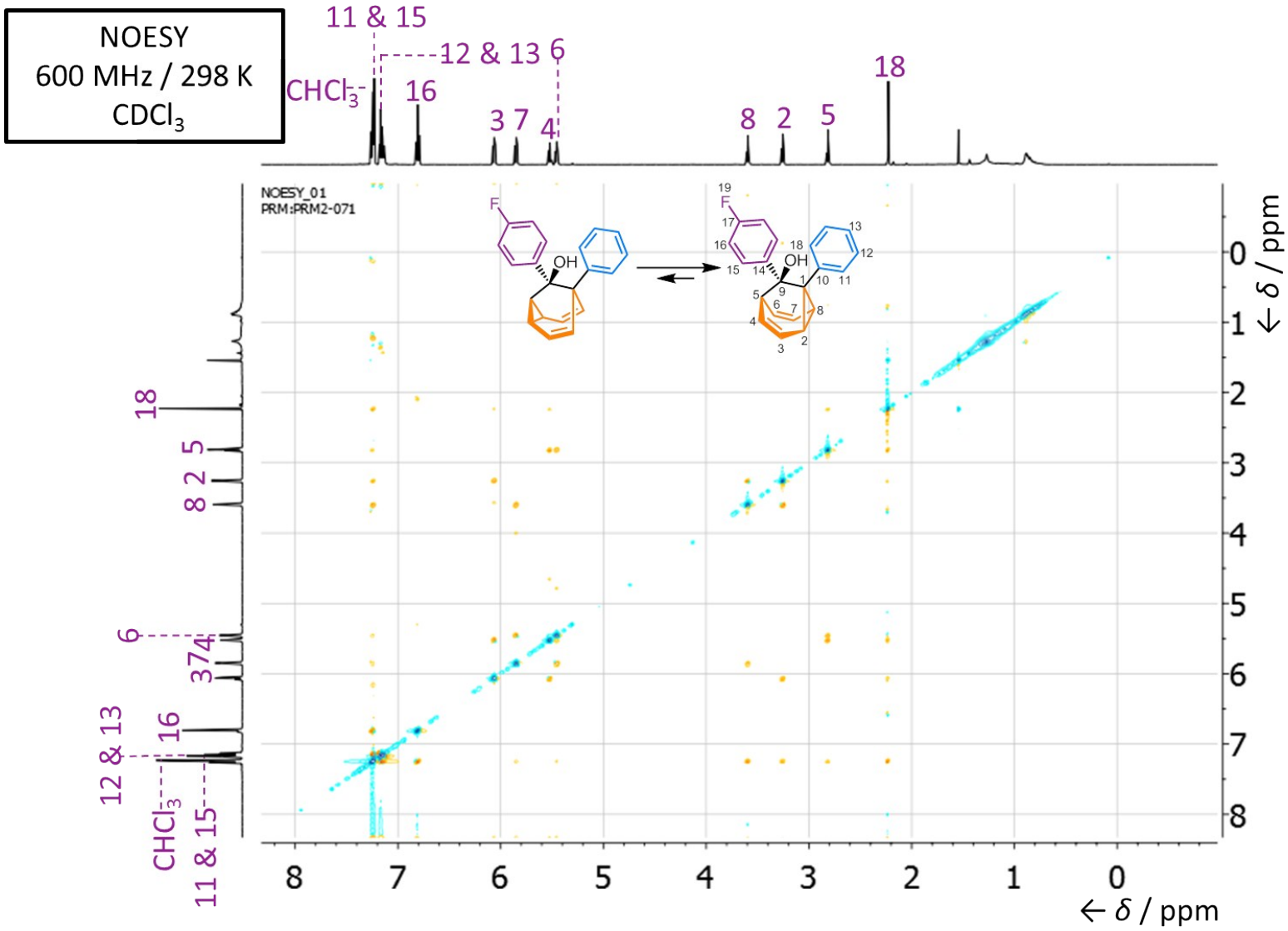

Figure S48. NOESY Spectrum of **1e**.

3.1 Structural Assignment by Two-Dimensional (2D) NMR

In order to determine which structure, **1** or **1′**, is the major species present in solution, we used 2D NMR spectroscopy. Briefly, we are able to differentiate the signals arising from the two barbaralane positions next to the tertiary alcohol based on the fact that one is a quaternary centre (position 1/5′), which gives rise to a lower intensity ^{13}C signal on account of its long relaxation time, and the other is a tertiary centre (position 5/1′). Position 5/1′ is easily distinguishable from the other tertiary alkyl ^{13}C signals as the protons at positions 2/4′ and 8/6′ (linked to the ^{13}C by HSQC) show a COSY correlation (e.g., Figure S17, blue dashed line). From here, we are then able to assign the structure as either **1** instead of **1′** because we observe that 5/1′ bridges the *cis*-dialkylolefins as it correlates *via* COSY (e.g., Figure S17, purple dashed line) to the olefins at positions 4 and 6 (in structure **1**) but not the cyclopropyl ring at positions 2′ and 8′ (in structure **1′**).

3.2 Estimation of Equilibrium Constants Based on Chemical Shifts

In solution, **1** and **1′** are present in unequal proportions ($p_{\mathbf{1}}$ and $p_{\mathbf{1'}}$). In the fast exchange regime, $p_{\mathbf{1}}$ and $p_{\mathbf{1'}}$ can be estimated by treating the experimentally observed chemical shift (δ_{obs}) as a weighted average of the chemical shifts of the individual components, $\delta_{\mathbf{1}}$ and $\delta_{\mathbf{1'}}$, according to Equation 1:

$$\delta_{obs} = p_1\delta_1 + p_{1'}\delta_{1'} \qquad \text{Equation 1}$$

We estimated equilibrium constants for **1**/**1′** in solution by comparing the δ_{obs} values measured from ^{13}C NMR spectra (Section 3) to those typical for the functional groups present in the molecule, allowing us to approximate $\delta_{\mathbf{1}}$ and $\delta_{\mathbf{1'}}$. A divinyl cyclopropane group has a ^{13}C chemical shift of ~25 ppm (see reference 9 of the main text), while a *cis*-dialkylolefin group has a ^{13}C chemical shift of ~135 ppm (see reference 10 of the main text) in $CDCl_3$ at 298 K. The equilibrium constant K relates to $p_{\mathbf{1}}$ and $p_{\mathbf{1'}}$, as well as the free energy difference ΔG, according to Equation 2:

$$K = \frac{p_1}{p_{1'}} = e^{-\frac{\Delta G}{RT}} \qquad \text{Equation 2}$$

4. Variable-Temperature (VT) and Solid-State NMR (ssNMR) Spectroscopy

4.1 Compound 1a/1a′

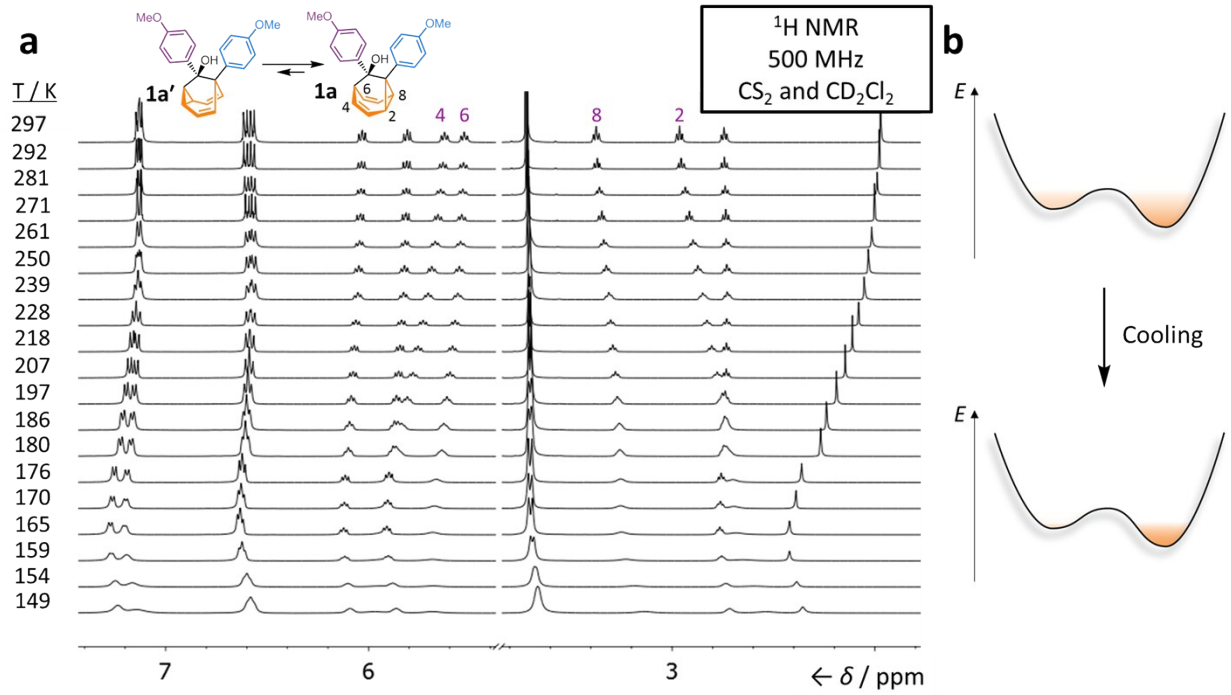

Figure S49. (**a**) Partial ^{1}H NMR spectra of **1a/1a′**, recorded from 297 K to 149 K and (**b**) schematic illustration of the change in equilibrium population on a simplified potential energy surface as temperature decreases.

The barbaralanes undergo a rapid and reversible Cope rearrangement in solution. Isomer **1a** is in fast exchange with isomer **1a′**, giving rise to a single set of resonances in the ^{1}H NMR spectrum recorded (Figure S49a) at ambient temperature. The chemical shift of each nucleus is indicative of its time-averaged chemical environment. For example, the proton labelled as position 2 in Figure S49a has character arising from being part of both a divinyl cyclopropane (**1a**) and a *cis*-dialkyl olefin (**1a′**) environment. Its chemical shift of 2.9 ppm falls between the limits of ~1.8 ppm (typical[7] for a divinyl cyclopropane) and ~5.4 ppm (typical[8] for a *cis*-dialkylolefin) that would be expected if the structure was fixed in either state. It is, however, closer to the limit expected for a divinyl cyclopropane, therefore, **1a** appears to be the major isomer in solution. Similarly, position 8 has mostly cyclopropane character, while position 4 and 6 have a majority of olefin character,

confirming this conclusion. Upon reducing the temperature, the signals relating to these nuclei undergo marked changes in their chemical shifts. The signals arising from protons 2 and 8 shift upfield, becoming more cyclopropane-like, while the resonances of protons 4 and 6 shift downfied, becoming more olefin-like. These changes arise (Figure 49b) from perturbation of the equilibrium position upon cooling. At lower temperatures, there is less of the minor isomer present, so the NMR resonances shift towards the limits expected if the major isomer was the sole species. The signals appear to remain in fast exchange, even at very low temperatures. Below 154 K, the signals begin to broaden into the baseline, suggesting that the coalescence temperature may be in that region.

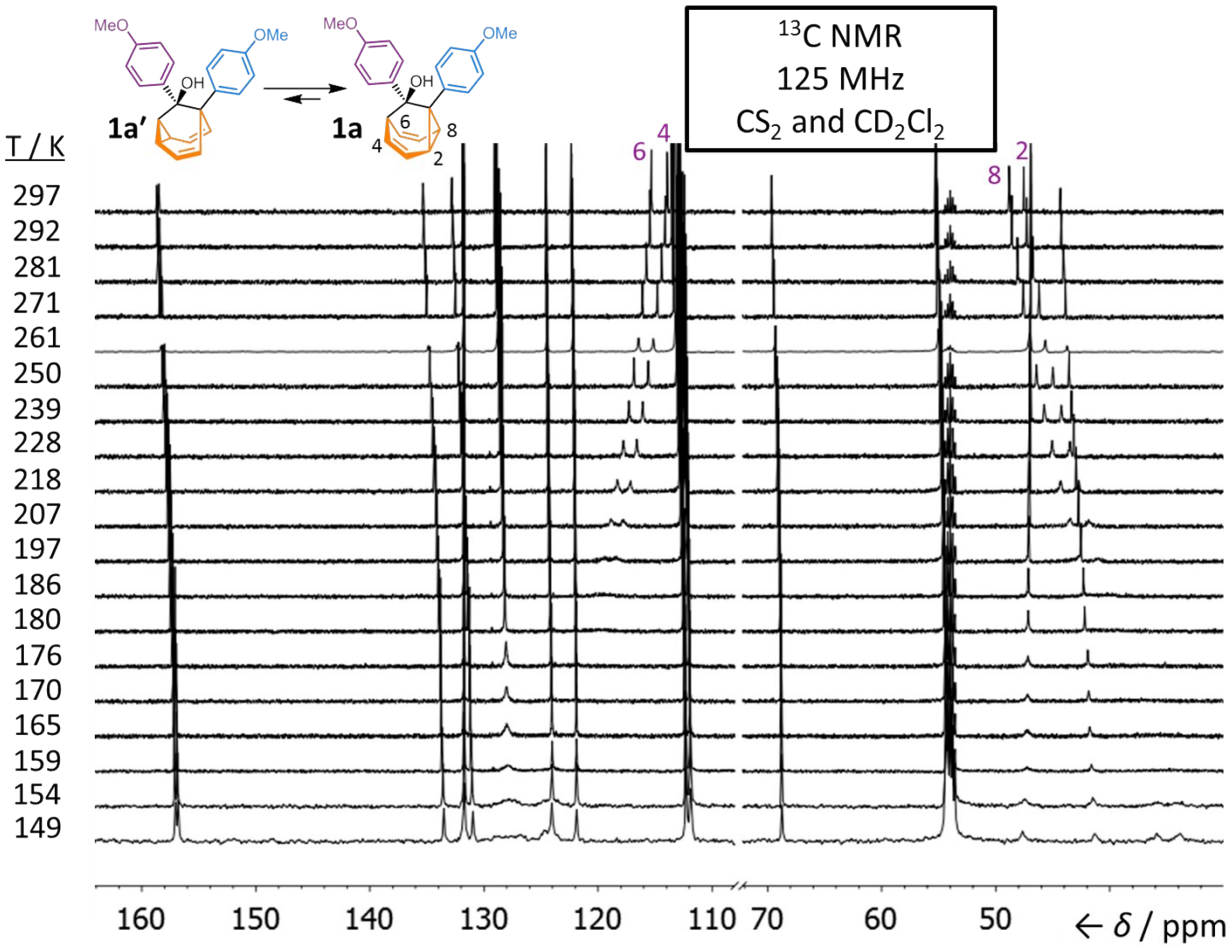

Figure S50. ^{13}C NMR spectra of **1a/1a'**, recorded from 297 K to 149 K.

The VT ^{13}C NMR spectra for **1a/1a′** also helps to confirm that the chemical shifts are a weighted average of both the isomers and that the equilibrium shifts in favour of the major isomer as the temperature is decreased. This is demonstrated in the ^{13}C NMR spectra (Figure S50) because the positions marked as 6 and 4 shift downfield becoming more olefin-like, whereas the positions marked as 8 and 2 shift further upfield becoming more cyclopropane-like.

Solid-state NMR spectroscopy for **1a** was acquired and then compared against the ^{13}C NMR spectra acquired at the temperature of 149 K in the solution state. An interrupted decoupling solid-state experiment was also acquired so that quaternary and primary carbons could be determined and then assigned correctly. The comparison between the spectra helps to corroborate our hypothesis that as we go lower in temperature in the solution state, the equilibrium shifts towards the major isomer (**1a**) and that less of the minor isomer (**1a′**) is present. We also observe that the solution state spectra acquired at 149 K is very similar to the solid-state spectra (especially in the upfield section of Figure S51). As the spectra are alike, this helps us to confirm that the assignment within the solution state is correct (at 298 K and at 149 K) and at the same time, the interrupted decoupling experiment and CASTEP calculations (*vide infra*), have allowed us to assign the majority of the peaks in the solid-state spectra.

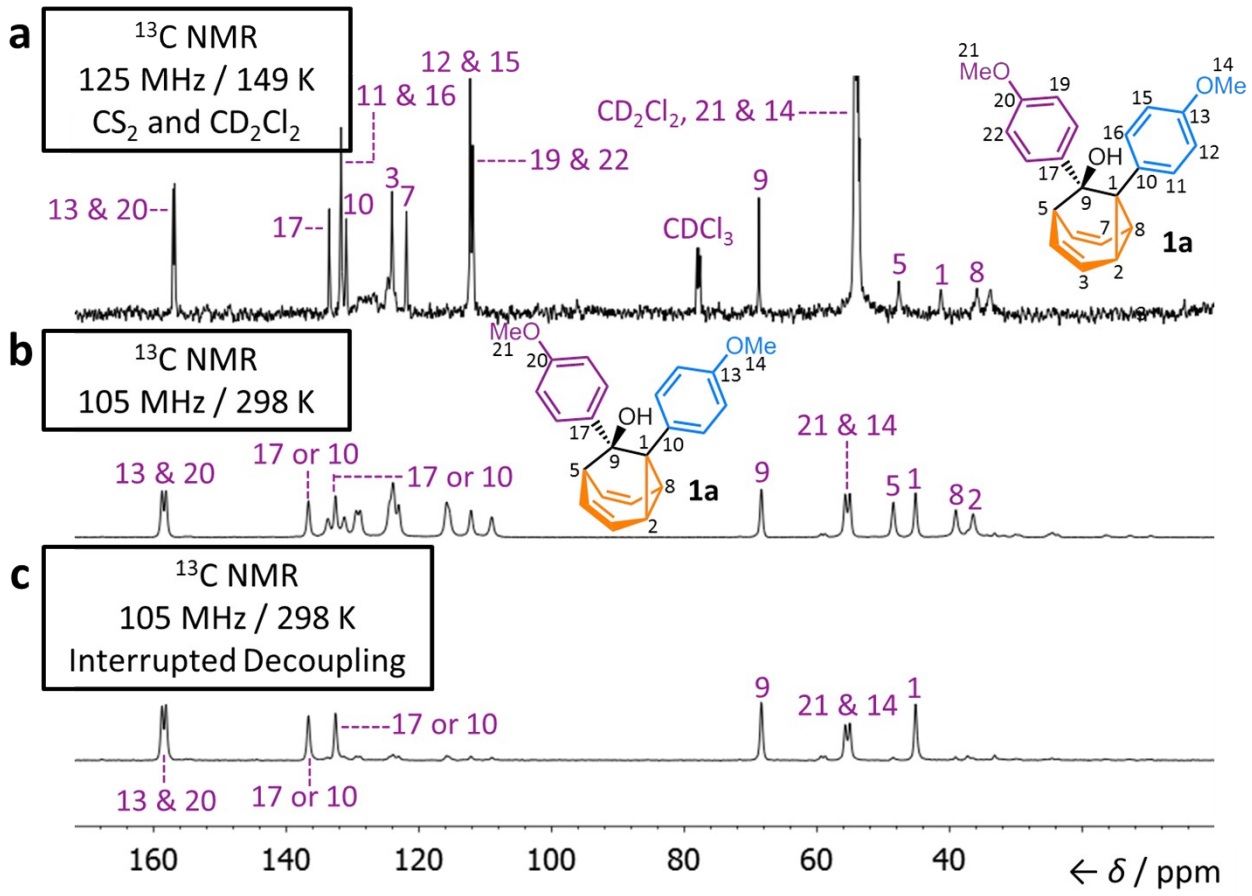

Figure S51. Comparison of ^{13}C NMR spectra of **1a** under different conditions: (**a**) in a CS_2–CD_2Cl_2 solution at 149 K, (**b**) in the solid state, and (**c**) in the solid state using an interrupted decoupling pulse sequence to determine quaternary and primary carbons.

4.2 Compound 1b/1b′

Compound **1b**/**1b′** is also a fluxional mixture (where the major isomer in solution is **1b**), which interconverts between two nondegenerate isomers. As with compound, **1a**/**1a′**, the ^{1}H NMR spectrum at ambient temperature only demonstrates a single set of resonances where the chemical shifts represent an average of both the chemical environments within the different valence isomers. As the temperature is reduced for **1b**/**1b′**, the resonances of the protons 4 and 6 shift downfield, whereas the resonances of the protons 8 and 2 shift upfield. The changes observed in the nuclei are identical to that of **1a**/**1a′**. This data from this compound corroborates that **1b** is the major isomer

at lower temperatures and that although the resonances shift the equilibrium towards the major isomer, the signals are still interconverting even at very low temperatures. The rearrangement only becomes slow relative to the chemical shift differences of exchanging sites at the lowest accessible[9] temperatures—the lineshapes of peaks such as 6/8′ and 8/6′ broaden (Figure 52) below 186 K and merge with the baseline at 149 K. This observation is consistent with a low energy barrier, $\Delta G^{\dagger}$, similar to those reported previously[10] for barbaralane Cope rearrangements, i.e., 30–40 kJ·mol^{-1}.[11]

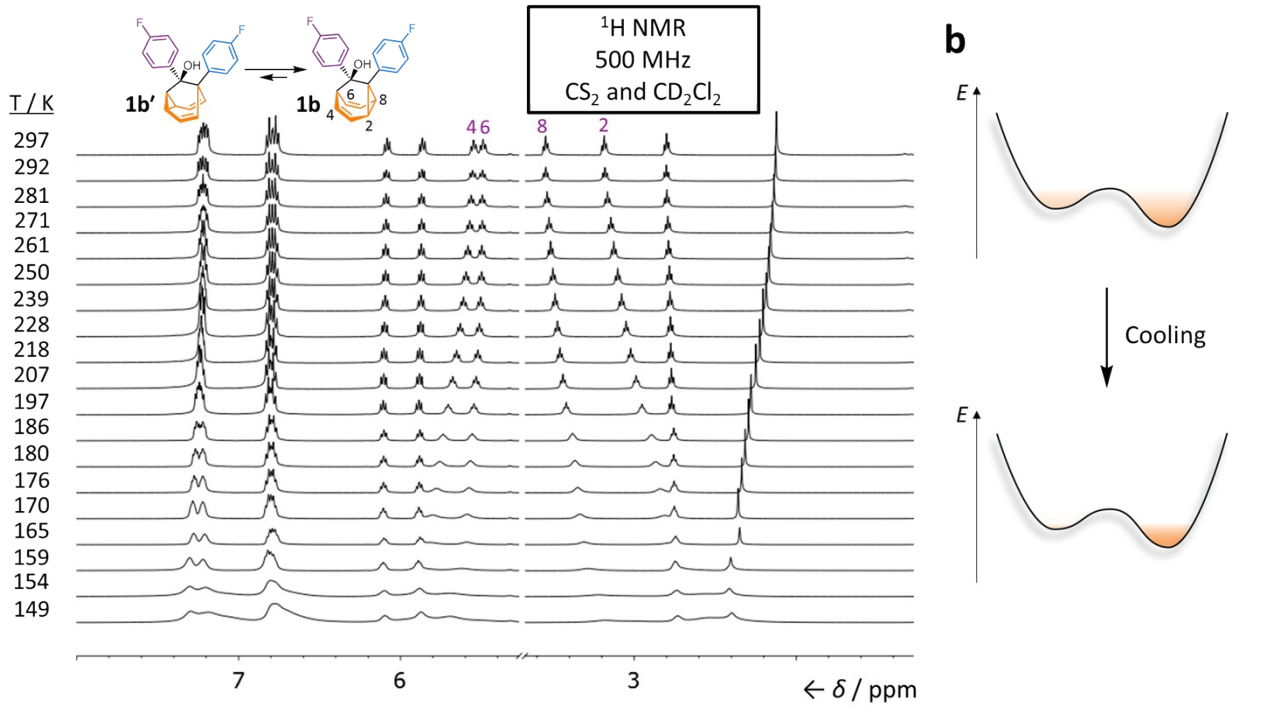

Figure S52. (**a**) Partial ^{1}H NMR spectra of **1b/1b′**, recorded from 297 K to 149 K and (**b**) schematic illustration of the change in equilibrium population on a simplified potential energy surface as temperature decreases.

The VT ^{13}C NMR spectra of **1b/1b′** (Figure S53) are near-identical to the VT ^{13}C NMR spectra of **1a/1a′**. As in Figure S50, the positions marked as 6 and 4 shift downfield becoming more olefin-like, whereas the positions marked as 8 and 2 shift further upfield becoming more cyclopropane-like. The data from the VT ^{13}C NMR for **1b/1b′** validates that the equilibrium shifts in favour of the major isomer as the temperature is lowered.

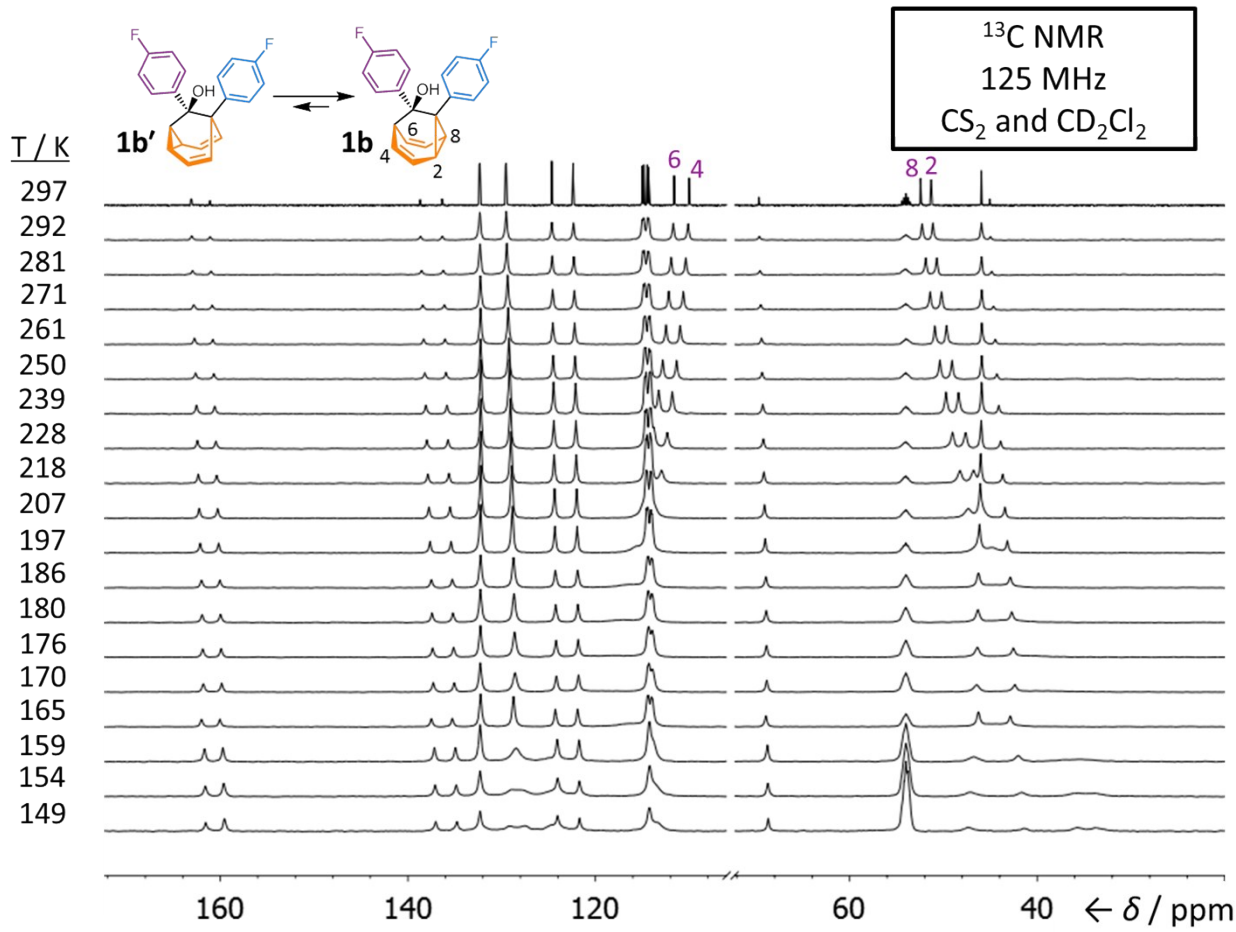

Figure S53. Partial ^{13}C NMR spectra of **1b/1b′**, recorded from 297 K to 149 K.

Solid-state NMR experiments for **1b′** were performed, including an interrupted decoupling experiment, and these were compared against the solution-sate ^{13}C NMR spectra for **1b/1b′** acquired at the temperature of 149 K. Comparing the solid-state NMR spectra and the solution state spectrum, there are clear differences. The solid-state NMR signals do not match up with the solution-state NMR signals, as would be expected if the structures are not the same. At 149 K, the solution phase equilibria is biased towards **1b**, whereas isomer **1b′** is present as the sole isomer in the solid state. The dissimilarity between the spectra confirms that the species in the solution and solid states are different. At the same time, the solid-state NMR spectrum helps to confirm the structure of **1b′**, as the interrupted decoupling experiment shows that the position marked as 5′ is a

quaternary carbon (Figure S54c), whereas in the solid-state NMR specturm of **1a**, the quaternary carbon is labelled as 1 (Figures S51b and S51c) and this peak lines up in a near-identical manner to the low-temperature solution state NMR spectrum. In Figure S54, the upfield peaks representing the tricyclic barbaralane framework in the solution state spectrum, do not line up with the peaks in the solid-state spectrum. Again, these observations show that different isomers are adopted in the solution and solid-state.

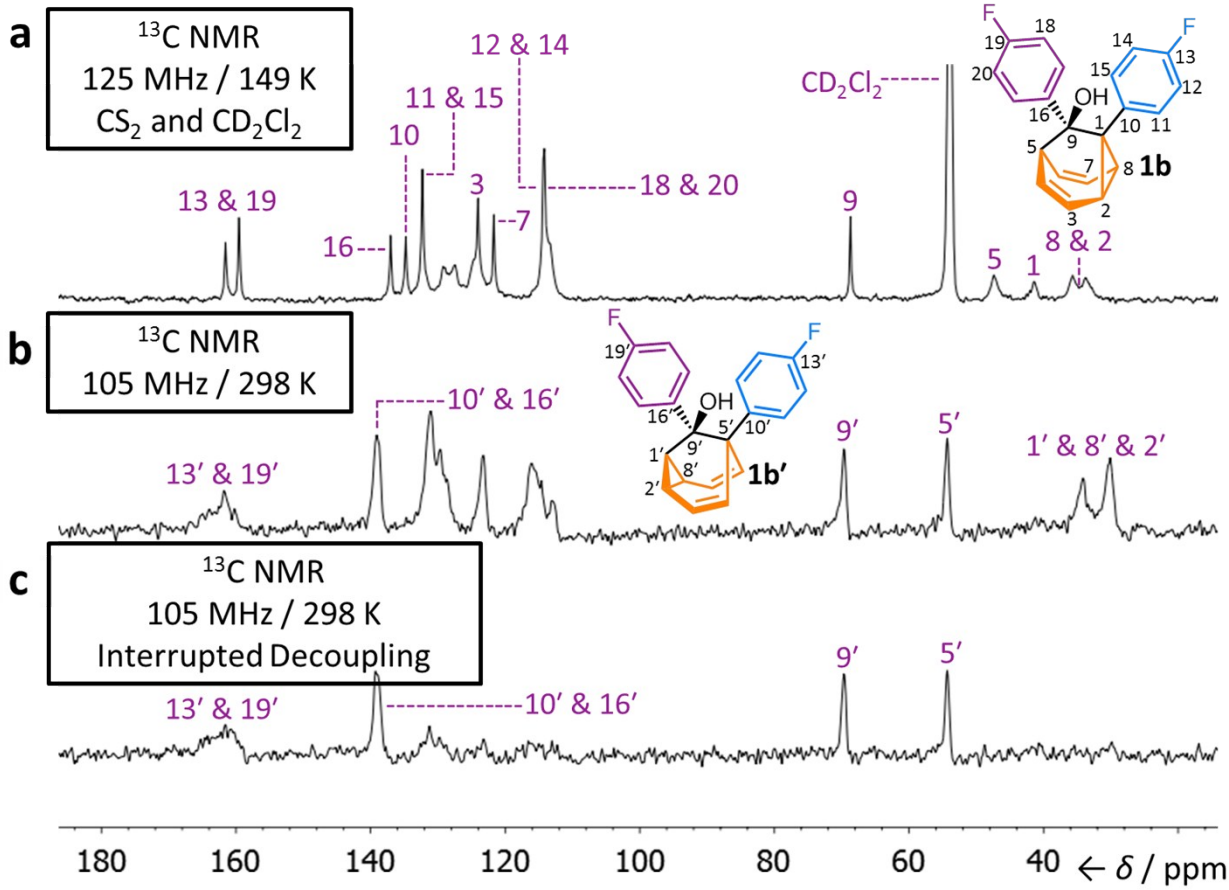

Figure S54. Comparison of ^{13}C NMR spectra of **1b/1b′** under different conditions: (**a**) in a CS_2–CD_2Cl_2 solution at 149 K, (**b**) in the solid state, and (**c**) in the solid state using an interrupted decoupling pulse sequence to determine quaternary carbons.

5. X-Ray Crystallographic Analysis

5.1 1-(4-Fluorophenyl)tricyclo[3.3.1.0^{2,8}]nona-3,6-dien-9-one

Crystals of 1-(4-fluorophenyl)tricyclo[3.3.1.^{2,8}]nona-3,6-dien-9-one suitable for X-ray diffraction were grown by slow evaporation of a hexanes–CH_2Cl_2 solution at 5 °C.

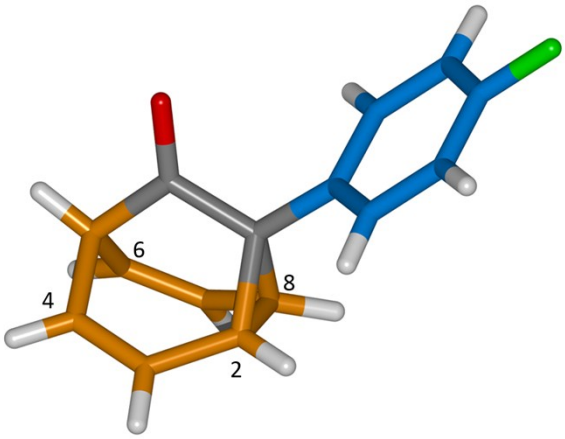

Figure S55. Solid-state structure of 1-(4-fluorophenyl)tricyclo[3.3.1.^{2,8}]nona-3,6-dien-9-one.

Crystal System: Orthohombic
Space group: $P2_12_12_1$
Unit Cell Parameters: a = 9.9209(4) Å, b = 9.9803(4) Å, c = 11.1024(4) Å, α = 90 °, β = 90 °, γ = 90 °, V = 1099.29(7) Å^3, Z = 4
Interatomic Distances / Å: C2–C8 = 1.54, C4···C6 = 2.41.
Calculated density: 1.36691 g·cm^{-3}

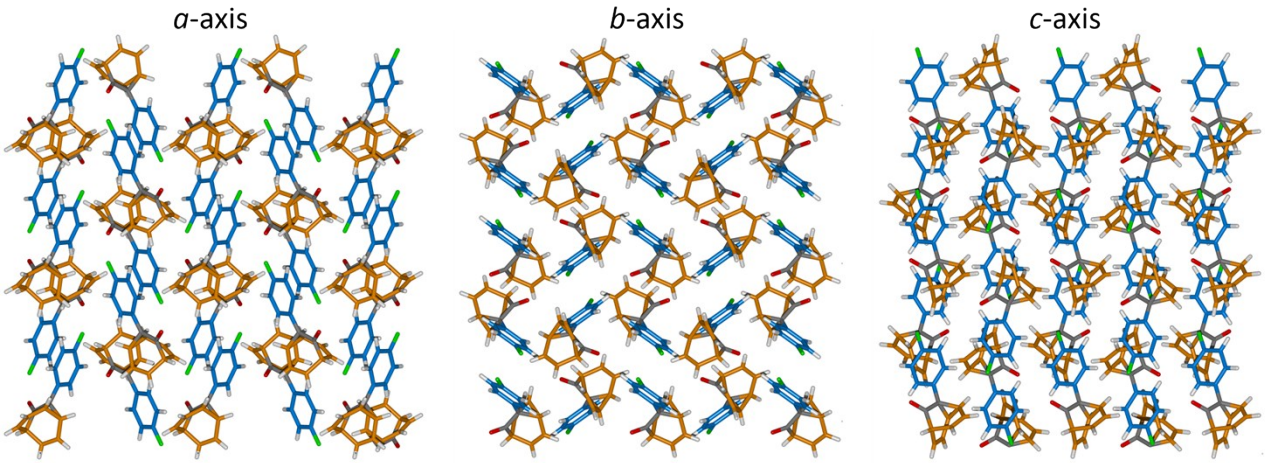

Figure S56. Solid-state superstructure of 1-(4-fluorophenyl)tricyclo[3.3.1.^{2,8}]nona-3,6-dien-9-one viewed along the three unit cell axes.

5.2 Compound 1a

Crystals of **1a** suitable for X-ray diffraction were formed through spontaneous crystallisation of a saturated CH_2Cl_2 solution upon standing. See Figure 3 in the main text.

Crystal System: Monoclinic
Space group: $P2_1/c$
Unit Cell Parameters: a = 13.5882(7) Å, b = 9.2068(5) Å, c = 14.8687(8) Å, α = 90 °, β = 111.2938(18) °, γ = 90 °, V = 1733.14(16) $Å^3$, Z = 4
Calculated density: 1.32748 $g \cdot cm^{-3}$

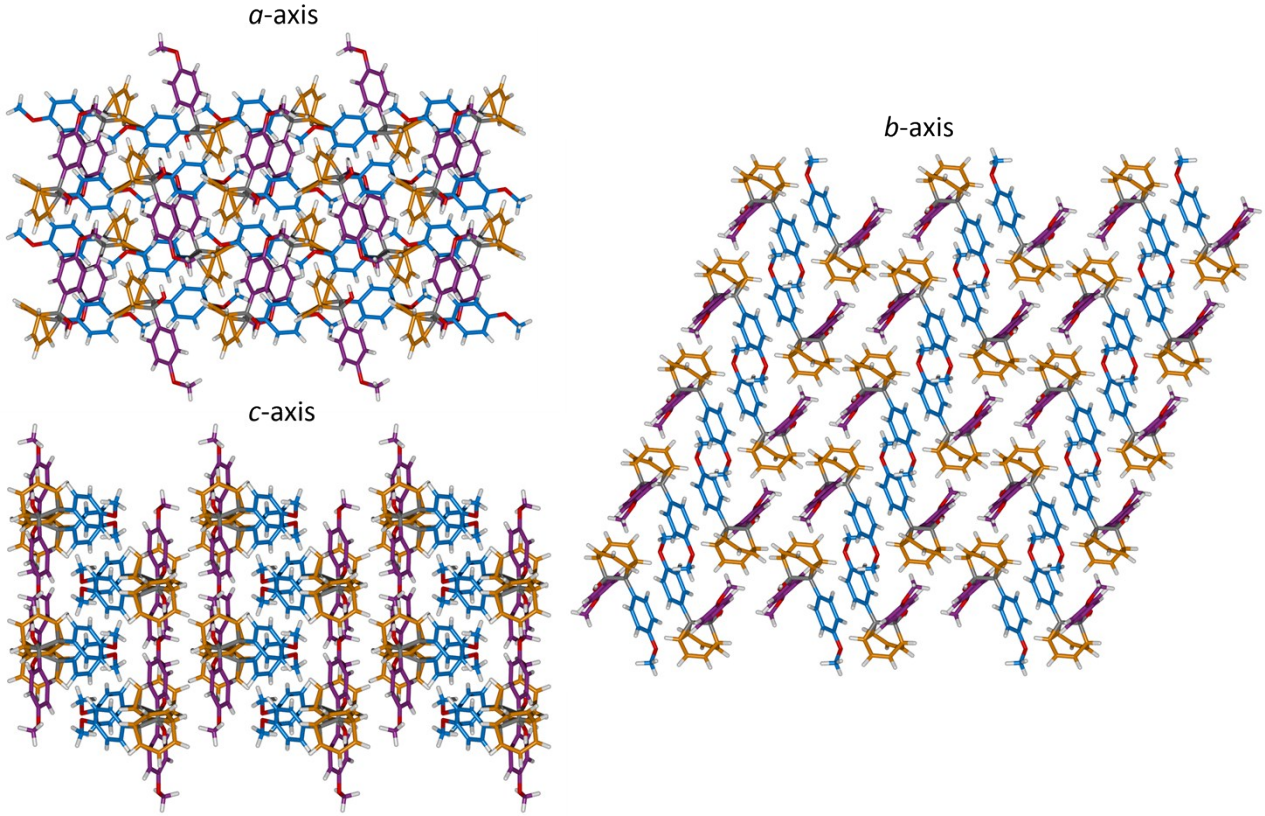

Figure S57. Solid-state superstructure of **1a** viewed along the three unit cell axes.

5.3 Compound 1b′

Crystals of **1b′** suitable for X-ray diffraction were grown by slow cooling of a hot and saturated MeCN solution. See Figure 3 in the main text.

Crystal System: Monoclinic
Space group: $P2_1/n$
Unit Cell Parameters: a = 9.7695(8) Å, b = 6.1770(5) Å, c = 24.650(2) Å, α = 90 °, β = 90.360(7) °, γ = 90 °, V = 1487.5(2) $Å^3$, Z = 4
Calculated density: 1.43926 $g \cdot cm^{-3}$

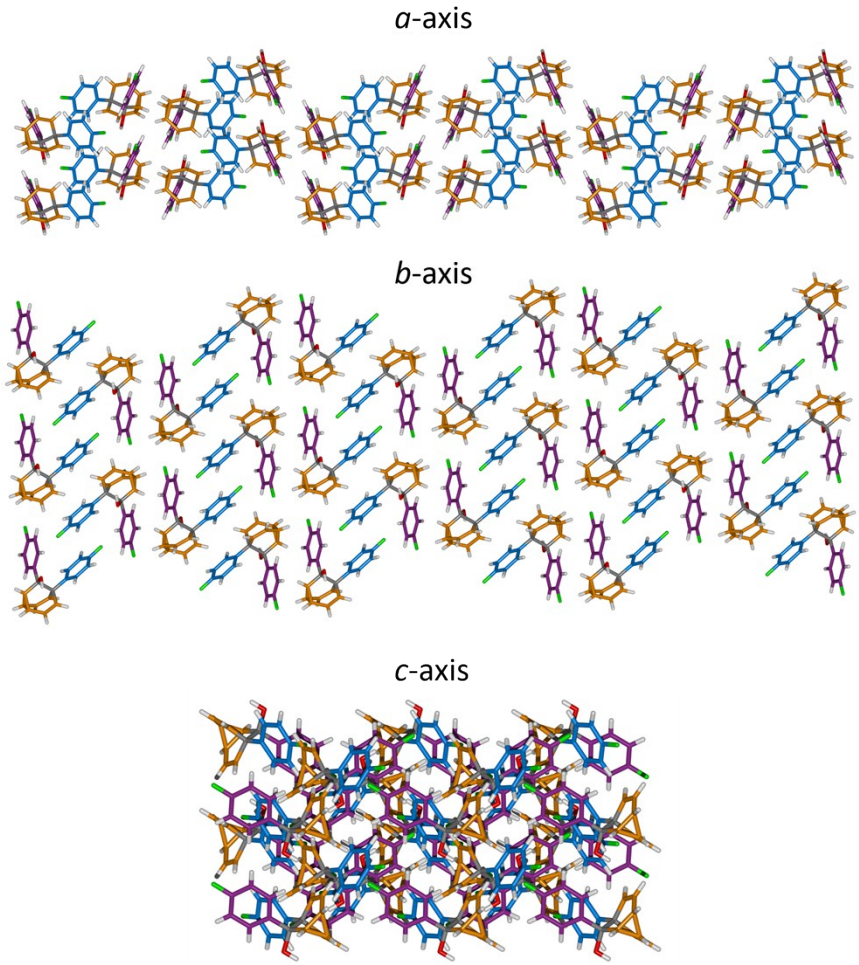

Figure S58. Solid-state superstructure of **1b′** viewed along the three unit cell axes.

5.4 Compound 1c

Crystals of **1c** suitable for X-ray diffraction were grown by slow cooling of a hot and saturated MeCN solution. See Figure 3 in the main text.

Crystal System: Monoclinic
Space group: $P2_1/c$
Unit Cell Parameters: a = 16.0612(11) Å, b = 7.1500(5) Å, c = 14.5266(10) Å, α = 90 °, β = 98.455(3)°, γ = 90 °, V = 1650.1(2) Å^3, Z = 4
Calculated density: 1.34589 g·cm^{-3}

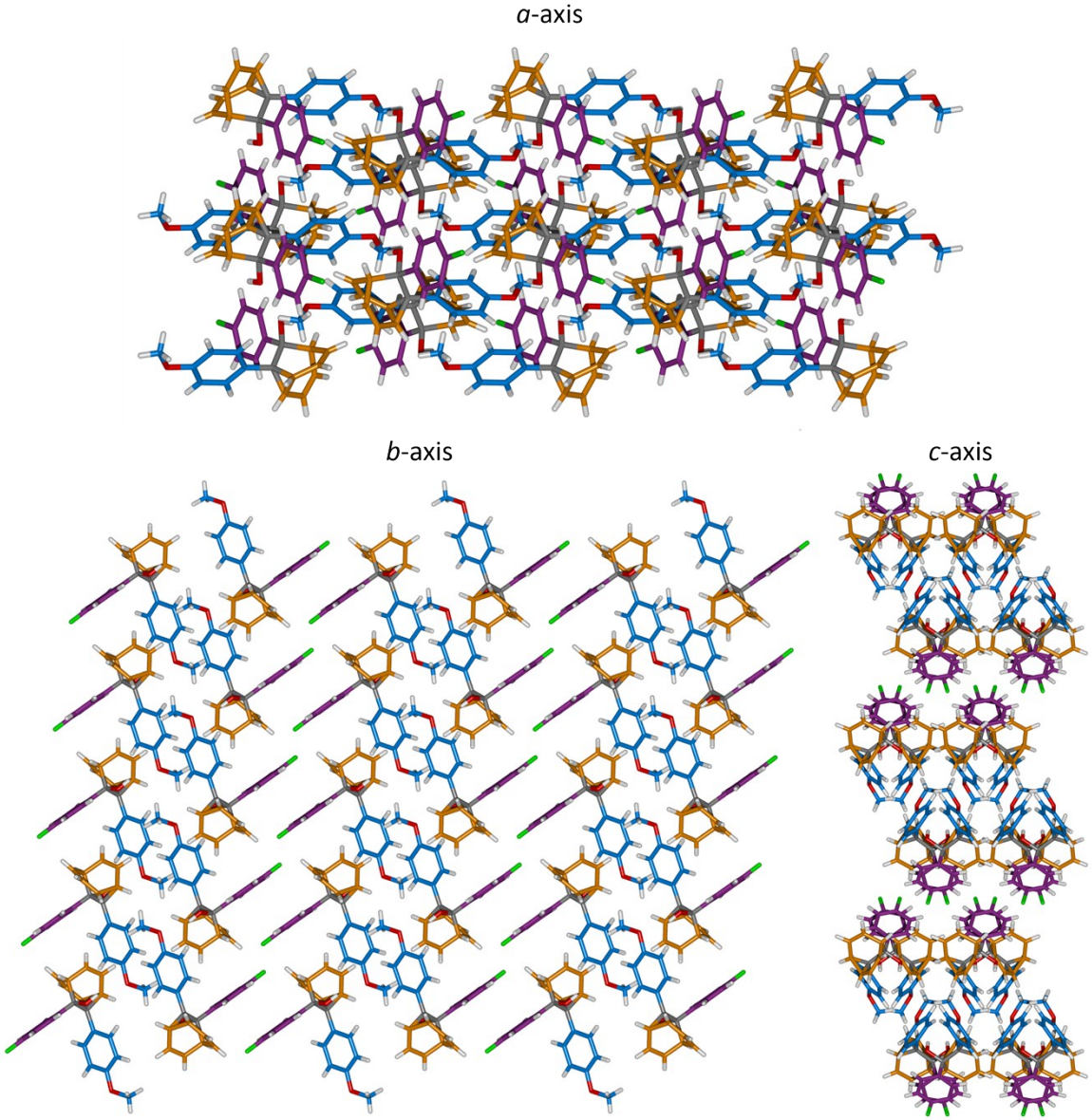

Figure S59. Solid-state superstructure of **1c** viewed along the three unit cell axes.

5.5 Compound 1d

Crystals of **1d** suitable for X-ray diffraction were grown by diffusion of H_2O vapour into a saturated MeOH solution. See Figure 3 in the main text.

Crystal System: Monoclinic
Space group: $P2_1/c$
Unit Cell Parameters: a = 18.8480(7) Å, b = 7.4991(3) Å, c = 12.2152(5) Å, α = 90 °, β = 107.6909(15)°, γ = 90 °, V = 1644.88(11) $Å^3$, Z = 4
Calculated density: 1.35013 $g \cdot cm^{-3}$

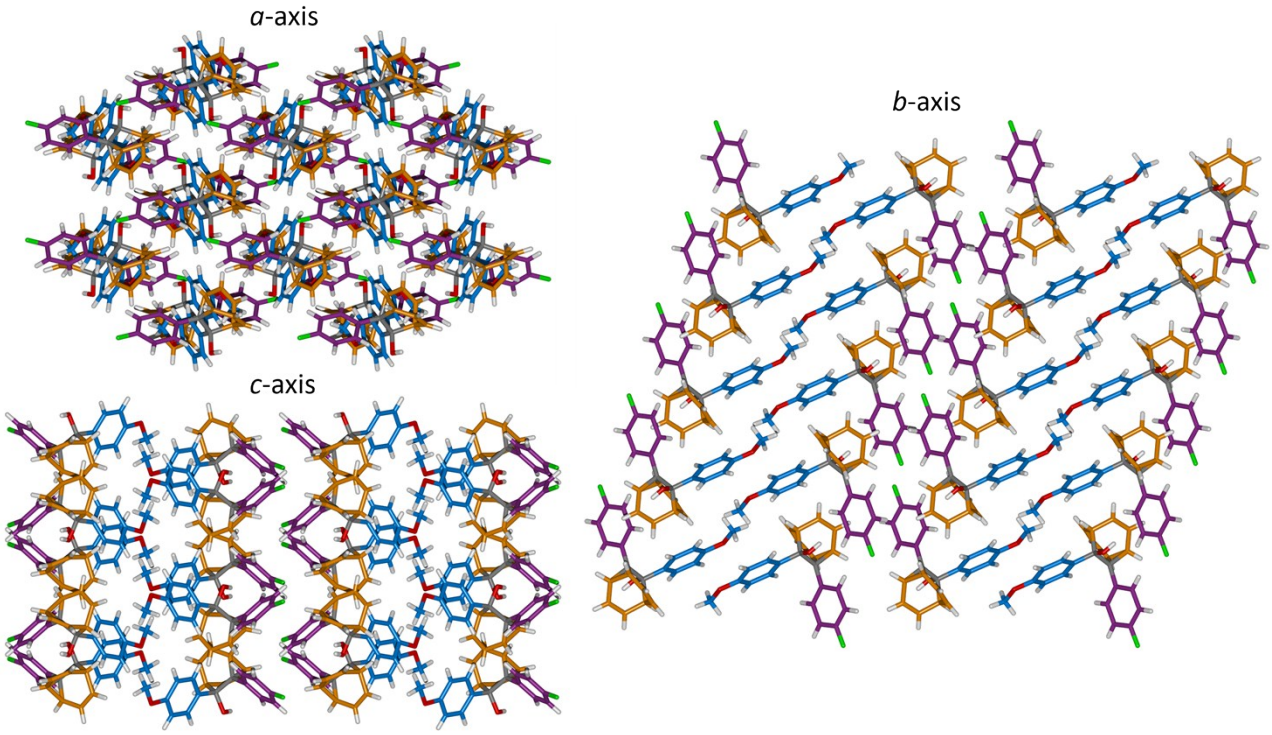

Figure S60. Solid-state superstructure of **1d** viewed along the three unit cell axes.

5.6 Compound 1e′

Crystals of **1e′** suitable for X-ray diffraction were grown by diffusion of H_2O vapour into a saturated MeOH solution. See Figure 3 in the main text.

Crystal System: Monoclinic
Space group: $P2_1/n$
Unit Cell Parameters: a = 9.7901(6) Å, b = 6.2016(4) Å, c = 24.0401(14) Å, α = 90 °, β = 92.931(2)°, γ = 90 °, V = 1457.67(16) Å^3, Z = 4
Calculated density: 1.38675 g·cm^{-3}

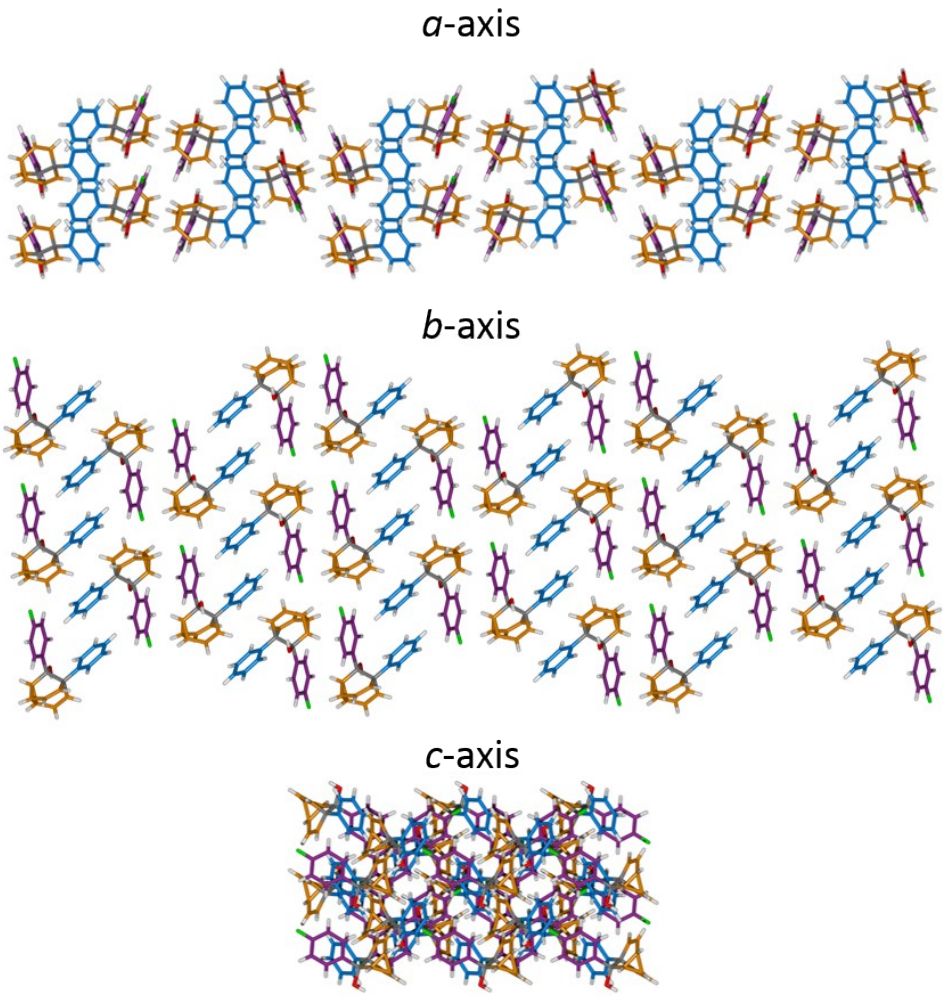

Figure S61. Solid-state superstructure of **1e′** viewed along the three unit cell axes.

5.7 Variable-Temperature (VT) X-Ray Crystallography

As the barbaralanes undergo a rapid and reversible Cope rearrangement in solution, we also investigated whether this rearrangement occurs within the solid state (Schemes S2 and S3). X-Ray crystallography data for **1a** and **1b′** was acquired at four different temperatures; 120 K, 270 K, 320 K and 370 K. At each temperature, the interatomic distances between specific nuclei were measured (Tables S1 and S3) and the distances were converted to percentages relative to the distances measured at 120 K (Tables S2 and S4).

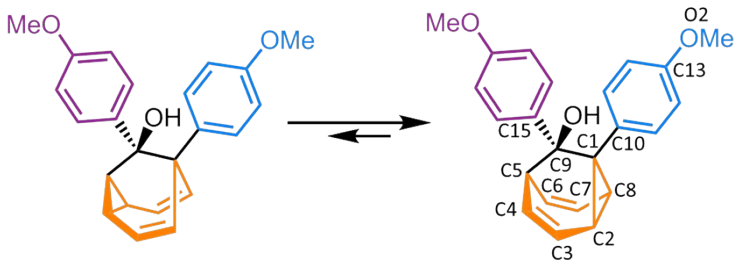

1a′ **1a**

Scheme S2. Potential solid-state equilibrium between **1a** and **1a′**. Atomic positions labelled here also apply to Tables S1–S2 and Figure S42.

Table S1. Interatomic distances for specific nuclei measured at various temperatures.

Nuclei	Interatomic Distance / Å			
	120 K	**270 K**	**320 K**	**370 K**
C9-C1	1.533(2)	1.533(2)	1.533(2)	1.536(2)
C1-C8	1.514(2)	1.507(2)	1.507(2)	1.505(3)
C1-C2	1.509(2)	1.511(2)	1.513(2)	1.511(2)
C8-C2	1.592(2)	1.590(2)	1.599(2)	1.604(2)
C2-C3	1.465(1)	1.460(2)	1.456(2)	1.452(2)
C6-C7	1.334(2)	1.325(3)	1.327(2)	1.332(3)
C7-C8	1.467(1)	1.463(2)	1.461(2)	1.454(2)
C3-C4	1.338(2)	1.331(2)	1.322(3)	1.325(3)
C5-C6	1.512(2)	1.504(2)	1.506(3)	1.502(2)
C4-C5	1.509(2)	1.506(2)	1.510(2)	1.505(3)
C9-C5	1.556(1)	1.557(2)	1.555(1)	1.556(2)
C9-C15	1.523(1)	1.523(2)	1.527(2)	1.525(2)
C1-C10	1.498(1)	1.503(2)	1.504(2)	1.501(2)
C13-O2	1.371(1)	1.376(2)	1.376(2)	1.375(2)
C4···C6	2.359(2)	2.345(2)	2.347(2)	2.335(3)
C3···C7	3.015(2)	3.004(2)	3.004(2)	3.001(3)
C2···C7	2.630(2)	2.627(2)	2.629(2)	2.628(2)
C8···C3	2.642(2)	2.632(2)	2.636(2)	2.635(3)

Table S2. Interatomic distances converted to percentages relative to 120 K for specific nuclei measured at various temperatures.

Nuclei	Interatomic Distance Relative to 120 K / %			
	120 K	**270 K**	**320 K**	**370 K**
C9-C1	100.0	100.0	100.0	100.2
C1-C8	100.0	99.5	99.5	99.4
C1-C2	100.0	100.1	100.3	100.1
C8-C2	100.0	99.9	100.4	99.3
C2-C3	100.0	99.7	99.4	99.1
C6-C7	100.0	99.3	99.5	99.9
C7-C8	100.0	99.7	99.6	99.1
C3-C4	100.0	99.5	98.8	99.0
C5-C6	100.0	99.5	99.6	99.3
C4-C5	100.0	99.8	100.1	99.7
C9-C5	100.0	100.1	99.9	100.0
C9-C15	100.0	100.0	100.3	100.1
C1-C10	100.0	100.3	100.4	100.2
C13-O2	100.0	100.4	100.4	100.3
C4···C6	100.0	99.4	99.5	99.0
C3···C7	100.0	99.6	99.6	99.5
C2···C7	100.0	99.9	100.0	99.9
C8···C3	100.0	99.6	99.8	99.7

The variable-temperature X-Ray crystallography data for **1a** reveals (Figure S62) that only minor changes occur between the specific nuclei measured as the temperature is raised. If the Cope rearrangement occurs within the solid state, we would expect there to be large changes between the nuclei. In particular, we would expect there to be significant changes between **C8-C2** and **C4···C6** – the positions where the Cope rearrangement occurs, i.e. a cyclopropyl ring is broken between **C8-C2** and forms between **C4···C6**. As the variation in the bond length is negligible (< 1%) for these nuclei and this indicates that the structures are fixed within the solid state, therefore no Cope rearrangement is occurring.

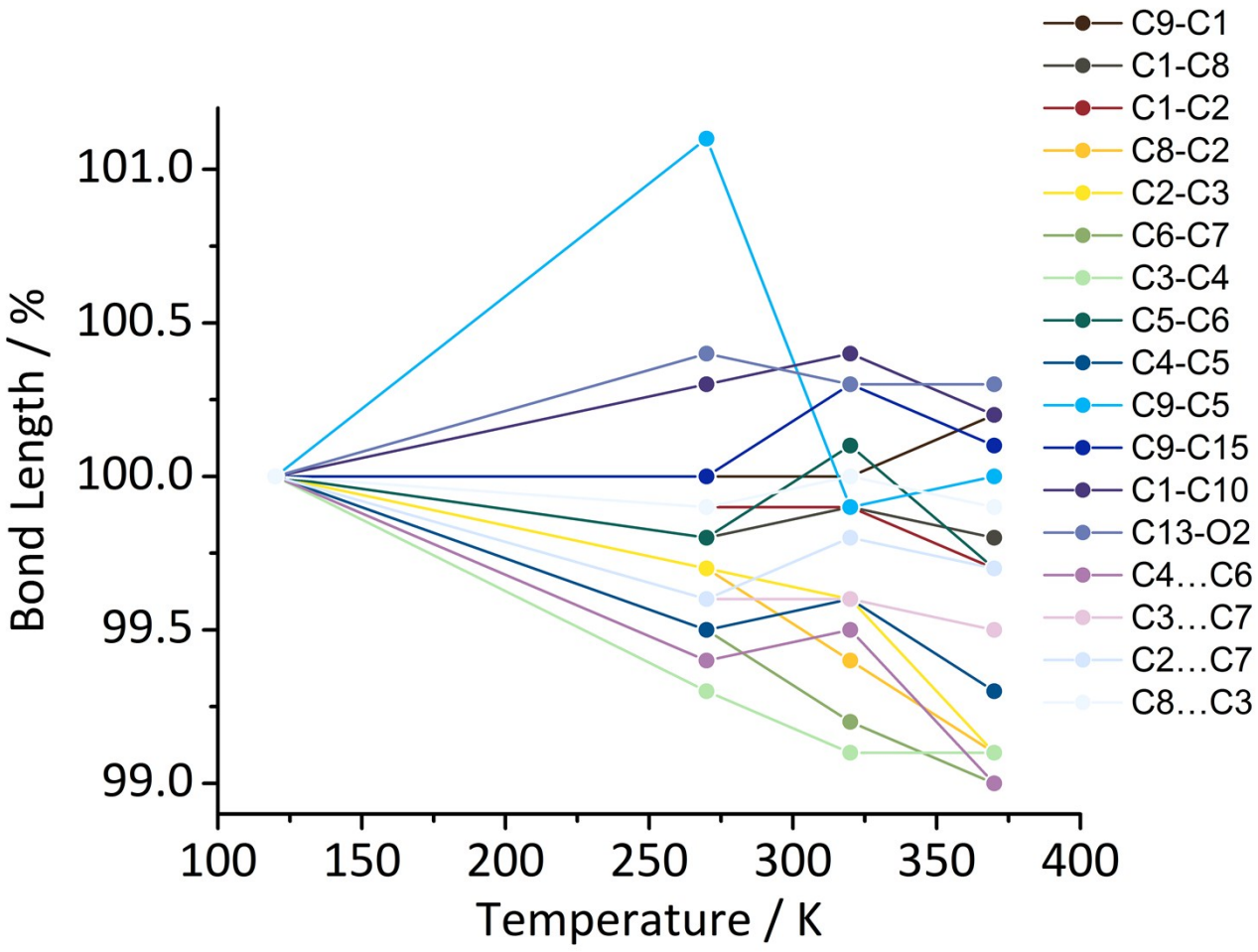

Figure S62. The bond lengths present in **1a** (as a percentage relative to the bond length at 120 K) plotted versus temperature.

The variable-temperature X-Ray crystallography data for **1b′** also confirms there is no Cope rearrangement occurring in the solid state. For **1b′**, we would expect there to be large changes in the distances between the nuclei **C1′-C2′** and **C4′···C6′**, as this is where a cyclopropyl ring is broken/formed. Figure S63 shows that the variation in the bond lengths for these nuclei is again minimal (< 1%).

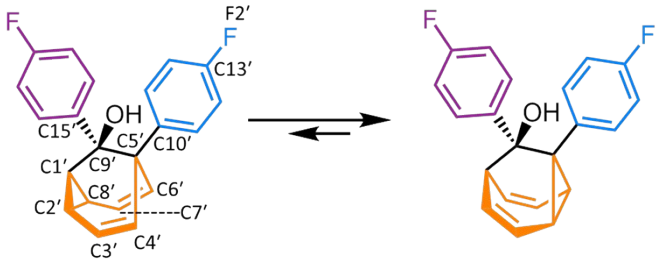

1b′ **1b**

Scheme S3. Potential solid-state equilibrium between **1b** and **1b′**. Atomic positions labelled here also apply to Tables S3–S4 and Figure S43.

Table S3. Interatomic distances for specific nuclei measured at various temperatures.

Nuclei	Interatomic Distance / Å			
	120 K	**270 K**	**320 K**	**370 K**
C9′-C1′	1.518(3)	1.509(2)	1.508(2)	1.508(2)
C1′-C8′	1.497(3)	1.496(2)	1.495(2)	1.494(3)
C1′-C2′	1.508(3)	1.503(2)	1.503(2)	1.500(3)
C8′-C2′	1.592(3)	1.591(2)	1.595(2)	1.610(3)
C8′-C7′	1.461(3)	1.455(2)	1.450(2)	1.440(3)
C2′-C3′	1.461(3)	1.462(2)	1.456(2)	1.446(3)
C6′-C7′	1.332(3)	1.328(2)	1.327(2)	1.325(3)
C3′-C4′	1.337(3)	1.333(2)	1.328(2)	1.331(3)
C5′-C6′	1.518(3)	1.519(2)	1.516(2)	1.517(2)
C4′-C5′	1.524(3)	1.520(2)	1.520(2)	1.521(2)
C9′-C5′	1.587(3)	1.593(2)	1.592(2)	1.590(2)
C5′-C10′	1.522(3)	1.517(2)	1.516(2)	1.514(2)
C9′-C15′	1.518(3)	1.521(2)	1.519(2)	1.520(2)
C13′-F2′	1.367(3)	1.363(2)	1.360(2)	1.358(3)
C4′⋯C6′	2.353(3)	2.342(2)	2.336(2)	2.328(3)
C3′⋯C7′	2.990(3)	2.989(2)	2.982(2)	2.976(3)
C2′⋯C7′	2.626(3)	2.622(2)	2.619(2)	2.622(3)
C8′⋯C3′	2.626(3)	2.626(2)	2.622(2)	2.621(3)

Table S4. Interatomic distances converted to percentages relative to 120 K for specific nuclei measured at various temperatures.

Bond	Interatomic Distance Relative to 120 K / %			
	120 K	**270 K**	**320 K**	**370 K**
C9′-C1′	100.0	99.4	99.3	99.3
C1′-C8′	100.0	99.9	99.9	99.8
C1′-C2′	100.0	99.7	99.7	99.5
C8′-C2′	100.0	99.9	100.2	101.1
C8′-C7′	100.0	99.6	99.2	98.6
C2′-C3′	100.0	100.1	99.7	99.0
C6′-C7′	100.0	99.7	99.6	99.5
C3′-C4′	100.0	99.7	99.3	99.6
C5′-C6′	100.0	100.1	99.9	99.9
C4′-C5′	100.0	99.7	99.7	100.1
C9′-C5′	100.0	100.4	100.3	100.2
C5′-C10′	100.0	99.7	99.6	99.5
C9′-C15′	100.0	100.2	100.1	100.1
C13′-F2′	100.0	99.7	99.5	99.3
C4′⋯C6′	100.0	99.5	99.3	98.9
C3′⋯C7′	100.0	100.0	99.7	99.2
C2′⋯C7′	100.0	99.8	99.9	99.8
C8′⋯C3′	100.0	100.0	99.8	99.8

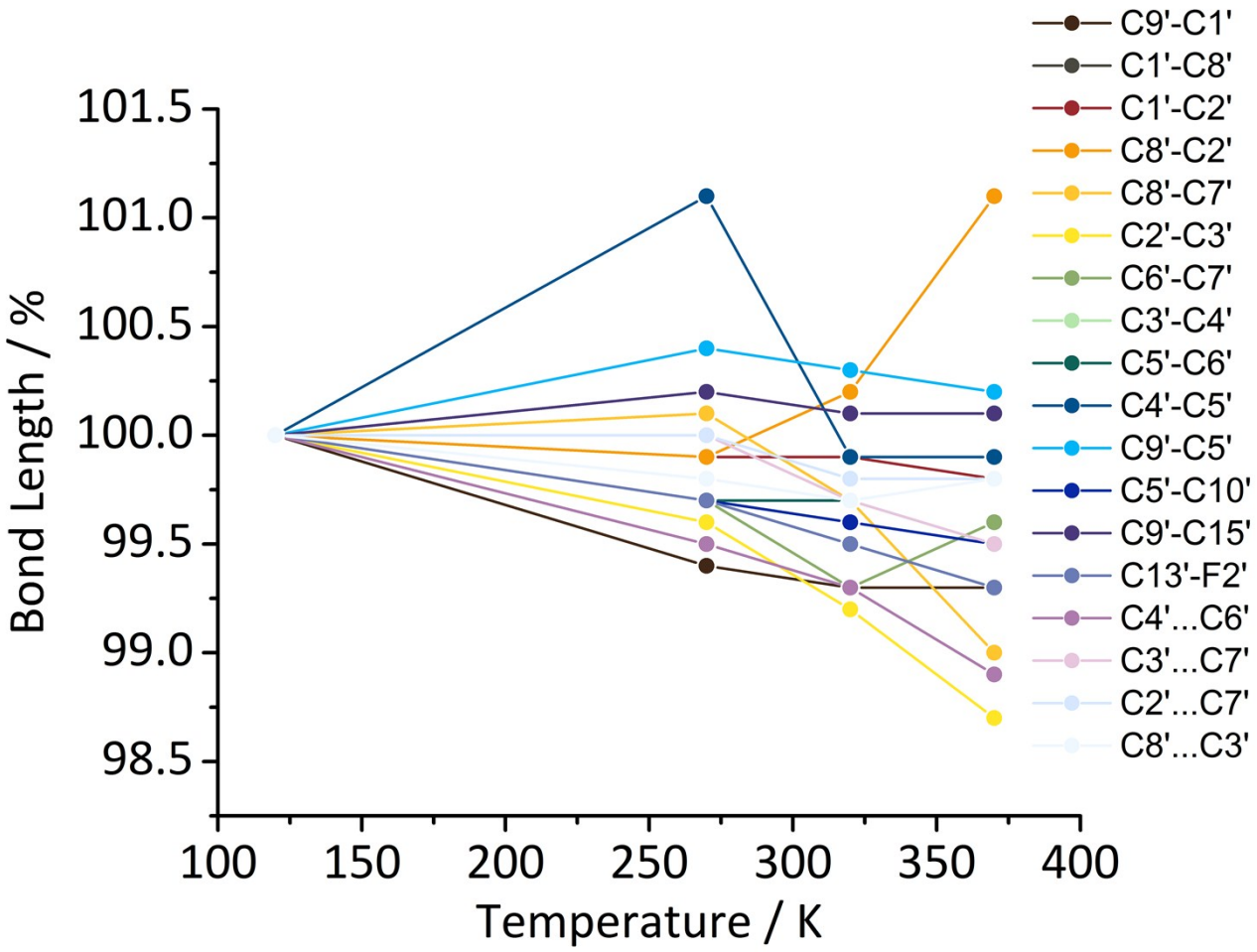

Figure S63. The bond lengths present in **1b'** (as a percentage relative to the bond length at 120 K) plotted versus temperature.

6. *In Silico* Modelling

6.1 Calculation of Solution-Phase Equilibria and Chemical Shifts

1 and **1′** interconvert *via* a [3,3]-sigmatropic Cope rearrangement. If one only one substituent is present on the barbaralane (i.e. on position 9), the isomers are energetically indistinguishable, i.e., degenerate. However, in the case of two substituents, the isomers are nondegenerate and the equilibrium is shifted towards one isomer. To determine the more stable isomer *in silico* methods were used to gain better insight into the processes. Both isomers were optimised in Gaussian 16, rev A.03[12] to minima (confirmed by frequency calculations on the same level of theory having no imaginary frequency) by DFT functionals (B3LYP,[13] CAM-B3LYP,[14] M06-2X[15]) using Def2-TZVP basis set and GD3 empirical dispersion[16] to take into account weak long-range interactions. C-PCM solvent model[17] was used to describe CS_2 as a solvent (as this solvent was used in NMR studies). For comparison, the calculations were also performed without GD3 dispersion using DFT functionals (B3LYP, ωB97X-D[18]), Def2-TZVP basis set and C-PCM model for CS_2. In all cases, isomer **1** was deemed to be more stable. In addition, the transition state was also found and the barrier connecting these two minima was estimated. The transition state was confirmed by frequency calculations to have one imaginary frequency, which corresponds to the displacement of atoms forming either **1** or **1′**. All Gibbs free energies were calculated at 298 K, including ZPE corrections and gas phase thermochemistry was not scaled. The ultrafine grid option was used in all calculations. The results are summarised in Table S5. Calculated energies are very similar to each other; except B3LYP DFT functional, which is known to underestimate reaction barriers more than the other DFT functionals.[19] The energy difference between **1** and **1′** is quite small and sometimes even **1′** is energetically favoured, although Gibbs energy favours **1**. This suggests that the enthalpy and entropy factors are dominant in the equilibrium formation.

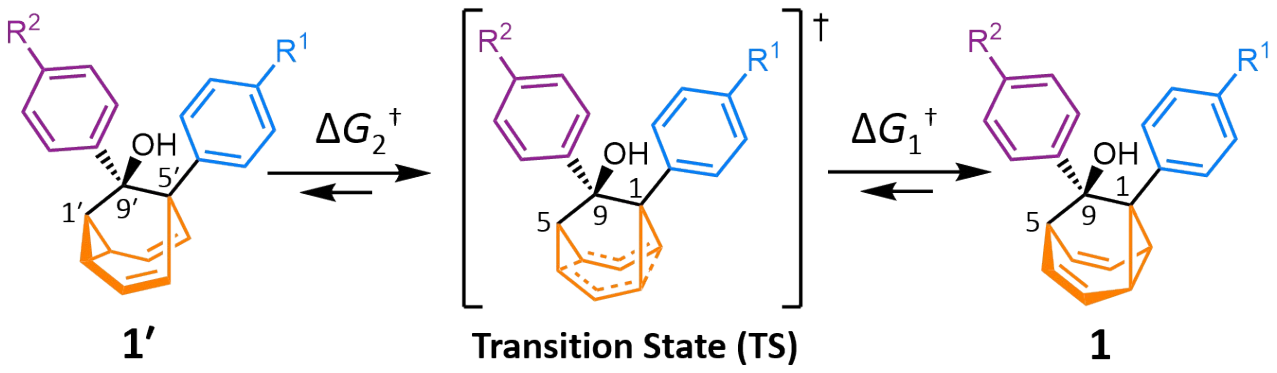

Scheme S4. The ground- and transition-state species modelled by DFT calculations.

Table S5. Calculated energies and Gibbs free energies in kJ·mol^{-1} compared to TS (taken as a reference).

DFT Functional	1a/1a′			1b/1b′		
	$\Delta G_1^{\dagger}$ ($\Delta E_1^{\dagger}$)[a]	$\Delta G_2^{\dagger}$ ($\Delta E_2^{\dagger}$) [b]	ΔG (ΔE) [c]	$\Delta G_1^{\dagger}$ ($\Delta E_1^{\dagger}$) [a]	$\Delta G_2^{\dagger}$ ($\Delta E_2^{\dagger}$) [b]	ΔG (ΔE) [c]
B3LYP – GD3	20.1 (25.4)	14.9 (21.0)	- 5.2 (- 4.4)	20.5 (25.0)	15.2 (20.9)	- 5.3 (- 4.1)
M06-2X – GD3	32.3 (37.6)	31.3 (38.1)	- 1.0 (0.5)	32.7 (37.0)	31.5 (37.8)	- 1.2 (0.8)
CAM-B3LYP – GD3	36.5 (42.6)	31.1 (38.1)	- 5.4 (- 4.5)	35.9 (42.2)	30.6 (38.0)	- 5.3 (- 4.2)
B3LYP	24.5 (29.0)	15.2 (20.4)	- 9.3 (- 8.6)	24.8 (28.9)	15.0 (20.3)	- 9.8 (- 8.6)
ωB97X-D	33.2 (37.8)	28.7 (34.9)	- 4.5 (- 2.9)	33.1 (37.3)	29.6 (34.7)	- 3.5 (- 2.6)

[a] calculated as $E_{TS} - E_1$; [b] calculated as $E_{TS} - E_1'$; [c] calculated as $\Delta G_2^{\dagger} - \Delta G_1^{\dagger}$.

Based on these results, the ^{13}C NMR chemical shifts were calculated using GIAO method implemented in Gaussian 16 for both structures to assist with the assignment of the measured data using B3LYP DFT functional, De2-TZVP basis set, GD3 empirical dispersion model, C-PCM solvent model for CS_2 and geometry from the previous optimisation at the same level of theory. The chemical shifts are referenced to tetramethylsilane optimised at the same level of theory. The ^{13}C NMR chemical shifts are summarised in Table S6 and S7, comparing against the experimental shifts observed at ambient temperatures for $CDCl_3$ solutions. There is much better agreement between the experimental values and the shifts calculated for the **1** isomer than those calculated for the **1′** isomer. This corroborates our assignment of **1** as the major isomer in solution.

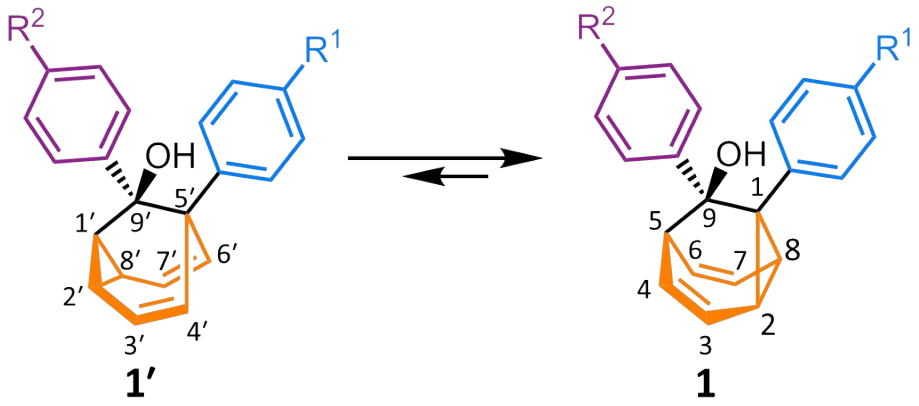

Scheme S5. Equilibrium between **1** and **1′** in the solution state at room temperature. Atomic positions labelled for Table S6–7.

Table S6. ^{13}C chemical shifts (ppm) observed at ambient temperature and calculated by DFT for **1**.

Atom	Observed ^{13}C Chemical Shift (δ)		Calculated ^{13}C Chemical Shift for 1′ (δ)	
	1a/1a′	**1b/1b′**	**1a**	**1b**
1	44.1	44.7	51.3	51.5
2	49.6	53.1	42.2	44.3
3	123.9	123.9	133.4	131.4
4	110.6	106.7	132.5	134.0
5	45.2	44.3	56.6	56.2
6	111.9	108.3	133.9	132.6
7	121.8	121.7	131.4	133.5
8	51.0	54.3	44.4	42.1
9	69.7	69.5	77.0	77.2

Table S7. ^{13}C chemical shifts (ppm) observed at ambient temperature and calculated by DFT for **1′**.

Atom	Observed ^{13}C Chemical Shift (δ)		Calculated ^{13}C Chemical Shift for 1′ (δ)	
	1a/1a′	**1b/1b′**	**1a′**	**1b′**
1′	44.1	44.7	63.0	63.1
2′	49.6	53.1	137.4	136.9
3′	123.9	123.9	130.5	129.0
4′	110.6	106.7	33.9	39.0
5′	45.2	44.3	36.7	36.8
6′	111.9	108.3	38.9	34.2
7′	121.8	121.7	128.5	130.8
8′	51.0	54.3	137.8	136.8
9′	69.7	69.5	78.5	78.6

6.2 Calculation of ^{13}C ssNMR Chemical Shifts

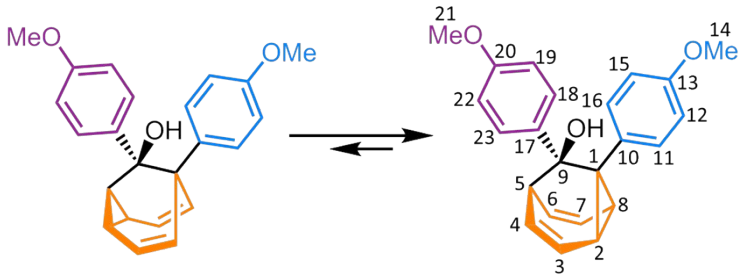

1a' **1a**

Scheme S6. Equilibrium between **1a** and **1a'** in the solution state at room temperature. Atomic positions labelled for Table S8.

Table S8. Comparison of experimental ^{13}C NMR chemical shifts (solid-state and solution state at 149 K) against calculated solid-state ^{13}C chemical shifts (ppm).

Atom	Solid-State Calculated ^{13}C NMR Chemical Shift (δ)[d]	Solid-State Experimental ^{13}C NMR Chemical Shift (δ)	Solution-State Experimental Low-Temperature ^{13}C NMR Chemical Shift (δ)
1	51.3	45.1	41.3
2	41.3	36.5 or 39.1	33.8
3	130.3	[c]	124.0
4	131.2	[c]	[a]
5	52.1	48.5	47.6
6	130.7	[c]	[a]
7	132.2	[c]	121.9
8	44.8	39.1 or 36.5	35.9
9	72.8	68.4	68.7
10	137.1	136.7 or 132.6	131.0
11 or 16	137.1	[c]	131.7
12 or 15	119.6	[c]	112.3
13	166.0	158.7 or 158.1	157.0
14 or 21	57.6	55.7 or 55.1	[b]
15 or 12	111.6	[c]	112.3
16 or 11	139.5	[c]	131.7
17	141.7	136.7 or 132.6	133.5
18 or 23	134.6	[c]	[a]
19 or 22	115.6	[c]	111.9
20	164.8	158.7 or 158.1	156.8
21 or 14	55.9	55.7 or 55.1	[b]
22 or 19	119.4	[c]	111.9
23 or 18	133.5	[c]	[a]

[a] peaks have broadened into baseline; [b] peaks are overlapping with the solvent (CD_2Cl_2); [c] unable to assign unambiguously; [d] ^{13}C shielding of 170 ppm used.

First principles calculations of NMR shifts in crystalline forms were carried out using the GIPAW method implemented in CASTEP v17.2.[20] All calculations were performed using the PBE functional[21] and on-the-fly generated ultrasoft pseudopotentials with a cut-off energy of 600 eV. Geometry optimisation of all atomic positions was carried out with the centre of mass and unit cell parameters fixed at the values determined by single-crystal X-ray diffraction. Integrals were taken over the Brillouin zone using a Monkhorst-Pack grid with a maximum *k*-point sample spacing of 0.1 $Å^{-1}$, corresponding to 1 × 2 × 1 and 2 × 2 × 1 grids for **1a** and **1b′**, respectively. ^{13}C isotropic shifts were obtained from calculations of NMR parameters from the optimised structures using tools relying on the magres file format and MagresPython library.[22]

Calculations of the ^{13}C NMR chemical shifts in the solid state are based on the X-ray crystallographic data and as both **1a** and **1b′** demonstrate different structures in the solid state, calculations of ^{13}C NMR chemical shifts in the solid state bear significant importance. The solid-state samples were prepared as powders (which were obtained by evaporating a solution of the barbaralane), and although the ^{13}C NMR chemical shifts in the solid state can be measured experimentally (Figure S51 and Figure S54), precise values were desired (Figure S64 and Figure S65).

Firstly, looking at the data for **1a** and comparing the calculated ^{13}C NMR chemical shifts in the solid state against the experimental chemical shifts, all the values are relatively similar. At the same time, from the ^{13}C and ^{1}H VT NMR for **1a/1a′** (Figure S49 and Figure S50) we have shown that as the temperature is lowered, the equilibrium shifts further towards **1a**. This means that as we reach the lowest temperature attainable (149 K), there is less of the minor isomer and the spectrum acquired will resemble a spectrum showing the major isomer as the sole species. The solution-state

experimental ^{13}C NMR chemical shifts are also similar to both the experimental and calculated solid-state ^{13}C NMR chemical shifts, and this observation reinforces the conclusion that the structure of the major isomer in the solid state is the same as that in the solution state at low temperature, due to a shift in the equilibrium.

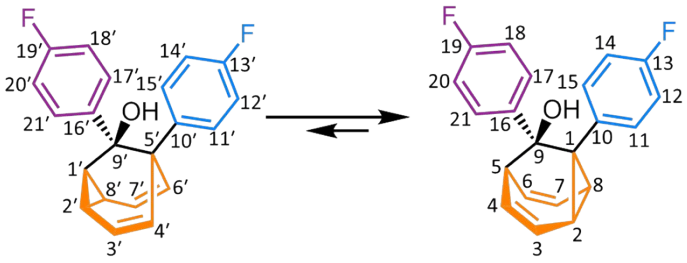

Scheme S7. Equilibrium between **1b** and **1b′** in the solution state at room temperature. Atomic positions labelled for Table S9.

Table S9. Comparison of experimental ^{13}C NMR chemical shifts (solid-state and solution-state at 149 K) against calculated solid-state ^{13}C chemical shifts (ppm).

Atom	Solid-State Calculated ^{13}C NMR Chemical Shift (δ)[d]	Solid-State Experimental ^{13}C NMR Chemical Shift (δ)	Solution State Experimental Low Temperature ^{13}C NMR Chemical Shift (δ)
1′/5	41.3	34.1 or 30.1[b]	41.4
2′/4	35.8	34.1 or 30.1[b]	[a]
3′/3	130.0	[c]	124.0
4′/2	135.0	[c]	33.8 or 35.7
5′/1	59.6	54.3	47.4
6′/8	137.1	[c]	35.7 or 33.8
7′/7	130.9	[c]	121.7
8′/6	33.2	34.1 or 30.1[b]	[a]
9′/9	75.8	69.7	68.7
10′/10	145.6	139.1[b]	134.8
11′ or 15′/11 or 15	137.7	[c]	132.3
12′ or 14′/12 or 14	120.9	[c]	114.3
13′ or 19′/13 or 19	172.3	161.8[b]	161.6
14′or 12′/14or 12	119.3	[c]	114.3
15′ or 11′/15 or 11	137.5	[c]	132.3
16′/16	145.8	139.1[b]	137.0
17′ or 21′/17 or 21	137.1	[c]	[a]
18′ or 20′/18 or 20	123.0	[c]	114.2
19′ or 13′/19 or 13	173.7	161.8[b]	159.6
20′ or 18′/20 or 18	116.6	[c]	114.2
21′ or 17′/21 or 17	135.5	[c]	[a]

[a] peaks have broadened into baseline; [b] assignments of overlapping peaks; [c] unable to assign unambiguously; [d] ^{13}C shielding of 170 ppm used.

As mentioned previously, the ^{13}C and ^{1}H VT NMR spectra acquired for **1b/1b′** show that as the temperature is decreased, the resonances shift in a manner so that the spectrum at the lowest temperature (149 K) shows mainly the structure for **1b** and only a minimal amount of **1b′**. Following from this observation, the solution-state experimental chemical shifts should differ from both the solid-state calculated and experimental ^{13}C NMR chemical shifts. This is indeed what is apparent in the comparison. The differences in the chemical shifts corroborate that the structure in the solid state is the minor isomer **1b′** and that the structure in the solution state at low temperature is mainly **1b**. Upon further inspection, the solid-state calculated chemical shifts for the atoms 4′/2

and 6′/8, in comparison to the solution-state low-temperature experimental chemical shifts are completely different and this is due to the dissimilar structures in the solid- and solution-states. As the structures are different, in the solid state (**1b′**) the protons labelled as 4′ and 6′ will resemble a *cis*-dialkyl olefin whereas in the solution state (**1b**) the protons labelled as 2 and 8 will resemble a divinyl cyclopropane. As the chemical environments are different in the adopted structures, there will be large differences in the chemical shifts, and this is what we observe.

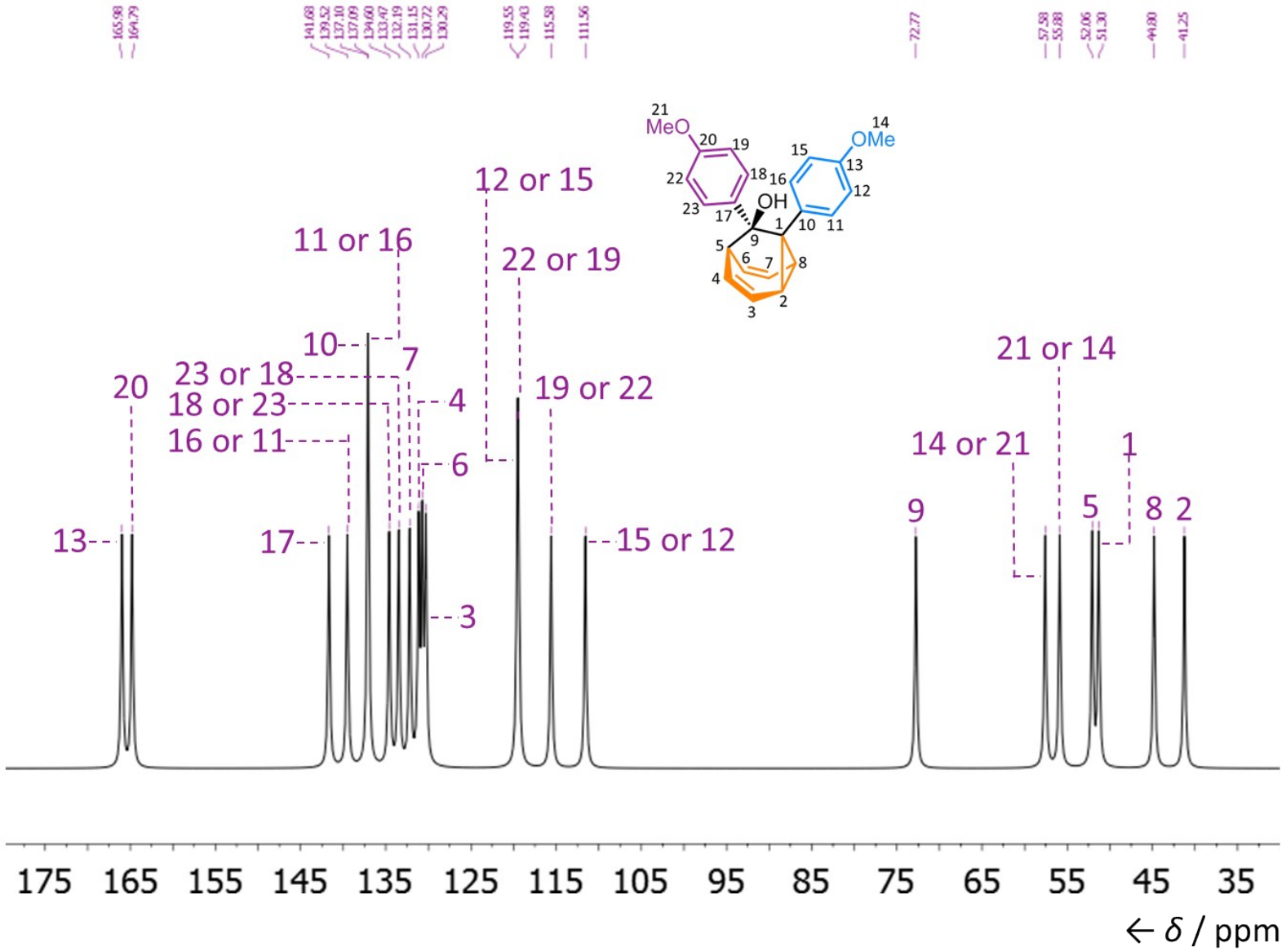

Figure S64. Calculated solid state ^{13}C NMR spectrum of **1a**.

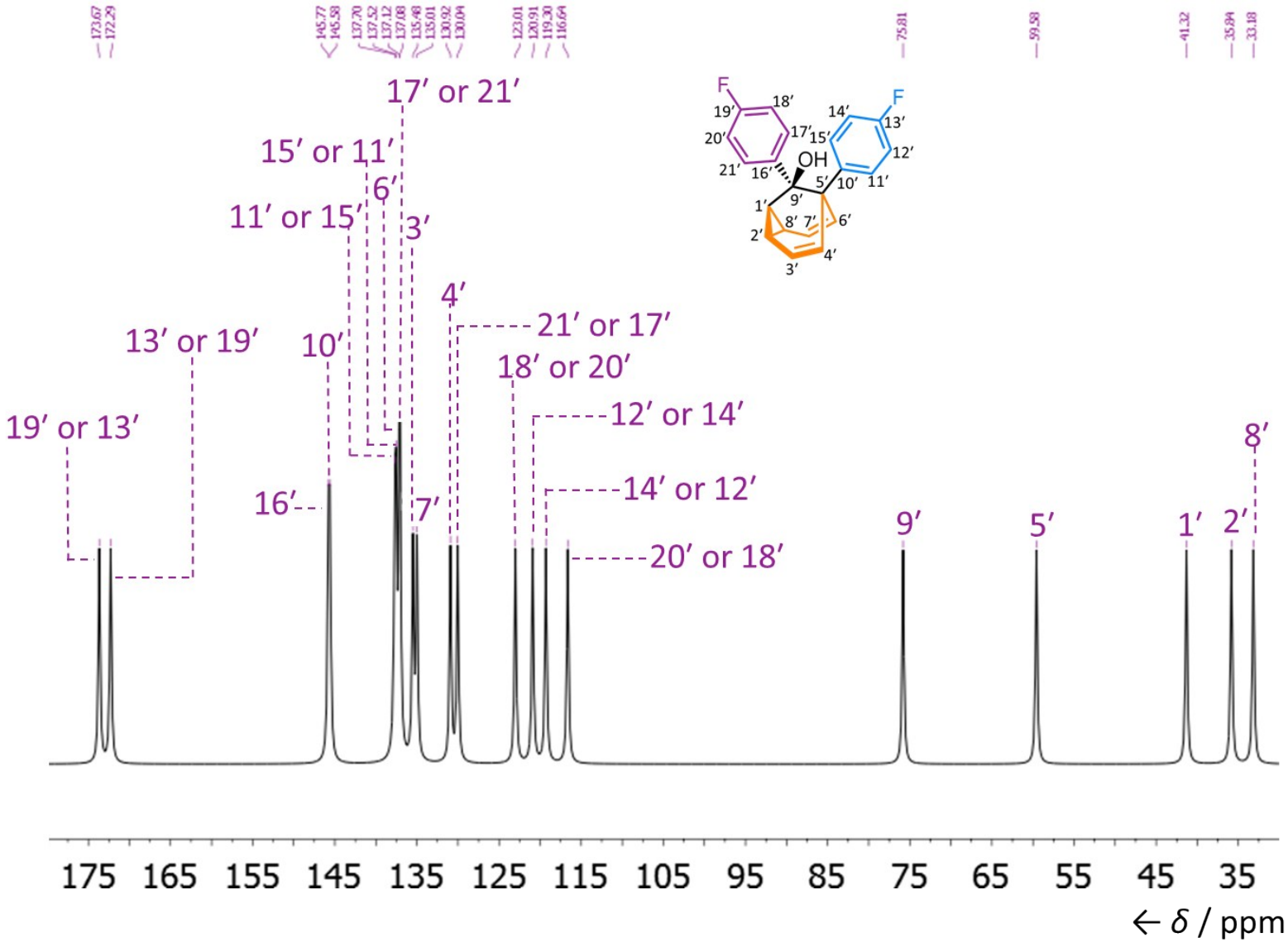

Figure S65. Calculated solid state ^{13}C NMR spectrum of **1b'**.

6.3 Electrostatic Potential Maps and Hirshfeld Surfaces of Solid-State Structures

In order to understand the crystal packing of the barbaralanes **1/1′**, we modelled electrostatic potential maps and Hirshfeld surfaces.

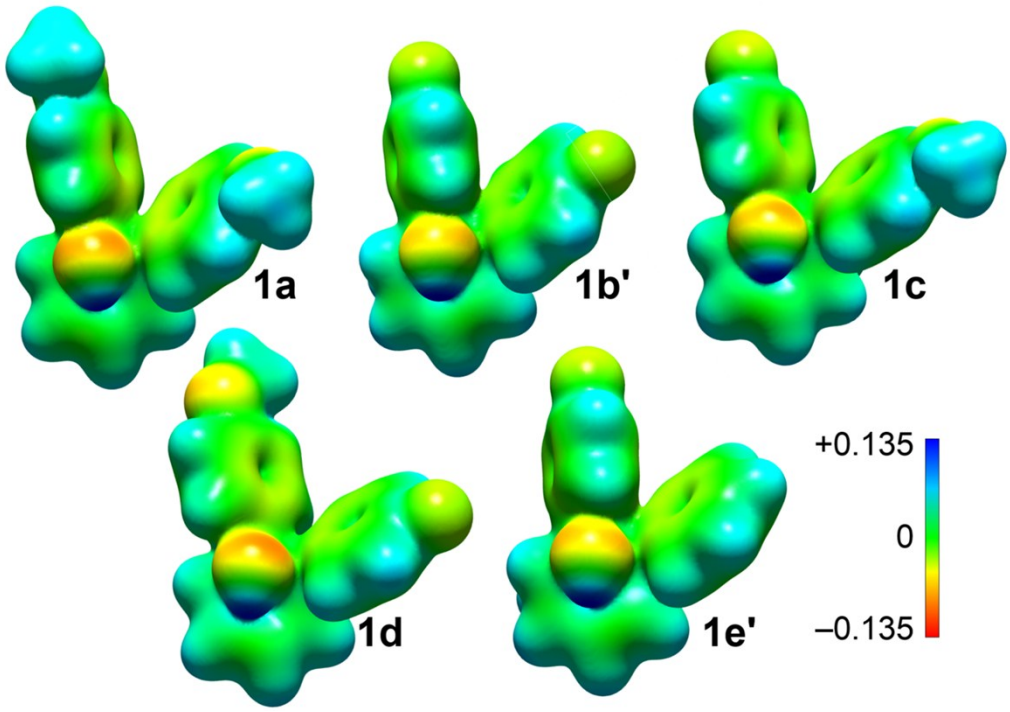

Figure S66. Calculated (B3LYP/3-21G) electrostatic potential maps for the solid-state geometries of the barbaralanes **1/1′**.

Electrostatic potential maps (Figure S66) were calculated using Gaussian 09, starting from the atomic coordinates obtained by X-ray crystallography and using the B3LYP functional and 3-21G basis set. Isovalues of 0.01 are used for mapped surface and the colour scale displays electrostatic potentials of –0.135 (red) to +0.135 (blue). It is clear from inspecting the maps that the heteroatoms are the most polarised areas of the structures, as would be expected, and that the aromatic surfaces are only mildly polarised. There is no indication that this mild polarisation gives

rise to any aromatic interactions in the solid state, as the partially polarised regions do not match up with one another in the crystal lattice.

Hirshfeld surfaces[23] give insights into the interactions between molecules in the crystal lattices. We calculated Hirshfeld surfaces for the crystal packing structures of **1/1′** in CrystalExplorer17[24] using an isovalue of 0.5 and mapping the normalised contact distance, d_{norm}. The surfaces highlight (Figures S67–71) in red any regions in which the molecular surfaces meet at distances shorter than the sum of van der Waals radii, while white and blue illustrate regions where they meet at distances that are the sum of the van der Waals radii or longer, respectively. Overall, the Hirshfeld surfaces of **1/1′** reveal there are only a few contacts that are slightly shorter than the sum of van der Waals radii – there are only a small number of red patches, which are faint in colour and small in size. This data suggests that there are no strong and specific noncovalent interactions in the solid state that direct the crystal packing. In two cases, **1a** and **1c**, the tertiary alcohol appears to be involved in a O–H···O contact with a neighbouring OMe group. However, the H···O distances are much longer (by ∼0.3 Å) than the mean distance[25] of 1.974 Å expected for a O–H···O hydrogen bond in the solid state, so these can only be considered very weak interactions, at most. The other contacts that appear shorter than the sum of van der Waals radii, e.g., some C–H···F and C–H···C contacts, are also rather weak and would not be expected to dictate the crystal packing.

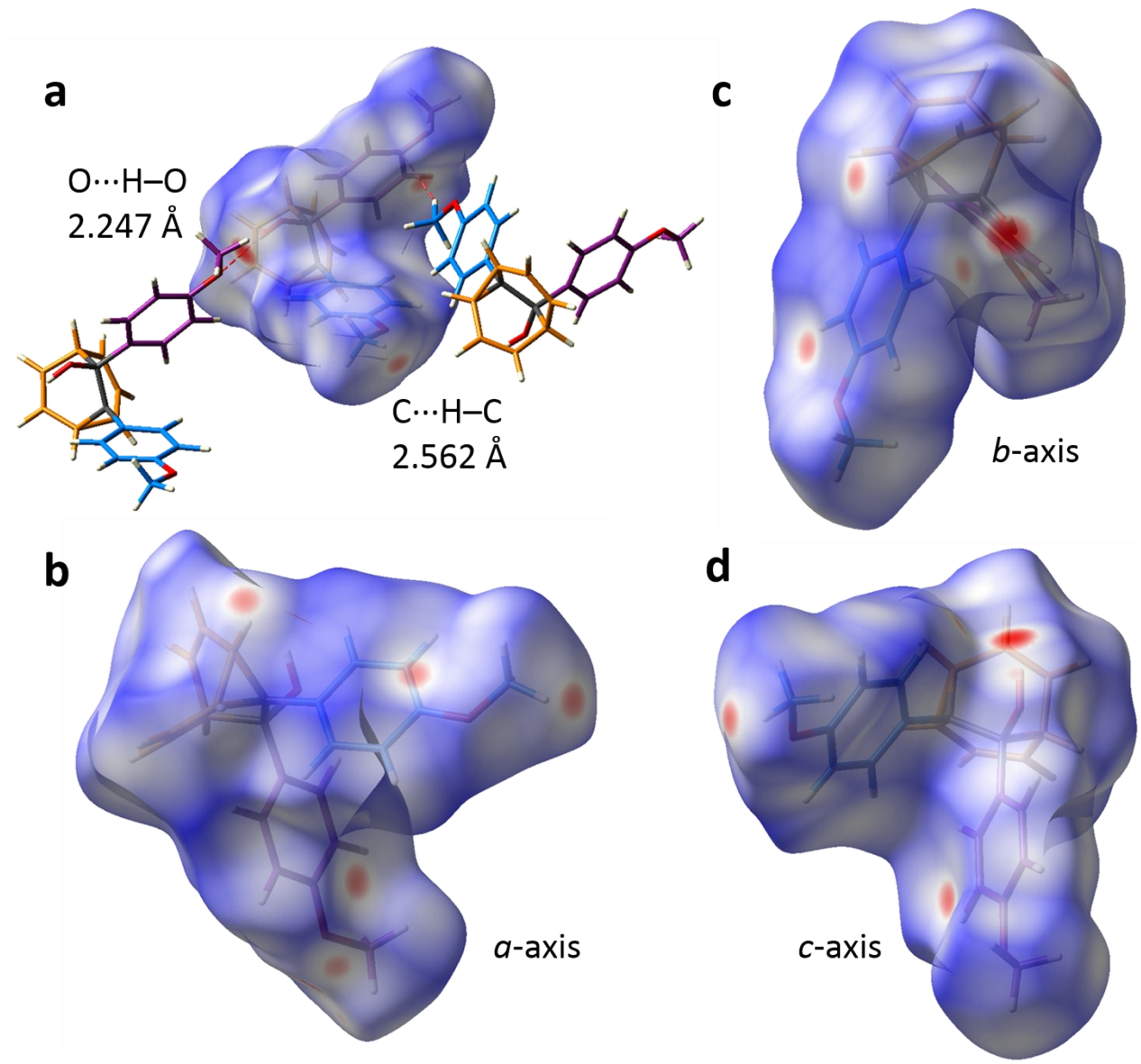

Figure S67. Hirshfeld surface of **1a**, showing (a) the most significant close contacts, as well as views of the surface along the crystallographic (b) *a*-axis, (c) *b*-axis, and (d) *c*-axis.

Crystals of **1a** exhibit (Figure S67) a few contacts that are slightly closer than the sum of van der Waals radii. Most are C–H···C contacts, but there is also a weak O–H···O interaction that measures 2.247 Å – significantly longer than the 1.974 Å expected for a O–H···O hydrogen bond.

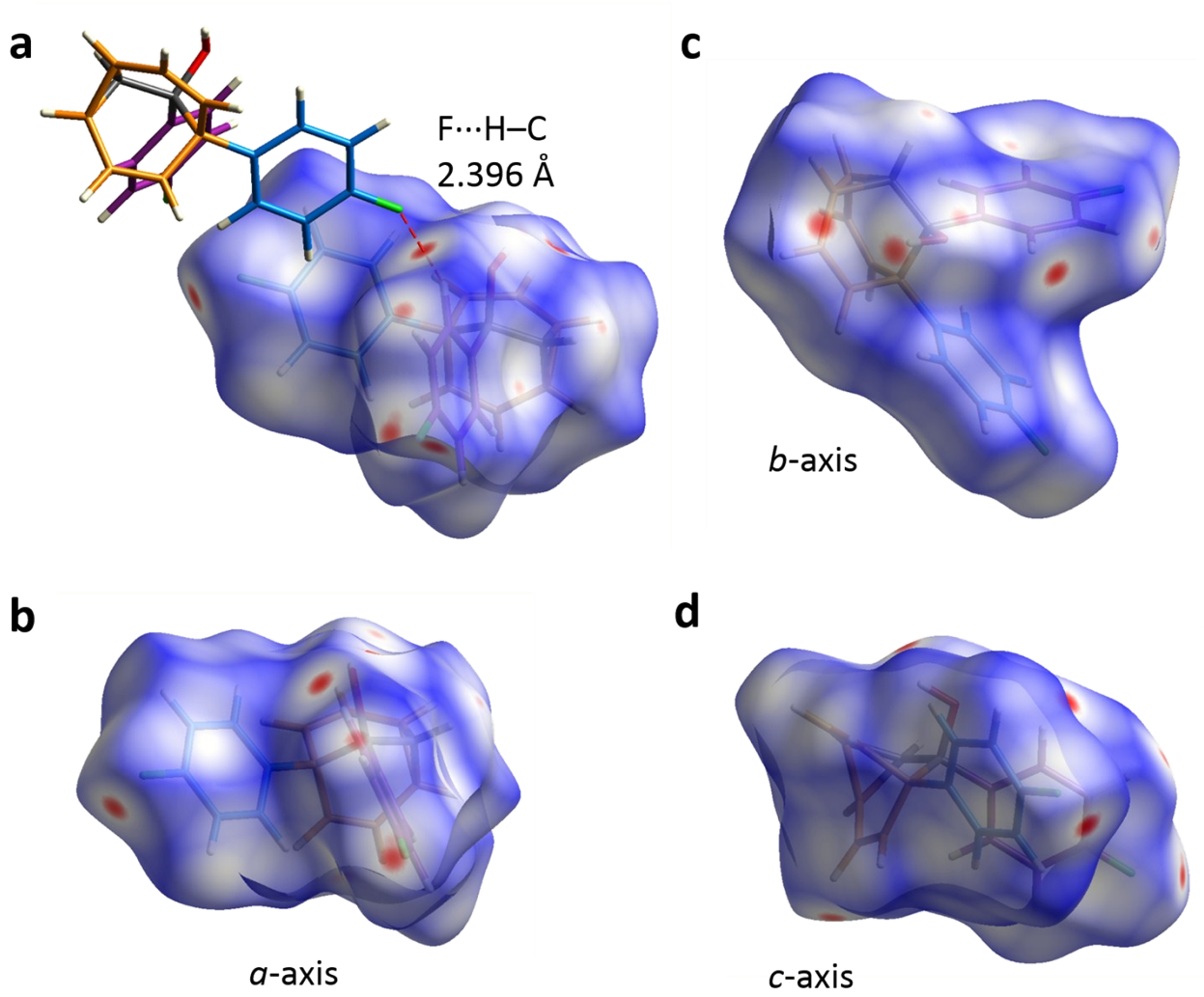

Figure S68. Hirshfeld surface of **1b′**, showing (a) the most significant close contact, as well as views of the surface along the crystallographic (b) *a*-axis, (c) *b*-axis, and (d) *c*-axis.

Crystals of **1b′** also exhibit (Figure S68) a few contacts that are slightly closer than the sum of van der Waals radii. Again, most of them are C–H···C contacts, but there is also a C–H···F contact involving a sp^2 C–H of one of the 4-fluorophenyl rings. None of the contacts correlate with a strong noncovalent bonding interaction.

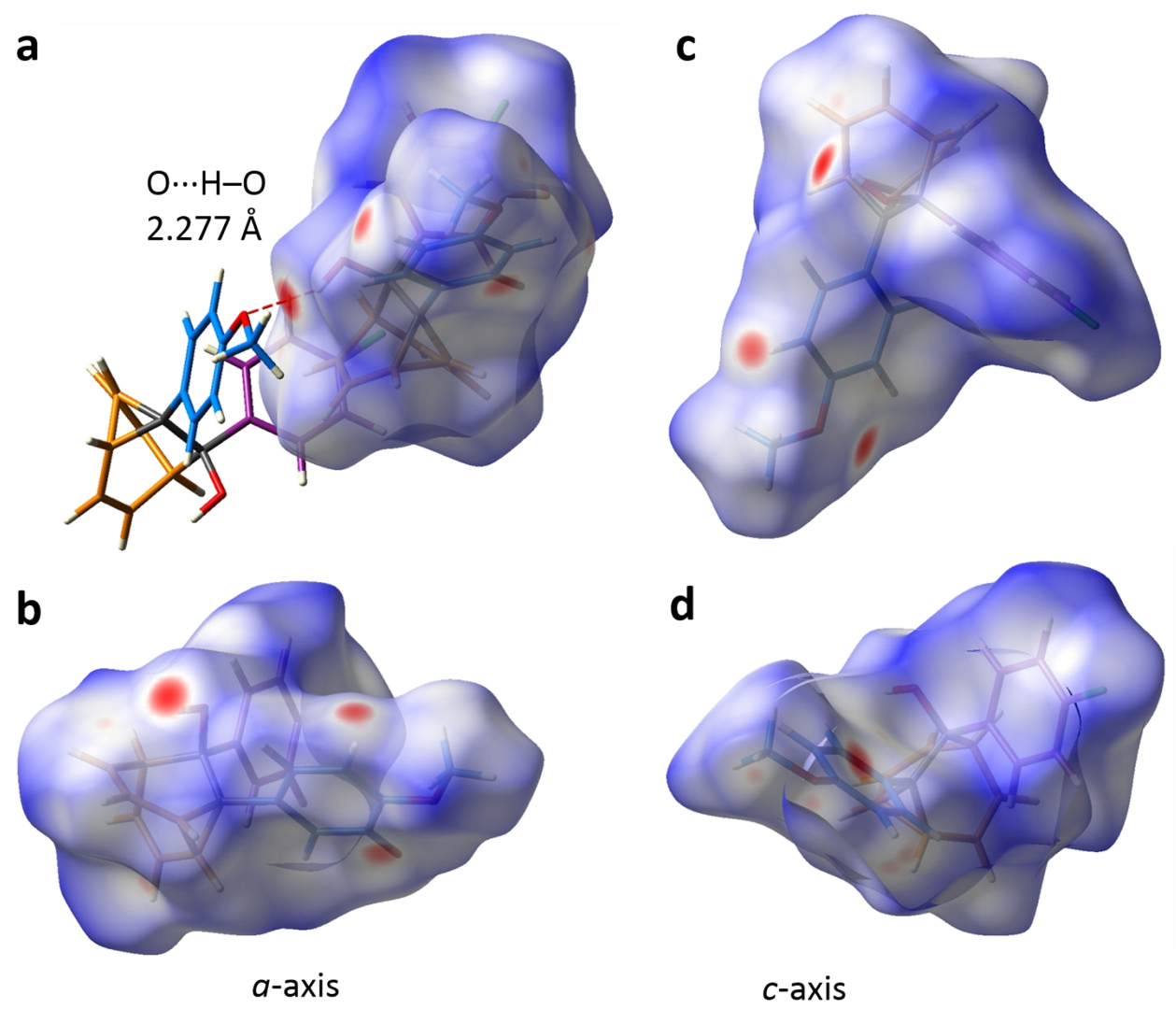

Figure S69. Hirshfeld surface of **1c** showing (a) the most significant close contact, as well as views of the surface along the crystallographic (b) *a*-axis, (c) *b*-axis, and (d) *c*-axis.

Crystals of **1c** pack in a manner that is similar to **1a** and close contacts present (Figure S69) are very similar. As for **1a**, there is a weak O–H···O interaction that measures 2.277 Å – significantly longer than the 1.974 Å expected for a O–H···O hydrogen bond.

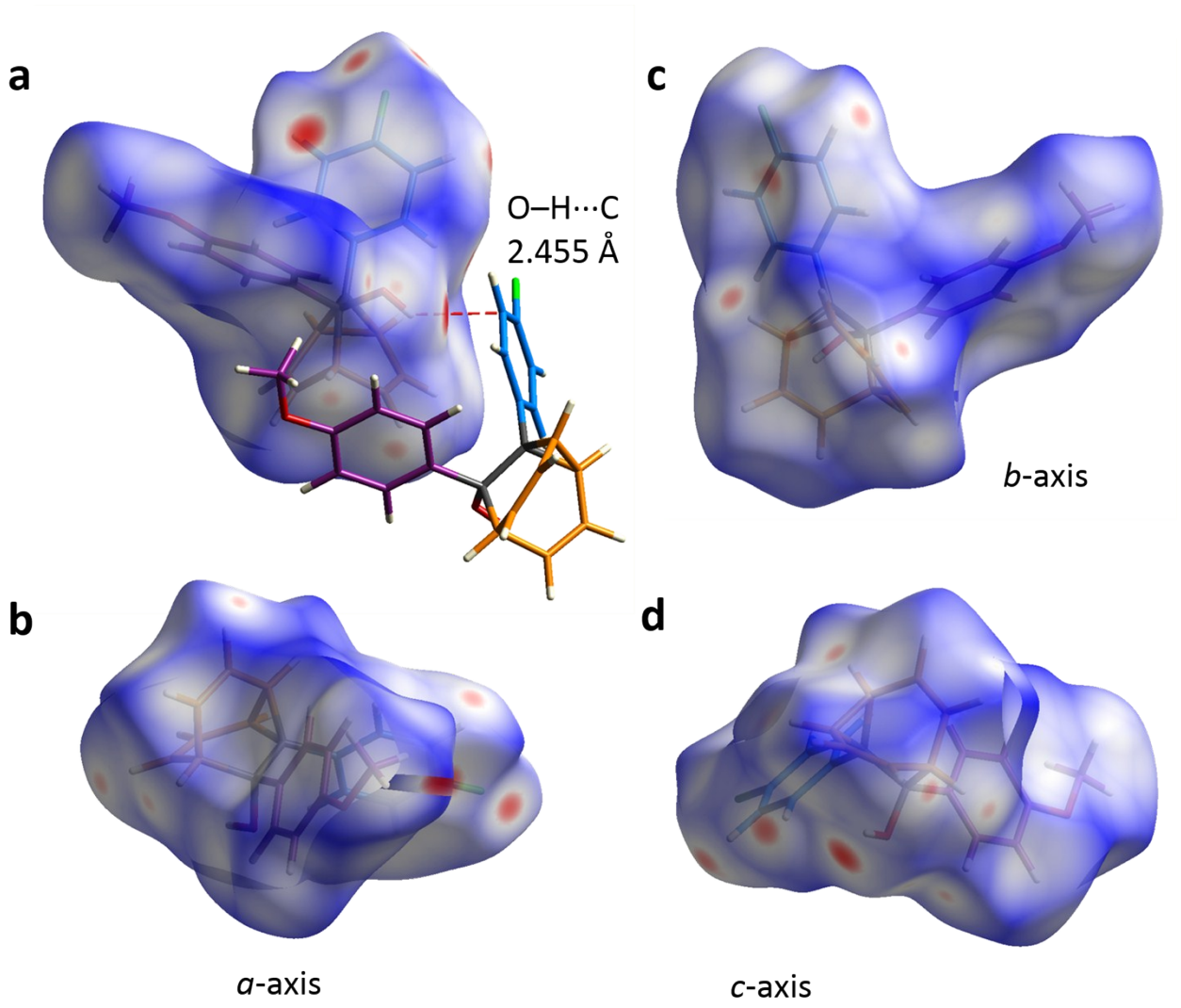

Figure S70. Hirshfeld surface of **1d** showing (a) the most significant close contact, as well as views of the surface along the crystallographic (b) *a*-axis, (c) *b*-axis, and (d) *c*-axis.

Crystals of **1d** are also similar to **1a** (and, therefore, with **1c**). Unlike **1a** and **1c**, however, there are no O–H···O close contacts (Figure S70). As the packing is essentially unchanged in the absence of these contacts, this observation confirms our assertion that any O–H···O hydrogen bonds present in the solid-state structures of **1a** or **1c** are weak and do not dictate the packing.

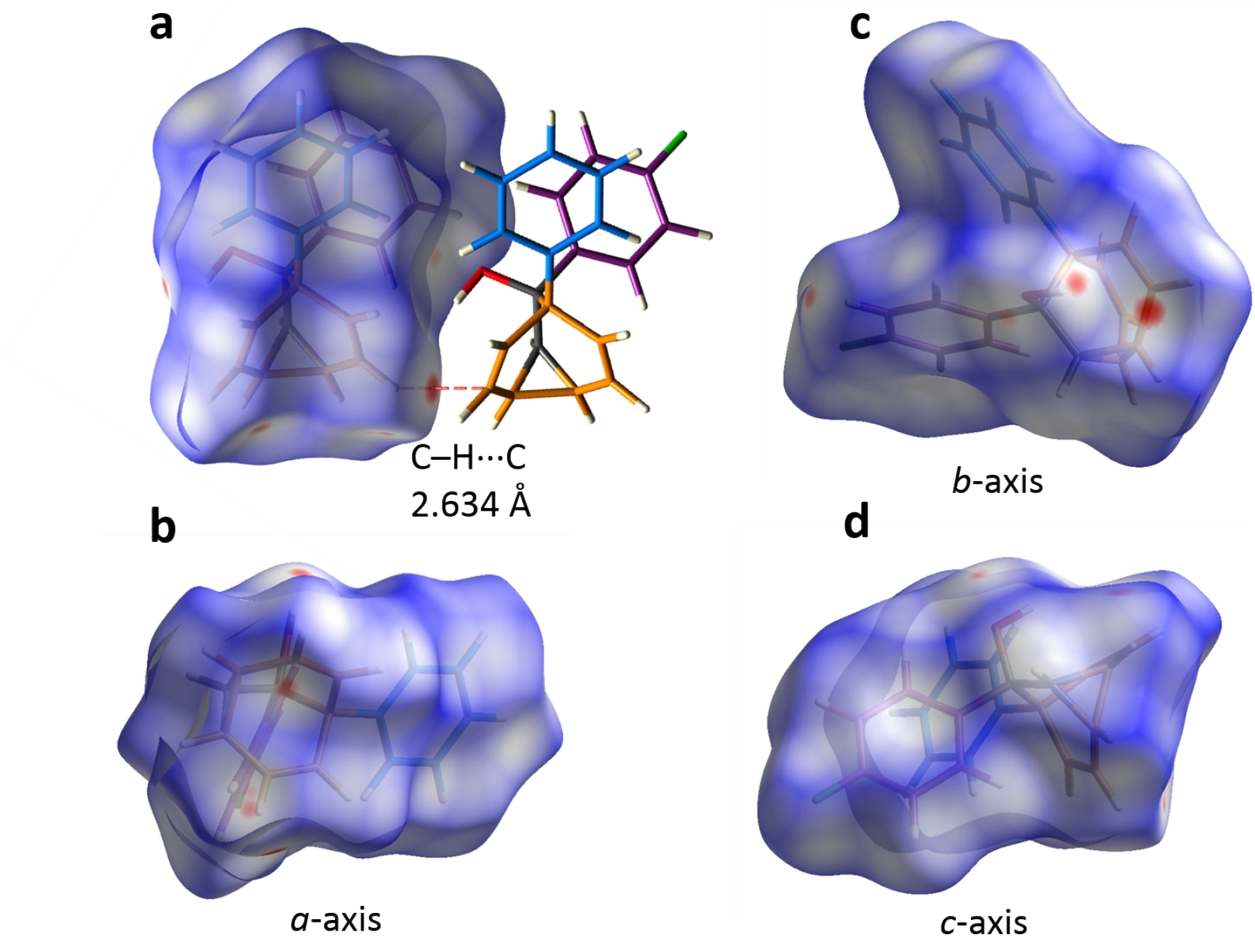

Figure S71. Hirshfeld surface of **1e′**, showing (a) the most significant close contact, as well as views of the surface along the crystallographic (b) *a*-axis, (c) *b*-axis, and (d) *c*-axis.

The packing structure of **1e′** is isostructural with **1b′**. As expected, the Hirshfeld surface (Figure S71) shows that there are only very few contacts closer than the sum of van der Waals radii. Those that are present do not correlate with any strong noncovalent bonding interactions.

Hirshfeld fingerprint diagrams show (Figure S72) similarities between **1a**, **1c**, and **1d** in one grouping and between **1b′** and **1e′** in another grouping. This observation confirms our categorisation of the packing structures into two groups and matches well with our hypothesis that it is the packing that causes the switch in preference for valence isomer **1** or **1′**.

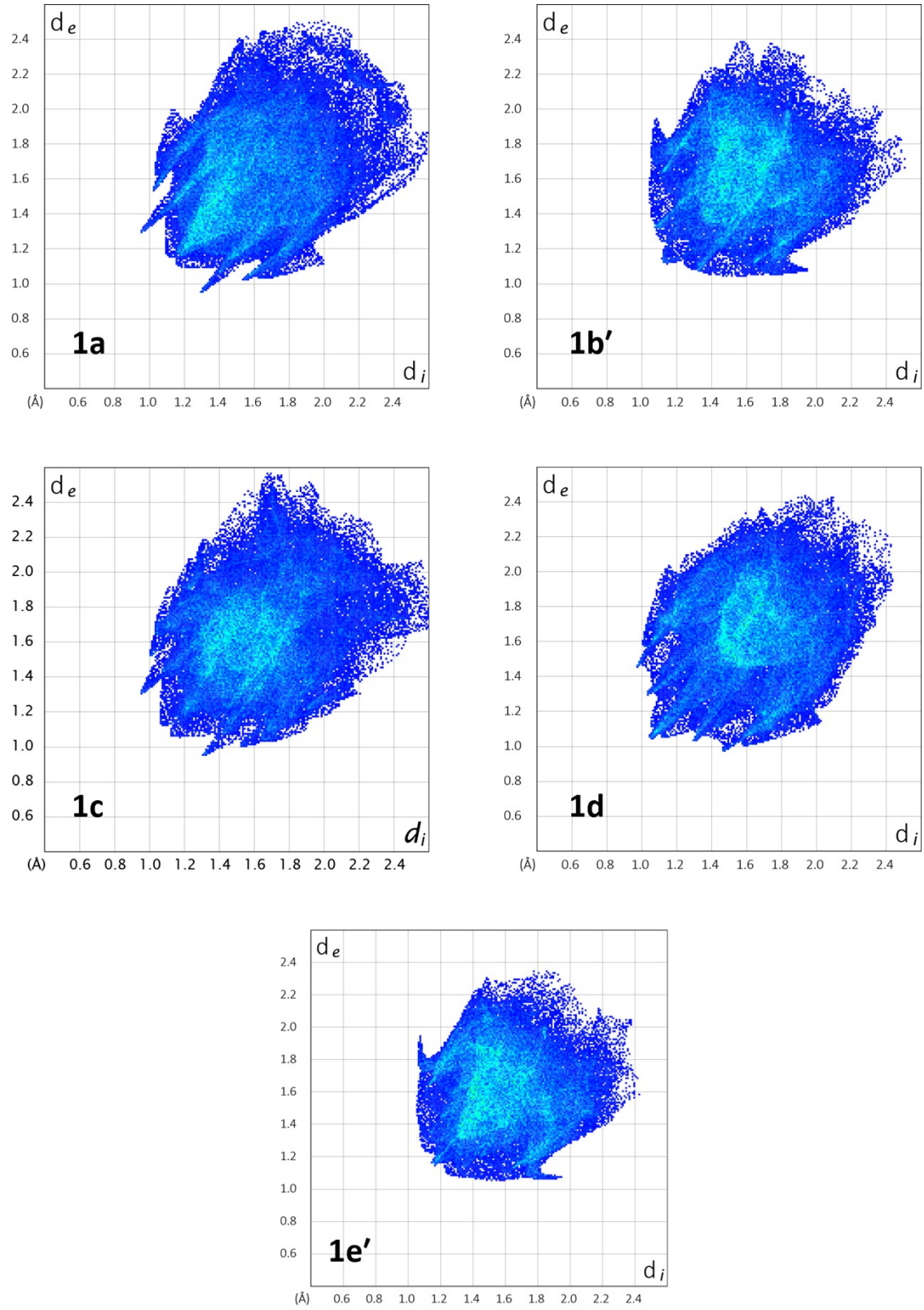

Figure S72. Calculated Hirshfeld fingerprints for the X-ray crystal structures of the barbaralanes **1/1′**.

6.4 Calculation of Intermolecular Interaction Energies in the Solid-State

We performed DFT calculations to quantify the interaction energies between neighbouring molecules in the solid state using the CE-B3LYP [B3LYP/6-31G(d,p)] energy model[23] in CrystalExplorer17.[24] Based on the X-ray crystal structure coordinates, a cluster was generated around a central molecule, extending to molecules that come within 3.8 Å of the central molecule at any point. As each of the crystal structures of **1**/**1′** have only one unique molecule in the unit cell (Z' = 1), all of the surrounding molecules are related to the central molecule by a symmetry operation (labelled 'Symmetry Op.' in Tables S10–14). These energy calculations allow us to elucidate the total interaction energies (E_{tot}, in kJ·mol^{-1}) between neighbouring molecules, based on the individual components for electrostatic (E_{ele}), polarization (E_{pol}), dispersion (E_{dis}), and repulsion (E_{rep}) energies. In each of the Tables below, N indicates the number of molecules of a particular symmetry operation included in the cluster. R is the distance between the molecular centroids (mean atomic position) of the central molecule and the molecule generated by the given symmetry operation. A colour code is given for each table entry, which matches the colouring of the relevant molecules in the corresponding cluster diagrams, Figures S73–77.

For all of the structures we modelled, not only is the overall lattice energy dominated (Tables S10–14) by the dispersion energy term, E_{dis}, but dispersion also makes the largest contribution to the total intermolecular interaction energy between each pair of neighbouring molecules. This observation is consistent with our description of these molecules packing in the solid state in a manner that is influenced more by molecular shape than by any specific noncovalent bonding interactions.

Table S10. Calculated intermolecular interaction energies (in kJ·mol^{-1}) for the solid-state structure of **1a**.

	N	Symmetry Op.	*R* / Å	E_{ele}	E_{pol}	E_{dis}	E_{rep}	E_{tot}
	1	-x, -y, -z	8.65	-10.3	-2.4	-30.8	24.0	-24.6
	2	-x, y+1/2, -z+1/2	8.98	-6.7	-1.5	-33.3	20.8	-24.4
	1	-x, -y, -z	14.98	-1.1	-0.1	-2.5	0.2	-3.2
	2	x, -y+1/2, z+1/2	7.51	-8.0	-2.5	-43.5	27.5	-31.3
	2	x, y, z	9.21	-19.8	-3.5	-29.9	30.6	-30.7
	1	-x, -y, -z	6.86	-2.2	-0.7	-29.5	13.8	-20.0
	2	-x, y+1/2, -z+1/2	9.79	-10.9	-2.1	-29.9	21.5	-25.8
	2	x, -y+1/2, z+1/2	11.01	-1.9	-0.4	-10.1	6.0	-7.3
	1	-x, -y, -z	8.18	-10.2	-1.7	-48.3	29.2	-36.1

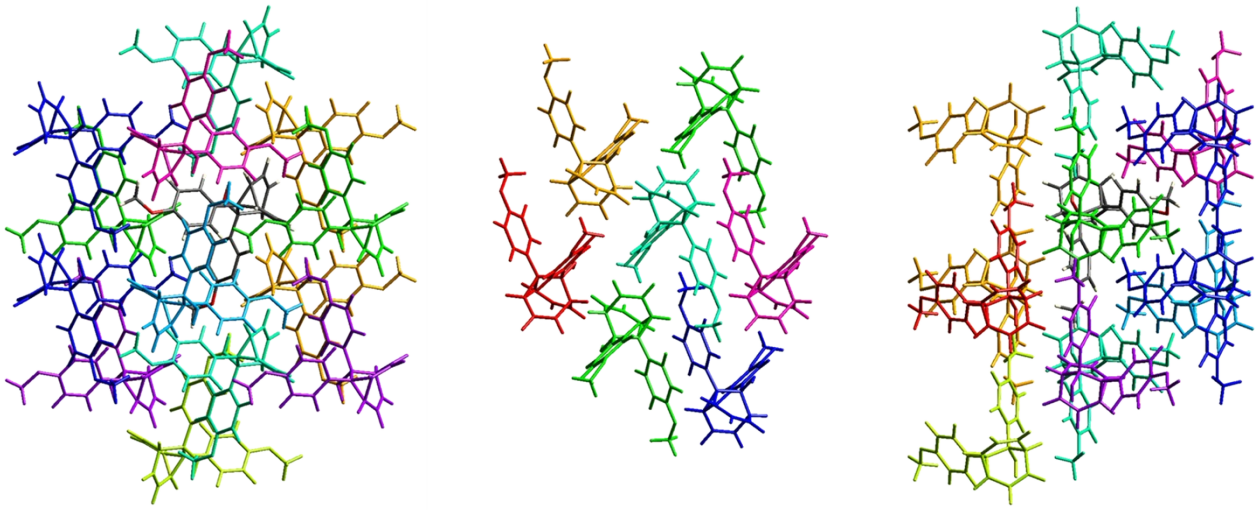

Figure S73. The cluster of molecules used to model intermolecular interaction energies listed in Table S10. The central molecule is coloured according to atom type (C, grey; H, white; O, red) and surrounding molecules are coloured to match the colour code in Table S10.

Table S11. Calculated intermolecular interaction energies (in kJ·mol^{-1}) for the solid-state structure of **1b'**.

N	Symmetry Op.	*R* / Å	E_{ele}	E_{pol}	E_{dis}	E_{rep}	E_{tot}
1	-x, -y, -z	11.65	1.8	-0.5	-7.5	1.5	-4.1
2	-x+1/2, y+1/2, -z+1/2	7.64	-7.7	-0.9	-33.5	18.8	-26.4
2	x, y, z	9.77	-5.5	-0.7	-16.6	12.6	-13.0
2	x, y, z	11.56	-2.3	-0.4	-3.9	0.6	-5.8
1	-x, -y, -z	8.30	-11.0	-1.4	-32.7	23.8	-26.5
2	-x+1/2, y+1/2, -z+1/2	8.20	-2.3	-1.4	-27.2	14.5	-18.2
2	x, y, z	6.18	-8.3	-2.5	-47.4	33.3	-31.4
1	-x, -y, -z	7.12	-14.9	-2.7	-50.6	30.1	-43.2
1	-x, -y, -z	13.22	1.7	-0.2	-1.4	0.0	0.5

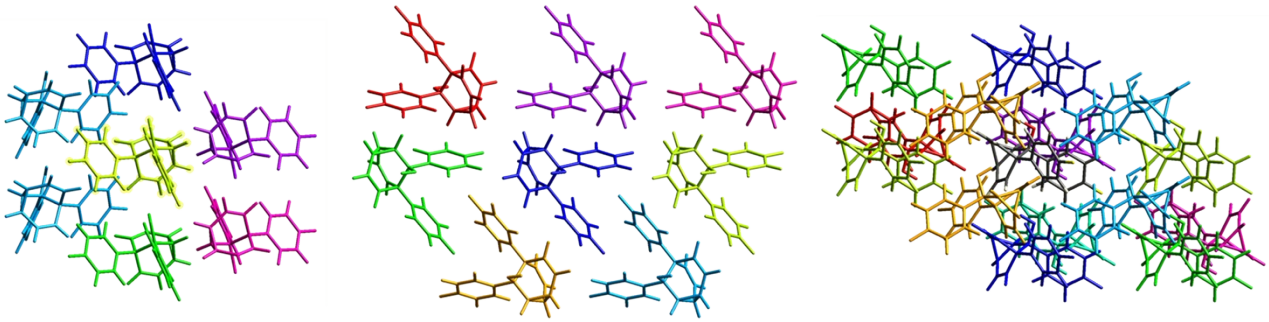

Figure S74. The cluster of molecules used to model intermolecular interaction energies listed in Table S11. The central molecule is coloured according to atom type (C, grey; H, white; O, red; F, yellow) and surrounding molecules are coloured to match the colour code in Table S11.

Table S12. Calculated intermolecular interaction energies (in kJ·mol^{-1}) for the solid-state structure of **1c**.

	N	Symmetry Op.	*R* / Å	E_{ele}	E_{pol}	E_{dis}	E_{rep}	E_{tot}
	2	x, -y+1/2, z+1/2	7.49	-17.5	-3.1	-57.6	44.8	-43.3
	1	-x, -y, -z	8.42	-8.0	-1.8	-31.9	20.8	-24.7
	1	-x, -y, -z	9.86	-0.9	-0.7	-13.3	2.3	-11.6
	2	-x, y+1/2, -z+1/2	11.13	-0.0	-0.4	-3.9	0.6	-3.4
	2	x, y, z	7.15	-4.9	-1.0	-25.1	14.0	-19.1
	2	x, -y+1/2, z+1/2	9.00	-6.1	-0.5	-21.7	13.8	-17.3
	1	-x, -y, -z	8.42	-4.2	-0.8	-26.8	15.0	-19.1
	2	-x, y+1/2, -z+1/2	9.48	-12.6	-2.5	-39.3	31.0	-30.3
	1	-x, -y, -z	13.95	-9.0	-1.3	-9.4	9.8	-12.6

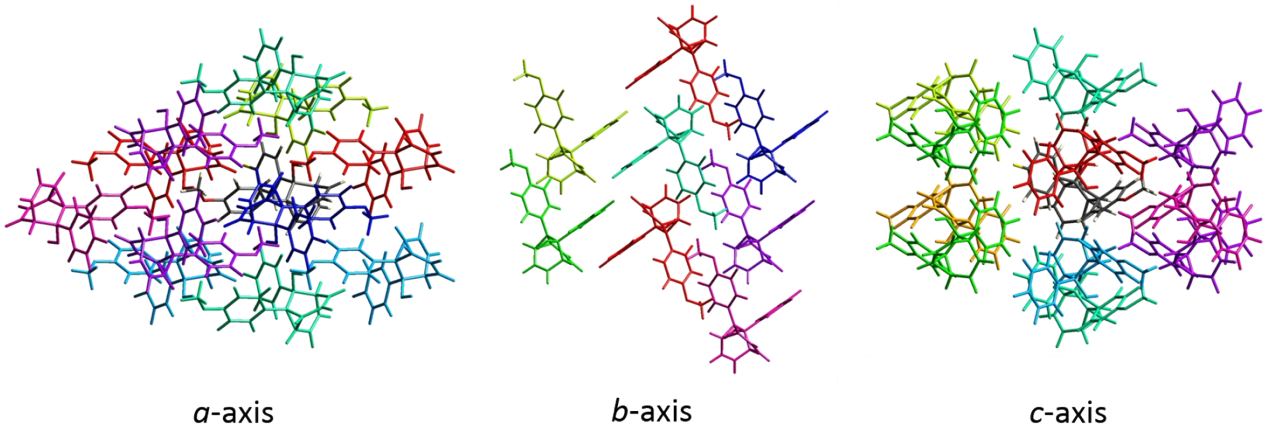

Figure S75. The cluster of molecules used to model intermolecular interaction energies listed in Table S12. The central molecule is coloured according to atom type (C, grey; H, white; O, red; F, yellow) and surrounding molecules are coloured to match the colour code in Table S12.

Table S13. Calculated intermolecular interaction energies (in kJ·mol^{-1}) for the solid-state structure of **1d**.

	N	Symmetry Op.	*R* / Å	E_{ele}	E_{pol}	E_{dis}	E_{rep}	E_{tot}
	2	-x, y+1/2, -z+1/2	9.58	-8.5	-1.3	-23.3	19.4	-18.3
	2	x, -y+1/2, z+1/2	6.63	-21.4	-3.7	-63.5	52.9	-48.0
	1	-x, -y, -z	11.99	-2.4	-0.9	-9.6	6.3	-7.6
	1	-x, -y, -z	9.42	-2.3	-0.6	-16.6	5.0	-14.3
	2	x, y, z	7.50	-6.6	-1.4	-15.8	10.2	-15.5
	2	-x, y+1/2, -z+1/2	12.92	-1.3	-0.6	-6.4	1.3	-6.5
	1	-x, -y, -z	9.69	-11.6	-2.7	-43.7	35.1	-30.6
	2	x, -y+1/2, z+1/2	7.84	-7.6	-0.9	-37.6	24.2	-26.4
	1	-x, -y, -z	11.52	-1.2	-0.4	-7.3	2.7	-6.2

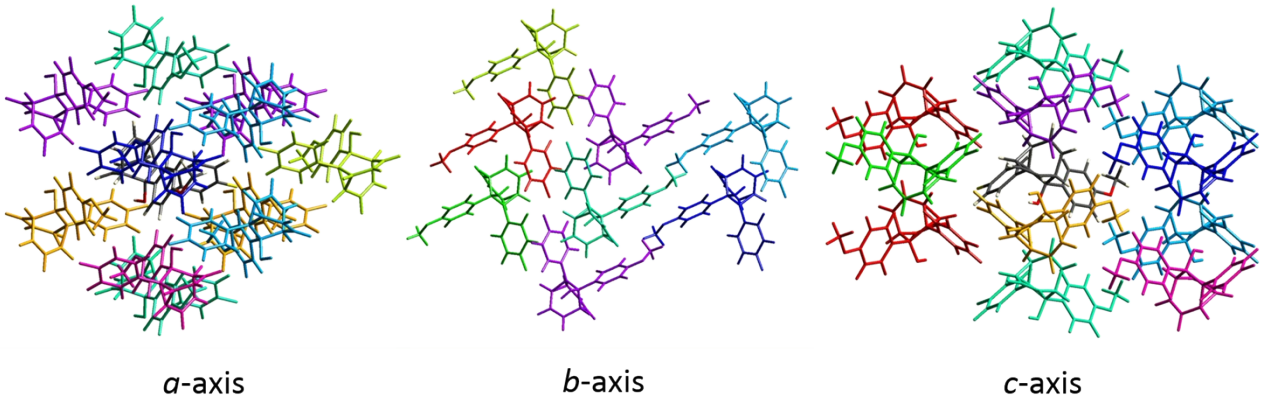

Figure S76. The cluster of molecules used to model intermolecular interaction energies listed in Table S13. The central molecule is coloured according to atom type (C, grey; H, white; O, red; F, yellow) and surrounding molecules are coloured to match the colour code in Table S13.

Table S14. Calculated intermolecular interaction energies (in kJ·mol^{-1}) of for the solid-state structure of **1e'**.

N	Symmetry Op.	*R* / Å	E_{ele}	E_{pol}	E_{dis}	E_{rep}	E_{tot}
1	-x, -y, -z	13.29	2.1	-0.2	-1.3	0.0	1.0
1	-x, -y, -z	7.94	-10.1	-1.4	-31.2	20.3	-26.3
2	x, y, z	11.59	-2.3	-0.4	-3.8	0.6	-5.6
2	x, y, z	6.20	-8.4	-2.4	-46.8	32.8	-31.1
2	-x+1/2, y+1/2, -z+1/2	8.26	-5.0	-0.9	-30.3	18.7	-20.8
1	-x, -y, -z	6.63	-14.8	-2.8	-51.4	30.9	-43.5
2	x, y, z	9.79	-5.0	-0.8	-16.1	11.7	-12.7
2	-x+1/2, y+1/2, -z+1/2	7.90	-6.3	-1.1	-31.5	17.9	-23.8
1	-x, -y, -z	11.04	1.1	-0.4	-8.1	1.8	-5.1

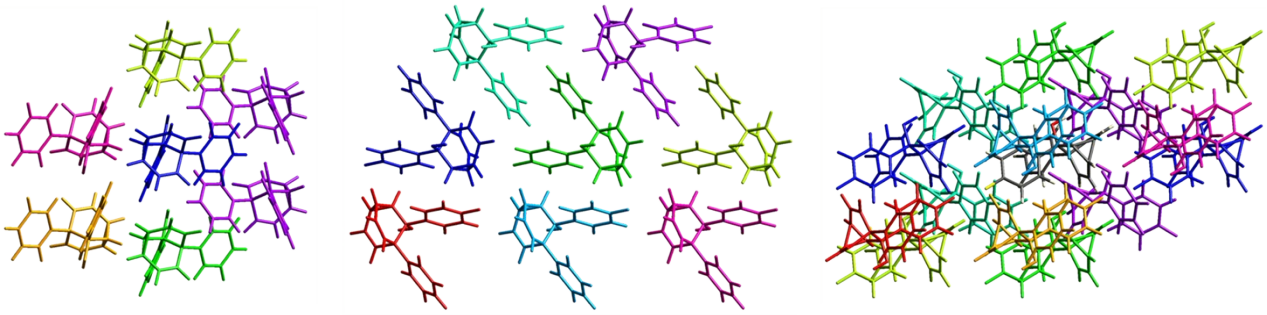

Figure S77. The cluster of molecules used to model intermolecular interaction energies listed in Table S14. The central molecule is coloured according to atom type (C, grey; H, white; O, red; F, yellow) and surrounding molecules are coloured to match the colour code in Table S14.

7. References

[1] Dolomanov, O. V.; Bourhis, L. J.; Gildea, R. J.; Howard, J. A. K.; Puschmann, H. *J. Appl. Crystallogr*. **2009**, *42*, 339.

[2] Sheldrick, G. M. *Acta Crystallogr. Sect. A Found. Crystallogr*. **2008**, *64*, 112.

[3] McGonigal, P. R.; de León, C.; Wang, Y.; Homs, A.; Solorio-Alvarado, C. R.; Echavarren, A. M. *Angew. Chem. Int. Ed.* **2012**, *51*, 13093.

[4] Ferrer, S.; Echavarren, A. M. *Angew. Chem. Int. Ed.* **2016**, *55*, 11178.

[5] Johnston, E. R; Barber, J. S.; Jacomet, M.; Barborak, J. C. *J. Am. Chem. Soc.* **1998**, *120*, 1489.

[6] Zong, H.; Hunag, H.; Liu, J.; Bian, G.; Song, L. *J. Org. Chem.***2012**, *77*, 4645.

[7] Moore, R. E.; Pettus, J. A., Jr.; Mistysyn, J. *J. Org. Chem.*, **1974**, *39*, 2201.

[8] Pretsch, E.; Bühlmann, P.; Affolter, C. *Structure Determination of Organic Compounds,* 3rd ed.; Springer-Verlag: Berlin Heidelberg, 2000.

[9] A CH_2Cl_2-CS_2 solvent mixture gave the best compromise of solubility and low freezing point, but freezes below 149 K.

[10] H. Günther, J. Runsink, H. Schmickler, P. Schmitt, *J. Org. Chem.* **1985**, *50*, 289.

[11] A metastable bullvalene isomer has been isolated by chromatography. a) M. He, J. W. Bode, *Proc. Natl Acad. Sci. USA* **2011**, *108*, 14752; b) M. He, J. W. Bode, *Org. Biomol. Chem.* **2013**, *11*, 1306.

[12] Guassian 16, Revision A.03, Frisch, M. J.; Trucks, G. W.; Schlegel, H. B.; Scuseria, G. E.; Robb, M. A.; Cheeseman, J. R.; Scalmani, G.; Barone, V.; Petersson, G. A.; Nakatsuji, H.; Li, X.; Caricato, M.; Marenich, A. V.; Bloino, J.; Janesko, B. G.; Gomperts, R.; Mennucci, B.; Hratchian, H. P.; Ortiz, J. V.; Izmaylov, A. F.; Sonnenberg, J. L.; Williams-Young, D.; Ding, F.; Lipparini, F.; Egidi, F.; Goings, J.; Peng, B.; Petrone, A.; Henderson, T.; Ranasinghe, D.; Zakrzewski, V. G.; Gao, J.; Rega, N.; Zheng, G.; Liang, W.; Hada, M.; Ehara, M.; Toyota, K.; Fukuda, R.; Hasegawa, J.; Ishida, M.; Nakajima, T.; Honda, Y.; Kitao, O.; Nakai, H.; Vreven, T.; Throssell, K.; Montgomery, J. A., Jr.; Peralta, J. E.; Ogliaro, F.; Bearpark, M. J.; Heyd, J. J.; Brothers, E. N.; Kudin, K. N.; Staroverov, V. N.; Keith, T. A.; Kobayashi, R.; Normand, J.; Raghavachari, K.; Rendell, A. P.; Burant, J. C.; Iyengar, S. S.; Tomasi, J.; Cossi, M.; Millam, J. M.; Klene, M.; Adamo, C.; Cammi, R.; Ochterski, J. W.; Martin, R. L.; Morokuma, K.; Farkas, O.; Foresman, J. B.; Fox, D. J. Gaussian, Inc., Wallingford CT, 2016.

[13] Becke, A. D. *J. Phys. Chem.* **1993**, *98*, 5648.

[14] Yanai, T.; Tew, D. P.; Handy, N. C. *Chem. Phys. Lett.* **2004**, *393*, 51.

[15] Zhao, Y.; Truhlar, D. *Theor. Chem. Acc.* **2008**, *120*, 215.

[16] Grimme, S.; Antony, J.; Ehrlich, S.; Krieg, H. *J. Chem. Phys.* **2010**, *132*, 154104.

[17] Cossi, M.; Rega, N.; Scalmani, G.; Barone, V. *J. Comput. Chem.* **2003**, *24*, 669.

[18] Chai, J.-D.; Head-Gordon, M. *Phys. Chem. Chem. Phys.* **2008**, *10*, 6615.

[19] Lingwood, M.; Hammond, J. R.; Hrovat, D. A.; Mayer, J. M.; Borden, W. T. *J. Chem. Theory Comput.* **2006**, *2*, 740.

[20] Clark, S. J.; Segall, M. D.; Pickard, C. J.; Hasnip, P. J.; Probert, M. J.; Refson, K.; Payne, M. C. *Z. Kristallogr.* **2005**, *220*, 567.

[21] Perdew, J. P.; Burke, K.; Ernzerhof, M. *Phys. Rev. Lett.* **1996**, *77*, 3865.

[22] Sturniolo, S.; Green, T. F. G.; Hanson, R. M.; Zilka, M.; Refson, K.; Hodgkinson, P.; Brown, S. P.; Yates, J. R. *Solid State Nucl. Magn. Reson.* **2016**, *78*, 64.

[23] Turner, M. J.; McKinnon, J. J.; Wolff, S. K.; Grimwood, D. J.; Spackman, P. R.; Jayatilaka, D.; Spackman, M. A. CrystalExplorer17 (2017). University of Western Australia.

[24] Spackman, M. A.; Jayatilaka, D. *CrystEngComm*, **2009**, 11, 19-31.

[25] Steiner, T.; Desiraju, G. R. *Chem. Commun.* **1998**, 891.